ECMWF COPERNICUS REPORT

Copernicus Atmosphere Monitoring Service

Validation report of the CAMS near-real time global atmospheric composition service

September-November 2016

Issued by: KNMI / Henk Eskes

Date: 14/02/2017

Ref: CAMS84_2015SC2_D84.1.1.6_2016SON_v0.5

IMPLEMENTED BY ECMWF

Validation report of the CAMS near-real-time global atmospheric composition service. September-November 2016

EDITORS:
H.J. ESKES (KNMI), A. WAGNER (MPG), M. SCHULZ (METNO),
Y. CHRISTOPHE (BIRA-IASB), M. RAMONET (LSCE)

AUTHORS:
S. BASART (BSC), A. BENEDICTOW (METNO), A.-M. BLECHSCHMIDT (IUP-UB),
S. CHABRILLAT (BIRA-IASB), H. CLARK (CNRS-LA), E. CUEVAS (AEMET),
H. FLENTJE (DWD), K. M. HANSEN (AU), U. IM (AU),
J. KAPSOMENAKIS (AA), B. LANGEROCK (BIRA-IASB), A. RICHTER (IUP-UB),
N. SUDARCHIKOVA (MPG), V. THOURET (CNRS-LA), T. WARNEKE (UBC),
C. ZEREFOS (AA)

REPORT OF THE COPERNICUS ATMOSPHERE MONITORING SERVICE, VALIDATION SUBPROJECT.

AVAILABLE AT:
HTTP://ATMOSPHERE.COPERNICUS.EU/QUARTERLY_VALIDATION_REPORTS

CITATION:
VALIDATION REPORT OF THE CAMS NEAR-REAL-TIME GLOBAL ATMOSPHERIC COMPOSITION SERVICE: SEPTEMBER-NOVEMBER 2016.
H.J. ESKES, A. WAGNER, M. SCHULZ, Y. CHRISTOPHE, M. RAMONET, S. BASART, A. BENEDICTOW, A.-M. BLECHSCHMIDT, S. CHABRILLAT, H. CLARK, E. CUEVAS, H. FLENTJE, K.M. HANSEN, U. IM, J. KAPSOMENAKIS, B. LANGEROCK, A. RICHTER, N. SUDARCHIKOVA, V. THOURET, T. WARNEKE, C. ZEREFOS,
COPERNICUS ATMOSPHERE MONITORING SERVICE (CAMS) REPORT,
CAMS84_2015SC2_D84.1.1.6_2016SON_v1.pdf, FEBRUARY 2017.

STATUS:
DRAFT, VERSION 0.5

DATE:
14/02/2016

1 Executive Summary

The Copernicus Atmosphere Monitoring Service (http://atmosphere.copernicus.eu, CAMS) is a component of the European Earth Observation programme Copernicus. The CAMS global near-real time (NRT) service provides daily analyses and forecasts of reactive trace gases, greenhouse gases and aerosol concentrations. The CAMS system was developed by a series of MACC research projects (MACC I-II-III) until July 2015. This document presents the validation statistics and system evolution of the CAMS NRT service for the period until 1 December 2016. Updates of this document appear every 3 months.

This summary is split according to areas of interest to users: Climate forcing, regional air quality, and stratospheric ozone. Specific attention is given to the ability of the CAMS system to capture recent events. We focus on the 'o-suite' composition fields, which are the daily analyses and forecasts produced by the C-IFS (Composition-IFS) modelling system at ECMWF, using the available meteorological and atmospheric composition observations which are ingested in the ECMWF 4D-Var assimilation system. For analyses and forecasts of trace gases the CB05 tropospheric chemistry is used, while for aerosol this is the CAMS prognostic aerosol module. We furthermore assess the impact of the composition observations by comparing the validation results from the 'o-suite' to a 'control' configuration without assimilation. Also the pre-operational high-resolution forecasts of CO_2 and CH_4 are assessed in this report.

The o-suite data availability for the period September-November 2016 was very good, with 100% of the forecasts delivered before the target time, 22:00 UTC (to be updated for SON 2016).

Climate forcing

Tropospheric ozone (O_3)

Model ozone is validated with respect to surface and free tropospheric ozone observations from the GAW and ESRL networks, IAGOS airborne data and ozone sondes. For free tropospheric ozone against sondes the o-suite modified normalized mean biases (MNMBs) are on average smaller ±10% over the Northern Hemisphere (NH), and between ± 20% for stations in the Tropics (Fig. S1). This is an improvement compared to the control experiment without the assimilation of composition observations. For September to November 2016 good agreement is found over the NH mid latitudes in the free troposphere, which is confirmed with IAGOS evaluations over Paris, Amsterdam and Frankfurt.

The o-suite shows an overestimation of surface ozone for Europe during September and November2016 with MNMBs of around 10% on average. For USA the o-suite shows an overestimation of surface ozone of around 15% on average. For Asia, the o-suite shows an overestimation of surface ozone MNMBs of around 35% on average. For the tropics, the surface ozone is overestimated around 15%. For Antarctic and Arctic stations, the o-suite shows a good correspondence with observed surface ozone mixing ratios (MNMBS < 15%). The data assimilation corrects the negative offset visible for the control run.

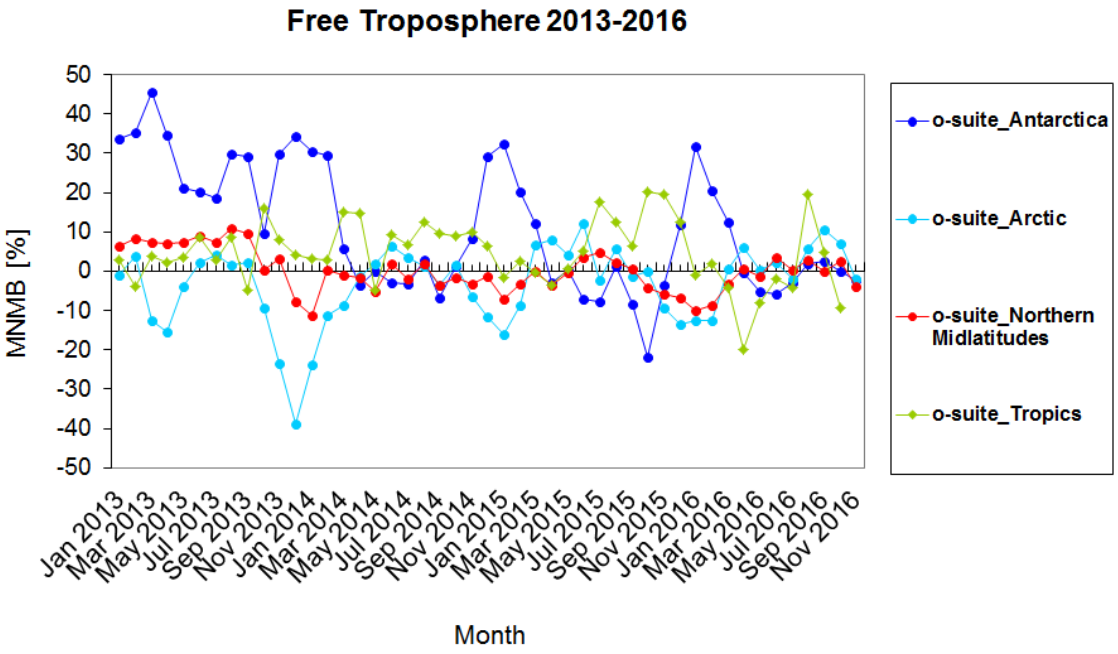

Figure S1: Time series of MNMB of ozone in the o-suite, compared against ozone sondes, averaged over different latitude bands.

Tropospheric Nitrogen dioxide (NO_2)

Model validation, with respect to SCIAMACHY/Envisat NO_2 data before April 2012 and GOME-2/MetOp-A NO_2 data afterwards, shows that tropospheric NO_2 columns are well reproduced by the NRT model runs, indicating that emission patterns and NO_x photochemistry are generally well represented, although modelled shipping signals are larger than the satellite retrievals. Tropospheric NO_2 columns over some emission hotspots are overestimated. Since December 2014, the agreement between satellite retrievals and model results for time series over East-Asia and Europe is better than for previous years (Fig. S2), as observed columns of NO_2 decreased recently, likely associated with reduced emissions. Spring and summertime values over East-Asia are overestimated by the o-suite in 2015 and 2016, a feature which does not occur for previous years. Compared to satellite data, tropospheric background values over Europe, Africa and South Americaare currently underestimated by the models, while local maxima over Central Africa are overestimated, likely due to overestimation of fire emissions for Central Africa. Evaluation against MAX-DOAS observations illustrates the positive impact of data assimilation for urban sites, leading to an increase in NO_2.

Tropospheric Carbon Monoxide (CO)

Model validation with respect to GAW network surface observations, IAGOS airborne data, FTIR observations (NDACC and TCCON) and MOPITT and IASI satellite retrievals reveals that the seasonality of CO can be reproduced well by both model versions. A small, consistent negative bias of -5% against MOPITT appears in the o-suite throughout the year over Europe and the US, but for the latest periods (JJA, SON) it is further reduced. Also compared to IAGOS aircraft observations over Europe and Asia, modelled free tropospheric CO mixing ratios show an underestimation compared to the measurements, whereas the control run partly overestimates the observations.

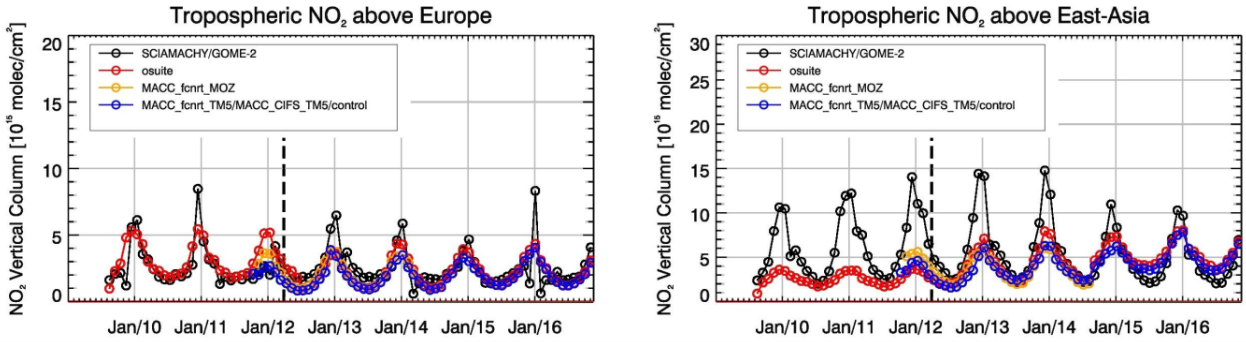

Figure S2: Time series of tropospheric NO_2 columns from SCIAMACHY (up to March 2012), GOME-2 (from April 2012 onwards) compared to model results for Europe and East-Asia. The o-suite is in red, control is in blue (before Sept 2014 blue and yellow represent older model configurations).

This is confirmed with comparison against GAW surface observations for Asia (MNMBs between 6% and -18%). During the fire season over Alaska and Siberia negative biases are within 5%. The two northern hemisphere TCCON sites, however, show a slight overestimation of CO in the o-suite (between 4 and 7%).

Especially the control run shows an overestimation of CO total columns in the tropics, SH and Asia. This overestimation is reduced by the data assimilation for the o-suite. The positive impact of the assimilation of satellite CO on model results shows especially over East and South Asia and North and South Africa, and Réunion Island, whereas for Europe and the US, the control run corresponds better to satellite and surface CO observations. The forecasts (D+1, D+4) are mostly identical to analysis (within 1% difference).

Formaldehyde

Model validation, with respect to SCIAMACHY/Envisat HCHO data before April 2012 and GOME-2/MetOp-A HCHO data afterwards, shows that modelled monthly HCHO columns represent well the magnitude of oceanic and continental background values and the overall spatial distribution in comparison with mean satellite HCHO columns. Compared to GOME-2 satellite retrievals, there is an overestimation of values for Northern and Central Australia and Central Africa. As for tropospheric NO_2, the latter may be due to an overestimation of HCHO emissions from fires for Central Africa. For time series over East-Asia and the Eastern US, both regions where HCHO columns are probably dominated by biogenic emissions, models and retrievals agree rather well. However, the yearly cycle over East-Asia is underestimated by the models.

The validation of model profiles with ground-based UV-VIS DOAS measurements over Xianghe, near Beijing, shows that background column values are underestimated by around 40-60%, in agreement with satellite observations for this region. Also local pollution events are not captured correctly, in part due to the relatively coarse horizontal resolution of the global models, and in part associated with uncertainties in HCHO and precursor emissions. Note that no formaldehyde observations are assimilated in the system.

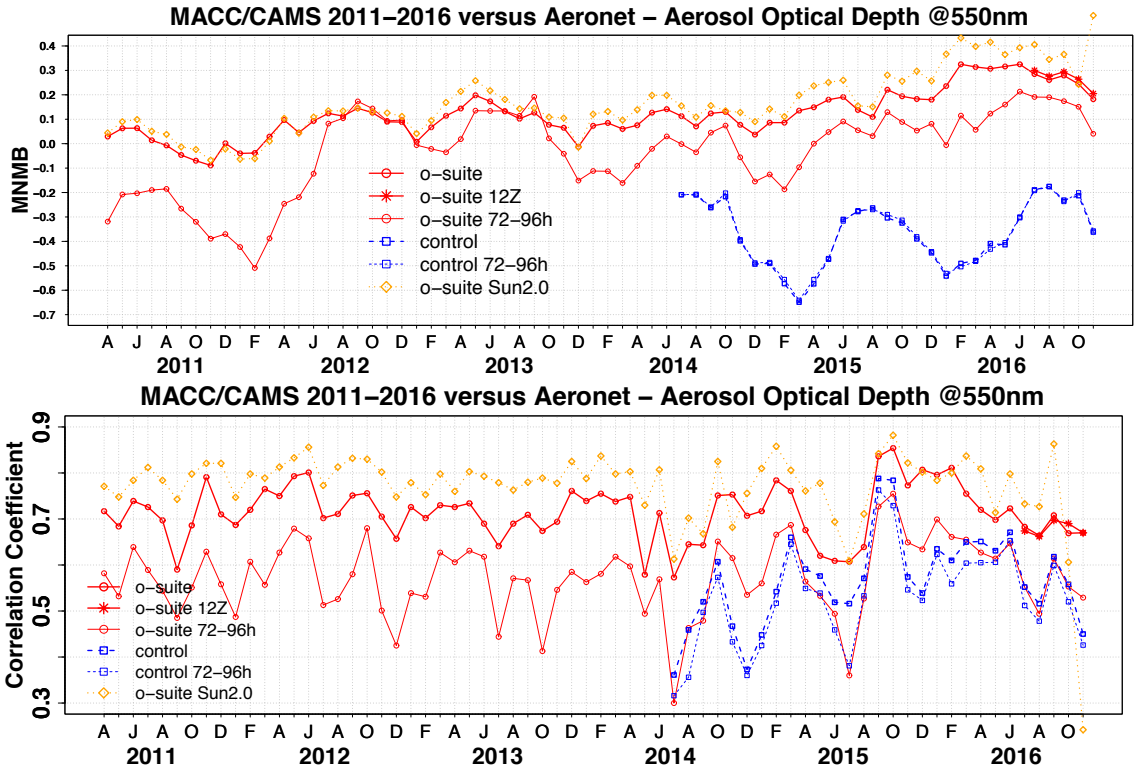

Figure S3. Aerosol optical depth at 550nm in IFS 00Z model simulations for April 2011 - November 2016 against daily matching Aeronet NRT level 1.5 and level 2.0 data a) Modified normalized mean bias (MNMB); o-suite (thick red curve); o-suite at last forecast day (light red curve); Control (blue dashed); Control at last forecast day (light blue dashed); o-suite but evaluated against quality assured Aeronet level 2.0 data (orange dashed); b) Corresponding correlation coefficient. Note that quality assured level 2.0 data amount decreases from ca 2800 daily data points per month (mean in 2014) to ca. 200 data points in the last two month of the time series. Correlation and MNMB of the 12Z forecast run is shown as well.

Aerosol

We estimate that the o-suite aerosol optical depth showed an average positive bias in the latest three months of +24%, measured as modified normalized mean bias against daily Aeronet sun photometer data. The +3 day forecasted aerosol distributions, since July 2012, show 10-30% less aerosol optical depth (AOD) than those from the initial day, as shown all in Figure S3a. The correlation, shown in figure S3b, shows month-to-month variation ranging from 0.65 to 0.85, indicating the simulation reproduces approximately 50% of the day to day AOD variability across all Aeronet stations. The more steady performance of the o-suite over the year indicates that assimilating MODIS deep blue product since September 2015 improves aerosol AOD simulation. The o-suite forecast at +3 days shows slightly lower correlation, as a consequence of imperfect forecasted meteorology and fading impact of the initial assimilation of MODIS AOD and MODIS fire info on model performance. The second o-suite running each day at 12UTC showed almost identical performance as the o-suite starting at 00UTC.

The regional AOD performance of the o-suite with respect to the AERONET data exhibits less and less a seasonal cycle depending on region. A lower correlation in autumn and winter in North

America can be noted. The smallest bias is shown in East Asia, and last months show a higher positive bias in North America (+50%).

The aerosol Ångström exponent contains information about the size distribution of the aerosol, and implicitly composition. The o-suite continues to show a positive global bias against Aeronet data of +20%, indicating too fine particles in the model, possibly dominated by sulphate, which represents ca 45% of global mean AOD. Correlation is lower in autumn and winter.

For this and the last validation report PM10 data were used directly as defined by the IFS system, and PM10 concentrations decreased by 50% compared to earlier validation reports, eg those in 2015. An evaluation of these PM10 surface concentrations against a climatological average (2000-2009) at 150 background sites in North America and Europe indicates overestimations at some sites closer to the coast, possibly due to high simulated sea salt concentrations. However, PM10 concentrations more inland exhibit an underestimation with MNMB bias of -30% both in Europe and North America.

From September to November, dust activity is low over Northern Africa and the Middle East in comparison the previous season. Satellites show that major dust activity is concentrated over the Sahara (in the Bodelé Basin and the Mali/Mauritania border), the dust corridor of North Western Maghreb and Iraq. CAMS o-suite model can simulate the main areas of dust activity in comparison with MODIS and the SDS-WAS multimodel product, although o-suite reduces the strong overestimations observed in control, some important dust sources (as the Bodélé and Iraq) appear underestimates. CAMS o-suite is the model that best reproduces the daily variability of AERONET observations with a correlation coefficient of 0.64 in average for all the AERONET sites. The performance of o-suite is particularly good over Sahel and Sahara regions (with correlation values of 0.41 and 0.57, respectively).

A preliminary evaluation of vertical profiles of aerosol backscatter coefficient derived from the German ceilometer network indicates that during dust events model profiles confirm the suspected presence of dust in the observations, and vice versa. Small-scale structures in dust plumes are not resolved, most likely due to model resolution. Profiles during elevated sea salt periods show more disagreement with observations and sea salt seems to be overestimated inland during storm events, confirming PM10 bias findings above.

Greenhouse gases

Pre-operational high-resolution forecasts of CO_2 and CH_4 have been compared to ICOS surface (15 sites) and TCCON total column (3 sites) measurements, for a one year period from (Dec. 2015 to Nov. 2016). Most of the stations are located in Europe (9 ICOS and 2 TCCON sites) providing a better representativeness over this continent. The third TCCON station is located in the tropical Indian ocean, at La Réunion Island where two surface stations are also monitoring CO_2 and CH_4 at the surface, one being installed at sea level, the other on a mountain site 2195 m asl. However the representation of CO_2 and CH_4 variabilities is challenging at this location, due to the complexity of the atmospheric transport (coastal and topography effects) combined to the presence of emission high spots due to anthropogenic and/or biogenic activities. The model simulates unrealistic short-term variations of CO_2 both at the mountain site and in the total column.

The amplitude of the CO_2 seasonal cycle in North Hemisphere is overestimated by the model. This feature observed both in total column and surface sites is characterized by too high concentrations in winter. The agreement is generally better in late summer and fall 2016 with a tendency to underestimate the concentrations at least at the surface. One important feature is the systematic improvement of the correlation coefficient at the three European tall towers when comparing measurements from the lowest to the highest sampling lines, which underline the importance of such infrastructure to improve the representativeness of surface sites.

CH_4 concentrations in the north hemisphere agree pretty well with surface and total column observations, with the exception of a three months period from August to November 2016. During this period a negative bias of about -20 ppb is observed at all locations. On the reverse, the negative bias observed at south hemisphere locations with the gf39 model experiment (Dec to Feb. 2016) has been solved with the new experiment (ghqy).

System performance in the Arctic

The CAMS model runs are validated using surface ozone measurements from the ESRL-GMD and the IASOA networks (5 sites) and ozone concentrations in the free troposphere are evaluated using balloon sonde measurement data.

For the period from December 2014 to November 2016 the simulations of the surface ozone concentrations are on average in good agreement with the observations apart from ozone depletion events in spring (March to June), which are not captured by the model simulations. These events are related to halogen chemistry reactions that are not represented in the C-IFS model.

During the period September 2016 – November 2016 the o-suite slightly underestimates observed O_3 mixing ratios (between -5 and -10%) for the five stations. MNMBs for the control run are larger (between -8 and -25%). The variability is better described by the control run. For the Arctic free troposphere, both o-suite and control run shows low MNMBs (between -10 and 10%).

System performance in the Mediterranean

The model is compared to surface O_3 observations from the AirBase network. Our analysis shows that both runs MNMBs vary between ±20% in the Mediterranean shore of Spain (MNMBs around ±20%) and between ±10% in the rest of the Mediterranean. Temporal correlation coefficients between simulated and observed surface ozone mixing for both o-suite and the control run are highly significant (on average around 0.7).

From September to November, CAMS o-suite can reproduce the AOD variability observed in the AERONET sites with MB of -0.01 and a correlation coefficient of 0.62 in average for all sites. The highest peaks on CAMS AOD simulations are linked to desert dust intrusions. During autumn, dust activity is low over all the Mediterranean Basin. Otherwise, overestimations are observed in Northwestern Mediterranean during background situations. On surface levels, CAMS o-suite can reproduce the timing of the most intense PM10 and PM2.5 events observed by Airbase sites although tends to overestimate them.

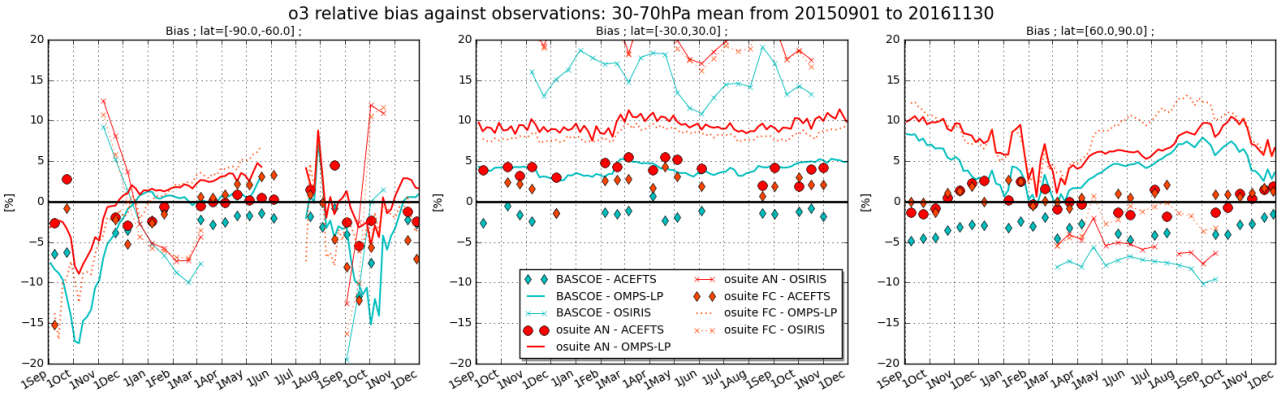

Figure S4: Time series of the normalized mean bias (%) between ozone from o-suite analyses (red, solid), 4th day forecasts (red, dotted) or BASCOE and observations from three satellite instruments: OMPS-LP, ACE-FTS and OSIRIS, in the middle stratosphere (30-70hPa averages).

Regional air quality

Ozone, CO and aerosol boundary conditions

Free tropospheric ozone concentrations in the o-suite in the northern midlatitudes are generally in good correspondence with ozone sondes, MNMBs in the range of ±10% (for the last nine months ±4%). The o-suite shows a positive bias in surface ozone concentrations in Europe, with MNMBs for GAW and ESRL stations ranging between 2% and 14% for the period September to November 2016, and also positive biases over North American stations (between 10% and 20%). The o-suite mostly underestimates surface CO concentration in Europe and Asia with MNMBs with respect to GAW of between -10% and -22%.

Ozone layer

Ozone partial columns and vertical profiles

Ozone columns and profiles have been compared with the following observations: vertical profiles from balloon-borne ozonesondes; ground-based remote-sensing observations from the NDACC (Network for the Detection of Atmospheric Composition Change, http://www.ndacc.org); and satellite observations by three instrument (OMPS-LP, ACE-FTS and OSIRIS). Furthermore, the o-suite analyses are compared with those delivered by two independent assimilation systems: BASCOE, and TM3DAM.

Compared to ozone sondes the model O_3 partial pressures are mostly slightly overestimated in all latitude bands (MNMB between 0 and +10%).

Comparisons with the NDACC network include microwave observations for Ny Alesund (78.9°N) and Bern (47°N) and LIDAR observations at Hohenpeissenberg (47.8°N) and Lauder (45°S). Among these stations the o-suite performs best at Bern with stratospheric columns evolving since September 2015 with seasonally averaged relative biases smaller than 5%, which is smaller than the reported measurement uncertainties. At Ny Alesund, the seasonally averaged bias of the stratospheric column almost vanishes during summer months , while during the rest of the year the o-suite overestimates (>10%) the ozone abundance between 25km and 35km. Compared with the LIDAR at

Lauder and Hohenpeissenberg, the o-suite does not show significant biases with the observed ozone between 20km and 35km.

The comparison with independent satellite observations is generally in good agreement for the considered period: for OMPS, the NMB is within 10% between 100hPa and 5hPa, except in the lower stratosphere of the North polar region where it reaches 15%; for ACE-FTS, the NMB is mainly within 10% between 5km and 40km, and mostly within 5% between 15km and 35km except in the tropics. The time evolution on the last 15 months of the normalized mean bias in the lower middle stratosphere (Figure S4) shows a systematic overestimation by the o-suite in the Tropics (~10% against OMPS and ~5% against ACE-FTS) and a variable bias for the polar regions. Also, the 4th day forecasts exhibits an higher bias in the polar regions.

Other stratospheric trace gases

Due to the lack of stratospheric chemistry in the C-IFS-CB05 scheme, the only useful product in the stratosphere is ozone. Other species, like NO_2, have also been evaluated but the results are only indicative.

Events

The selected dust event corresponds to a dust plume that originated in Algeria, and move towards Central and Eastern Mediterranean in early November 2016 as it was detected ground visibility stations. The full episode was well predicted by CAMS o-suite as it is showed the comparison of the dust aerosol optical depth (DOD) predicted by CAMS o-suite and observed AOD by satellites and AERONET sites from 6th to 9th November 2016.

Several big fire events took place in Siberia, Russian Federation, in September 2016. Both the o-suite and the free model run capture well the location of the plume and the eastward transport of CO. In the beginning of the fire event, both runs overestimated CO values in the plume, but both show an underestimation of CO after 4-7 days of transport.

A synoptic event at Amsterdam Island occurred in June 2016. During this season we observed increases of trace gases like Radon, CO_2, CH_4, CO, and black carbon. Such events cannot be explained by local emissions and are due to rapid advections (2-3 days) of pollutants from the southern Africa. This example demonstrates the capacity of the model to simulate this transportation over Indian Ocean, since both the amplitude and timing of the CH_4 spike is perfectly reproduced. For CO_2, the model underestimates the increase of concentrations and fails to reproduce the daily variation, indicating that the biospheric surface flux should be improved.

Table of Contents

1. Introduction

The Copernicus Atmosphere Monitoring Service (CAMS, http://atmosphere.copernicus.eu/) is a component of the European Earth Observation programme Copernicus. The CAMS global near-real time (NRT) service provides daily analyses and forecasts of trace gas and aerosol concentrations. The CAMS system was developed by a series of MACC research projects (MACC I-II-III). The CAMS near-real time services consist of daily analysis and forecasts with the Composition-IFS system with data assimilation of trace gas concentrations and aerosol properties. This document presents the system evolution and the validation statistics of the CAMS NRT global atmospheric composition analyses and forecasts. The validation methodology and measurement datasets are discussed in Eskes et al. (2015).

In this report the performance of the system is assessed in two ways: both the longer-term mean performance (seasonality) as well as its ability to capture recent events are documented. Table 1.1 provides an overview of the trace gas species and aerosol aspects discussed in this CAMS near-real time validation report. This document is updated every 3 months to report the latest status of the near-real time service.

This report covers results for a period of at least one year to document the seasonality of the biases. Sometimes reference is made to other model versions or the reanalysis to highlight aspects of the near-real time products.

Key CAMS NRT products and their users are: Boundary conditions for regional air quality models (e.g. AQMEII, air quality models not participating in CAMS); Long range transport of air pollution (e.g. LRTAP); Stratospheric ozone column and UV (e.g. WMO, DWD); 3D ozone fields (e.g. SPARC).

As outlined in the MACC-II Atmospheric Service Validation Protocol (2013) and MACC O-INT document (2011), relevant user requirements are quick looks of validation scores, and quality flags and uncertainty information along with the actual data. This is further stimulated by QA4EO (Quality Assurance Framework for Earth Observation, http://www.qa4eo.org) who write that “all earth observation data and derived products is associated with it a documented and fully traceable quality indicator (QI)”. It is our long-term aim to provide such background information. The user is seen as the driver for any specific quality requirements and should assess if any supplied information, as characterised by its associated QI, are "fit for purpose" (QA4EO task team, 2010).

CAMS data are made available to users as data products (grib or netcdf files) and graphical products from ECMWF, http://atmosphere.copernicus.eu/global-near-real-time-data-access. The stratospheric ozone service is provided by BIRA-IASB at http://copernicus-stratosphere.eu.

A summary of the system and its recent changes is given in section 2. Section 3 gives an overview of the performance of the system from a seasonal (climatological) perspective, for various species. Section 4 describes the performance of the system during recent events. Extended validation can be found online via regularly updated verification pages, http://atmosphere.copernicus.eu/user-support/validation/verification-global-services. Table 1.2 lists all specific validation websites that can also be found through this link.

Table 1.1: Overview of the trace gas species and aerosol aspects discussed in this CAMS near-real time validation report. Shown are the datasets assimilated in the CAMS analysis (second column) and the datasets used for validation, as shown in this report (third column). Green colors indicate that substantial data is available to either constrain the species in the analysis, or substantial data is available to assess the quality of the analysis. Yellow boxes indicate that measurements are available, but that the impact on the analysis is not very strong or indirect (second column), or that only certain aspects are validated (third column).

Species, vertical range	Assimilation	Validation
Aerosol, optical properties	MODIS Aqua/Terra AOD	AOD, Ångström: AERONET, GAW, Skynet, MISR, OMI, lidar, ceilometer
Aerosol mass (PM10, PM2.5)	-	European AirBase stations
O_3, stratosphere	MLS, GOME-2A, GOME-2B, OMI, SBUV-2	Sonde, lidar, MWR, FTIR, OMPS, BASCOE and MSR analyses
O_3, UT/LS	Indirectly constrained by limb and nadir sounders	IAGOS, ozone sonde
O_3, free troposphere	Indirectly constrained by limb and nadir sounders	IAGOS, ozone sonde
O_3, PBL / surface	-	Surface ozone: WMO/GAW, NOAA/ESRL-GMD, AIRBASE
CO, UT/LS	-	IAGOS
CO, free troposphere	IASI, MOPITT	IAGOS, MOPITT, IASI, TCCON
CO, PBL / surface	Indirectly constrained by satellite IR sounders	Surface CO: WMO/GAW, NOAA/ESRL
NO_2, troposphere	OMI, partially constrained due to short lifetime	SCIAMACHY, GOME-2, MAX-DOAS
HCHO	-	GOME-2, MAX-DOAS
SO_2	GOME-2A, GOME-2B (Volcanic eruptions)	-
Stratosphere, other than O_3	-	NO_2 column only: SCIAMACHY, GOME-2
CO_2, surface, PBL		ICOS
CO_2, column		TCCON
CH_4, surface, PBL		ICOS
CH_4, column		TCCON

Table 1.2: Overview of quick-look validation websites of the CAMS system.

Reactive gases – Troposphere
GAW surface ozone and carbon monoxide: **http://macc.copernicus-atmosphere.eu/d/services/gac/verif/grg/gaw/gaw_station_ts/** IAGOS tropospheric ozone and carbon monoxide: **http://www.iagos.fr/cams/** Surface ozone from EMEP (Europe) and NOAA-ESRL (USA): **http://www.academyofathens.gr/cams** Tropospheric nitrogen dioxide and formaldehyde columns against satellite retrievals: **http://www.doas-bremen.de/macc/macc_veri_iup_home.html** Tropospheric CO columns against satellite retrievals: **http://cams.mpimet.mpg.de**
Reactive gases - Stratosphere
Stratospheric composition: **http://www.copernicus-stratosphere.eu** NDACC evaluation in stratosphere and troposphere (the NORS server) **http://nors-server.aeronomie.be**
Aerosol
Evaluation against selection of Aeronet stations: **http://www.copernicus-atmosphere.eu/d/services/gac/verif/aer/nrt/** Aerocom evaluation: **http://aerocom.met.no/cgi-bin/aerocom/surfobs_annualrs.pl?PROJECT=MACC&MODELLIST=MACC-VALreports&** WMO Sand and Dust Storm Warning Advisory and Assessment System (SDS-WAS) model intercomparison and evaluation: **http://sds-was.aemet.es/forecast-products/models**
Satellite data monitoring
Monitoring of satellite data usage in the Reanalysis and Near-Real-Time production: **http://copernicus-atmosphere.eu/d/services/gac/monitor/**

This validation report is accompanied by the "Observations characterization and validation methods" report, Eskes et al. (2016), which describes the observations used in the comparisons, and the validation methodology. This report can also be found on the global validation page, http://atmosphere.copernicus.eu/user-support/validation/verification-global-services.

2. System summary and model background information

The specifics of the different CAMS model versions are given (section 2.1) with a focus on the model changes (section 2.2). An overview of products derived from this system is given in section 2.3. Several external products used for validation and intercomparison are listed in section 2.4. Timeliness and availability of the CAMS products is given in section 2.5.

2.1 System based on the ECMWF IFS model

Key model information is given on the CAMS data-assimilation and forecast run o-suite and its control experiment, used to assess the sensitivity to assimilation. The forecast products are listed in Table 2.1. Table 2.2 provides information on the satellite data used in the o-suite. Further details on the different model runs and their data usage can be found at http://atmosphere.copernicus.eu/documentation-global-systems.
Information on older experiment types, including MACC_fcnrt_MOZ and MACC_CIFS_TM5 can be found in older Validation reports available from http://www.gmes-atmosphere.eu/services/aqac/global_verification/validation_reports/.

2.1.1 o-suite

The o-suite consists of the C-IFS-CB05 chemistry combined with the CAMS bulk aerosol model. The chemistry is described in Flemming et al. (2015), aerosol is described ub Morcrette et al. (2009). The forecast length is 120 h. The o-suite data is stored under expver '0001' of class 'MC'. On 21 June 2016 the model resolution has seen an upgrade from T255 to T511, and forecasts are produced twice per day. Here a summary of the main specifications of this version of the o-suite is given. We note that on 24 January 2017 the system has been upgraded to cy43r1, but the present report is evaluating the period up to 1 December 2016.

- The meteorological model is based on IFS version cy41r1_CAMS, see also http://www.ecmwf.int/en/forecasts/documentation-and-support/changes-ecmwf-model/cy41r1-summary-changes; the model resolution is T511L60.
- The modified CB05 tropospheric chemistry is used (Williams et al., 2013), originally taken from the TM5 chemistry transport model (Huijnen et al., 2010)
- Stratospheric ozone during the forecast is computed from the Cariolle scheme (Cariolle and Teyssèdre, 2007) as already available in IFS, while stratospheric NOx is constrained through a climatological ratio of HNO_3/O_3 at 10 hPa.
- Monthly mean dry deposition velocities are based on the SUMO model provided by the MOCAGE team.
- Data assimilation is described in Inness et al. (2015) and Benedetti et al. (2009) for chemical trace gases and aerosol, respectively. Satellite data assimilated is listed in Table 2.2 and Fig. 2.1.
- Anthropogenic and biogenic emissions are based on MACCity (Granier et al., 2011) and a climatology of the MEGAN-MACC emission inventories (Sindelarova et al., 2014)
- NRT fire emissions are taken from GFASv1.2 (Kaiser et al. 2012).

Table 2.1: Overview of model runs assessed in this validation report.

Forecast system	Exp. ID	Brief description	Status
o-suite	0001	Operational CAMS DA/FC run	20160621-20170124 (0067) 20150903-20160620 (g9rr) 20140918-20150902 (g4e2)
Control	gjjh geuh g4o2	control FC run without DA	20160621-20170124 (gjjh) 20150901-20160620 (geuh) 20140701-20150902 (g4o2)
GHG run	gf39 ghqy	High resolution, NRT CO_2 and CH_4 runs without DA	20150101-20160229 (gf39) 20160301-present (ghqy)

Table 2.2: Satellite retrievals of reactive gases and aerosol optical depth that are actively assimilated in the o-suite.

Instrument	Satellite	Provider	Version	Type	Status
MLS	AURA	NASA	V3.4	O3 Profiles	20130107 -
OMI	AURA	NASA	V883	O3 Total column	20090901 -
GOME-2A	Metop-A	Eumetsat	GDP 4.7	O3 Total column	20131007 -
GOME-2B	Metop-B	Eumetsat	GDP 4.7	O3 Total column	20140512 -
SBUV-2	NOAA	NOAA	V8	O3 21 layer profiles	20121007 -
IASI	MetOp-A	LATMOS/ULB	-	CO Total column	20090901 -
IASI	MetOp-B	LATMOS/ULB	-	CO Total column	20140918 -
MOPITT	TERRA	NCAR	V5-TIR	CO Total column	20130129-
OMI	AURA	KNMI	DOMINO V2.0	NO2 Tropospheric column	20120705 -
OMI	AURA	NASA	v003	SO2 Tropospheric column	20120705-20150901
GOME-2A/2B	METOP A/B	Eumetsat	GDP 4.7	SO2 Tropospheric column	20150902-
MODIS	AQUA / TERRA	NASA	Col. 5 Deep Blue	Aerosol total optical depth, fire radiative power	20090901 - 20150902 -

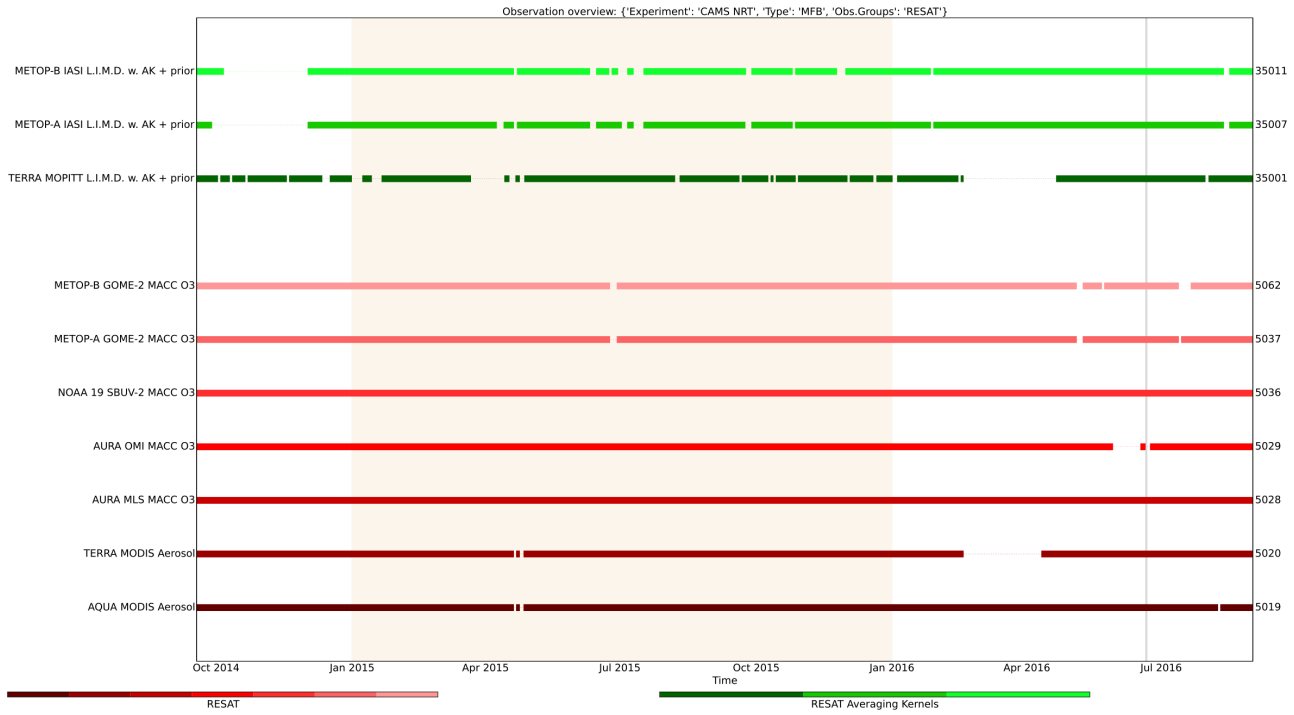

Figure 2.1: Satellite observation usage in the real-time analysis, from Oct. 2014 onwards. CO: Top three rows; O_3 columns and profiles: rows 4-8; Aerosol Optical Depth: rows 9-10. Figure will be updated

The aerosol model includes 12 prognostic variables, which are 3 bins for sea salt and desert dust, hydrophobic and hydrophilic organic matter and black carbon, sulphate aerosols and its precursor trace gas SO_2 (Morcrette et al., 2009). Aerosol total mass is constrained by the assimilation of MODIS AOD (Benedetti et al. 2009). A variational bias correction for the MODIS AOD is in place based on the approach used also elsewhere in the IFS (Dee and Uppala, 2009).

A brief history of updates of the o-suite is given in Table 2.4, and is documented in earlier MACC-VAL reports:
http://www.gmes-atmosphere.eu/services/aqac/global_verification/validation_reports/

2.1.2 Control

The control run (expver=gjjh/geuh/g4o2) applies the same settings as the respective o-suites, based on the coupled C-IFS-CB05 system with CAMS aerosol for cy41r1/cy40r2, except that data assimilation is not switched on. The only two exceptions with regard to this setup are:

- at the start of every forecast the ECMWF operational system is used to initialise *stratospheric* ozone, considering that stratospheric ozone, as well as other stratospheric species are not a useful product of this run. As a consequence, the behavior of this control run will not be discussed in the stratospheric contribution of this report. The reason for doing so is that this ensures reasonable stratospheric ozone as boundary conditions necessary for the tropospheric chemistry.
- The full meteorology in the control run is also initialized from the ECMWF operational NWP analyses. Note that this is different from the o-suite, which uses its own data assimilation setup for meteorology. This can cause slight differences in meteorological fields between o-suite and control, e.g. as seen in evaluations of upper stratospheric temperatures.

2.1.3 High-resolution CO_2 and CH_4 forecasts

The pre-operational forecasts of CO_2 and CH_4 use an independent setup of the IFS as the osuite, at a resolution of TL1279, i.e. ~16 km horizontal, and with 137 levels. This system runs in NRT, and does not apply data assimilation for the greenhouse gases.

The land vegetation fluxes for CO_2 are modelled on-line by the CTESSEL carbon module (Boussetta et al., 2013). A biogenic flux adjustment scheme is used in order to reduce large-scale biases in the net ecosystem fluxes (Agusti-Panareda, 2015). The anthropogenic fluxes are based on the annual mean EDGARv4.2 inventory using the most recent year available (i.e. 2008) with estimated and climatological trends to extrapolate to the current year. The fire fluxes are from GFAS (Kaiser et al., 2012).

Methane fluxes are prescribed in the IFS using inventory and climatological data sets, consistent with those used as prior information in the CH_4 flux inversions from Bergamaschi et al. (2009). The anthropogenic fluxes are from the EDGAR 4.2 database (Janssens-Maenhout et al, 2012) valid for the year 2008. The biomass burning emissions are from GFAS v1.2 (Kaiser et al., 2012).

The high resolution forecast experiments analyzed in this report correspond to two experiments:

- "gf39" from Jan 2015 to Feb 2016. This run was set up to replace run gcbt, which had a bug in the code resulting in spikes in concentration fields.
- "ghqy" from March 2016 to present. The initial conditions used in ghqy on 1st of March 2016 are from the GHG analysis (experiment gg5m). Furthermore, the meteorological analysis used to initialize the ghqy forecast changed resolution and model grid in March 2016.

The high-resolution model run also include a linear CO scheme (Massart et al., 2015), which is also briefly assessed in this report.

2.2 Evolution of the IFS-based system

A list with o-suite system changes are given in Table 2.3. A full list with all changes concerning the assimilation system can be found at http://atmosphere.copernicus.eu/user-support/operational-info/global-system-changes. The CAMS o-suite system is upgraded regularly, following updates to the ECMWF meteorological model as well as CAMS-specific updates such as changes in chemical data assimilation. These changes are documented in e-suite validation reports, as can be found from the link above. Essential model upgrades are also documented in Table 2.4.

Table 2.3: Recent changes in the CAMS o-suite setup.

Date	Change
2015.03.23-2014.04.14	Temporarily no assimilation of MOPITT CO
2015.04.15	Only allow OMI - SO2 assimilation for rows 1-20.
2015.09.03	Update of o-suite to CY41R1 C-IFS-CB05 with experiment id g9rr
2016.02.18-2016.04.21	Terra satellite went into safe mode, implying no data available for MODIS (until 2016.04.11) and MOPITT (until 2016.04.21).
2016.02.26-2016.03.01	Problem with GFAS fire emissions due to TERRA MODIS coming back on with inaccurate data, mostly pronounced on CO and aerosol over western United States.
2016.05.30-2016.06.16	Missing NO2 and O3 data from OMI, due to temporary problems with OMI instrument.

Table 2.4: Long-term o-suite system updates.

Date	o-suite update
2009.08.01	Start of first NRT experiment f7kn with coupled MOZART chemistry, without aerosol. Also without data assimilation.
2009.09.01	Start of first MACC NRT experiment f93i, based on meteo cy36r1, MOZART v3.0 chemistry, MACC aerosol model, RETRO/REAS and GFEDv2 climatological emissions, T159L60 (IFS) and 1.875°×1.875° (MOZART) resolution.
2012.07.05	Update to experiment fnyp: based on meteo cy37r3, MOZART v3.5 chemistry, where changes mostly affect the stratosphere, MACCity (gas-phase), GFASv1 emissions (gas phase and aerosol), T255L60 (IFS) and 1.125°×1.125° (MOZART) resolution. Rebalancing aerosol model, affecting dust.
2013.10.07	Update of experiment fnyp from e-suite experiment fwu0: based on meteo cy38r2, no changes to chemistry, but significant rebalancing aerosol model. Assimilation of 21 layer SBUV/2 ozone product
2014.02.24	Update of experiment fnyp from e-suite experiment fzpr: based on meteo cy40r1. No significant changes to chemistry and aerosol models.
2014.09.18	Update to experiment g4e2: based on meteo cy40r2. In this model version C-IFS-CB05 is introduced to model atmospheric chemistry.
2015.09.03	Update to experiment g9rr: based on meteo cy41r1.
2016.06.21	Update to experiment 0067: based on meteo cy41r1, but a resolution increase from T255 to T511, and two production runs per day
2017.01.24	Update to cycle cy43r1, T511L60

2.3 Other systems

2.3.1 BASCOE

The NRT analyses and forecasts of ozone and related species for the stratosphere, as delivered by the Belgian Assimilation System for Chemical ObsErvations (BASCOE) of BIRA-IASB (Lefever et al., 2014; Errera et al., 2008), are used as an independent model evaluation of the CAMS products. The NRT BASCOE product is the ozone analysis of Aura/MLS-SCI level 2 standard products, run in the following configuration (version 05.07):

- The following species are assimilated: O_3, H_2O, HNO_3, HCl, HOCl, N_2O and ClO.
- It lags by typically 4 days, due to latency time of 4 days for arrival of non-ozone data from Aura/MLS-SCI (i.e. the scientific offline Aura/MLS dataset).
- Global horizontal grid with a 3.75° longitude by 2.5° latitude resolution.
- Vertical grid is hybrid-pressure and consists in 86 levels extending from 0.01 hPa to the surface.
- Winds, temperature and surface pressure are interpolated in the ECMWF operational 6-hourly analyses.
- Time steps of 20 minutes, output every 3 hours

See the stratospheric ozone service at http://www.copernicus-stratosphere.eu/.
It delivers graphical products dedicated to stratospheric composition and allows easy comparison between the results of o-suite, BASCOE and TM3DAM. The BASCOE data products (HDF4 files) are also distributed from this webpage. Other details and bibliographic references on BASCOE can be found at http://bascoe.oma.be/. A detailed change log for BASCOE can be found at http://www.copernicus-stratosphere.eu/4_NRT_products/3_Models_changelogs/BASCOE.php.

2.3.2 TM3DAM and the multi-sensor reanalysis

One of the MACC products was a 30-year reanalysis, near-real time analysis and 10-day forecast of ozone column amounts performed with the KNMI TM3DAM data assimilation system, the Multi-Sensor Reanalysis (MSR) system (van der A et al., 2010, 2013),
http://www.temis.nl/macc/index.php?link=o3_msr_intro.html.
The corresponding validation report can be found at
http://www.copernicus-atmosphere.eu/services/gac/global_verification/validation_reports/.

The NRT TM3DAM product used for the validation of the CAMS NRT streams is the ozone analysis of Envisat/SCIAMACHY (until April 2012), AURA/OMI, and MetOp-A/GOME-2, run in the following configuration:

- total O_3 columns are assimilated
- Global horizontal grid with a 3° longitude by 2° latitude resolution.
- Vertical grid is hybrid-pressure and consists in 44 levels extending from 0.1 hPa to 100 hPa.
- Dynamical fields from ECMWF operational 6-hourly analysis.

An update of the MSR (MSR-2) was presented in van der A et al. (2015), which extended the record to 43 years based on ERA-interim reanalysis meteo and with an improved resolution of 1x1 degree.

2.3.3 SDS-WAS multimodel ensemble

The World Meteorological Organization's Sand and Dust Storm Warning Advisory and Assessment System (WMO SDS-WAS) for Northern Africa, Middle East and Europe (NAMEE) Regional Center (http://sds-was.aemet.es/) has established a protocol to routinely exchange products from dust forecast models as the basis for both near-real-time and delayed common model evaluation. Currently, nine (BSC-DREAM8b, MACC-ECMWF, DREAM-NMME-MACC, NMMB/BSC-Dust, NASE GEOS-5, NCEP NGAC, EMA_RegCM, DREAMABOL and NOA) provides daily operational dust forecasts (i.e. dust optical depth, DOD, and dust surface concentration).

Different multi-model products are generated from the different prediction models. Two products describing centrality (multi-model median and mean) and two products describing spread (standard deviation and range of variation) are daily computed. In order to generate them, the model outputs are bi-linearly interpolated to a common grid mesh of 0.5º x 0.5º. The multimodel DOD (at 550 nm) Median from nine dust prediction models participating in the SDS-WAS Regional Center is used for the validation of the CAMS NRT streams.

2.4 CAMS products

An extended list of output products from the NRT stream o-suite are available as 3-hourly instantaneous values up to five forecast days. These are available from ECMWF (through ftp in grib2 and netcdf format, http://atmosphere.copernicus.eu/global-near-real-time-data-access).

2.5 Availability and timing of CAMS products (will be updated)

Table 2.6: Timeliness of the o-suite from March 2013 – to February 2016

Months	On time, 22 utc	80th perc	90th perc	95th perc
March-May 2013	97%	D+0, 17:54	D+0, 18:36	D+0, 18:49
June-August 2013	97%	D+0, 18:34	D+0, 18:46	D+0, 19:23
Sept-Nov 2013	99%	D+0, 19:14	D+0, 19:22	D+0, 19:29
Dec-Feb '13-'14	94%	D+0, 19:45	D+0, 20:40	D+0, 21:55
Mar-May 2014	98%	D+0, 19:44	D+0, 19:57	D+0, 20:03
Jun-Aug 2014	95%	D+0, 20:03	D+0, 20:57	D+0, 22:43
Sept-Nov 2014	96%	D+0, 19:24	D+0, 20:31	D+0, 21:14
Dec-Feb '14-'15	97%	D+0, 19:43	D+0, 20:28	D+0, 21:13
Mar-May 2015	96%	D+0, 19:38	D+0, 21:03	D+0, 21:40
Jun-Aug 2015	95%	D+0, 20:24	D+0, 20:53	D+0, 21:54
Sept-Nov 2015	95%	D+0, 19:44	D+0, 20:55	D+0, 21:51
Dec-Feb '15-'16	100%	D+0, 18:39	D+0, 18:57	D+0, 19:43
Mar-May 2016	98%	D+0, 19:32	D+0, 19:47	D+0, 20:00
Jun-Aug 2016 (00 and 12 cycle)	100%	D+0, 08:53 D+0, 20:55	D+0, 09:04 D+0, 21:01	D+0, 09:18 D+0, 21:18
Sep-Nov 2016	tbd	tbd	tbd	tbd

The availability statistics provided in Table 2.6 are computed for the end of the 5-day forecast run, and are obtained from July 2012 onwards. A forecast is labeled "on time", if everything is archived on MARS before 22UTC. This is based on requirements from the regional models. We note that at present most regional models can still provide their forecasts even if the global forecast is available a bit later.

For the period September-November 2016, 100% of the forecasts were delivered before 22:00.

3. Validation results for reactive gases and aerosol

This section describes the validation results of the CAMS NRT global system (the o-suite) for reactive gases and aerosol up to December 2016. The validation focuses on the results from the NRT analysis (or D+0 FC) stream. For a selection of instances 2-4 day forecasts issued from them have been explicitly considered. Naming and color-coding conventions predominantly follow the scheme as given in Table 3.1.

Table 3.1 Naming and color conventions as adopted in this report.

Name in figs	experiment	Color
{obs name}	{obs}	**black**
o-suite D+0 FC	0001	**red**
Control	geuh, gjjh	**blue**

3.1 Tropospheric Ozone

3.1.1 Validation with sonde data in the free troposphere

Model profiles of the CAMS runs were compared to free tropospheric balloon sonde measurement data of 38 stations taken from the NDACC, WOUDC, NILU and SHADOZ databases for November 2015 to November 2016 (see Fig. 3.1.1 - 3.1.3). Towards the end of the period, the number of available soundings decreases, which implies that the evaluation results may become less representative. The figures contain the number of profiles in each month that are available for the evaluation. The methodology for model comparison against the observations is described in Annex 2 in CAMS VAL report #1. The free troposphere is defined as the altitude range between 750 and 200 hPa in the tropics and between 750 and 300 hPa elsewhere.

In all zonal bands MNMBs for the o-suite are within the range -20 to +30%, for all months, see Fig. 3.1.1-3.1.3. The control run shows larger negative MNMBs for Antarctica (up to -38%). Over the Arctic, the o-suite mostly shows slightly positive MNMBs during summer and spring (MNMBs up to 6%), while during the winter season the MNMBs get negative (within -13%) see, Fig. 3.1.1. The o-suite mostly shows lower MNMBs than the control run during the last six months. Over the NH mid-latitudes MNMBs for the o-suite are on average close to zero all year round (maxima are -10% to +3%), which is a clear improvement compared to the control run, which shows larger MNMBs (up to ±13%) during the respective period. MNMBs for the o-suite are generally larger (up to 30%) over Antarctica, where tropospheric O_3 values are comparatively lower than over the polluted NH. For the Tropics, MNMBs are between ±20% for the o-suite and the control run.

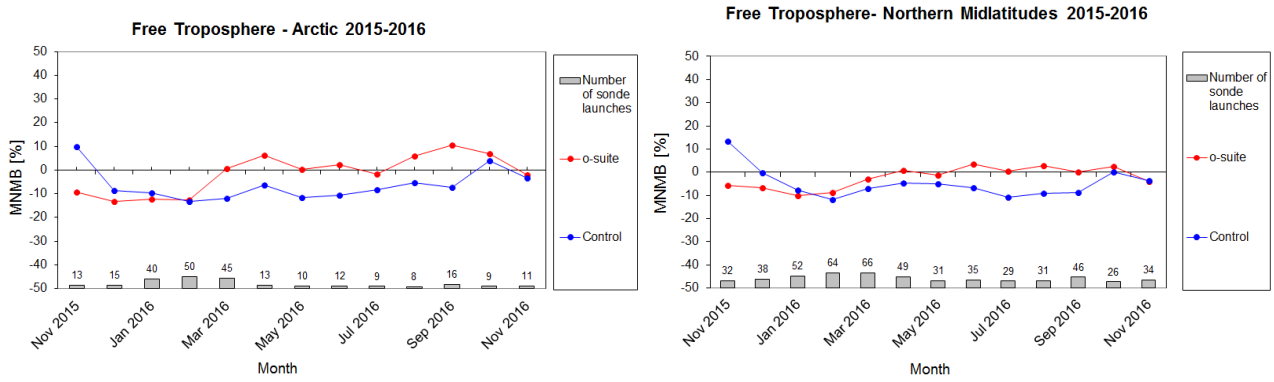

Figure 3.1.1: MNMBs (%) of ozone in the free troposphere (between 750 and 300 hPa) from the IFS model runs against aggregated sonde data over the Arctic (left) and the Northern mid latitudes (right). The numbers indicate the amount of individual number of sondes.

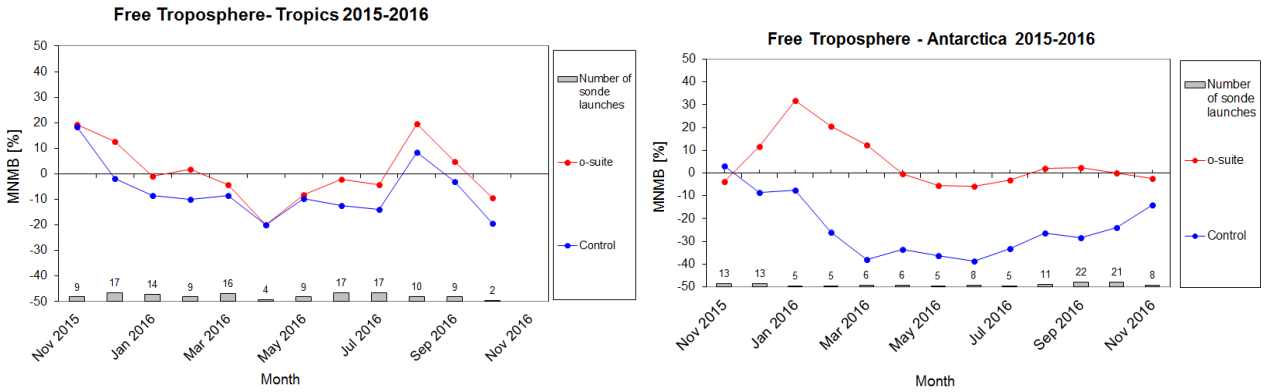

Figure 3.1.2: MNMBs (%) of ozone in the free troposphere (between 750 and 200 hPa (Tropics) / 300 hPa) from the IFS model runs against aggregated sonde data over the Tropics (left) and Antarctica (right). The numbers indicate the amount of individual number of sondes.

3.1.2 Ozone validation with IAGOS data

The daily profiles of ozone measured at airports around the world, are shown on the website at http://www.iagos.fr/macc/nrt_day_profiles.php. For the period from September 2016 to November 2016, the data displayed on the web pages and in this report include only the data as validated by the instrument PI. The available flights and available airports are shown in Figure 3.1.3 top and bottom respectively. Performance indicators have been calculated for different parts of the IAGOS operations.

A new aircraft was equipped during the summer, taking the fleet to 7. However since one aircraft has not been providing data for some time, we will consider the fleet to remain at 6. With the 6 aircraft, operating fully over the three month period, we can expect a total of about 1260 flights. The actual number of flights within the period was 985 (1970 profiles) giving a performance of 78%. The actual number of flights with usable data was 600 (60% of the total possible). These flights are shown in Figure 3.1.3 (top). Fifty percent (63%) (1242 profiles) of the operational flights had usable measurements of ozone and 54% of flights had usable CO. Delivering these O_3 and CO data are two aircraft from China Airlines based in Taipei, an aircraft operated by Air France based in Paris and

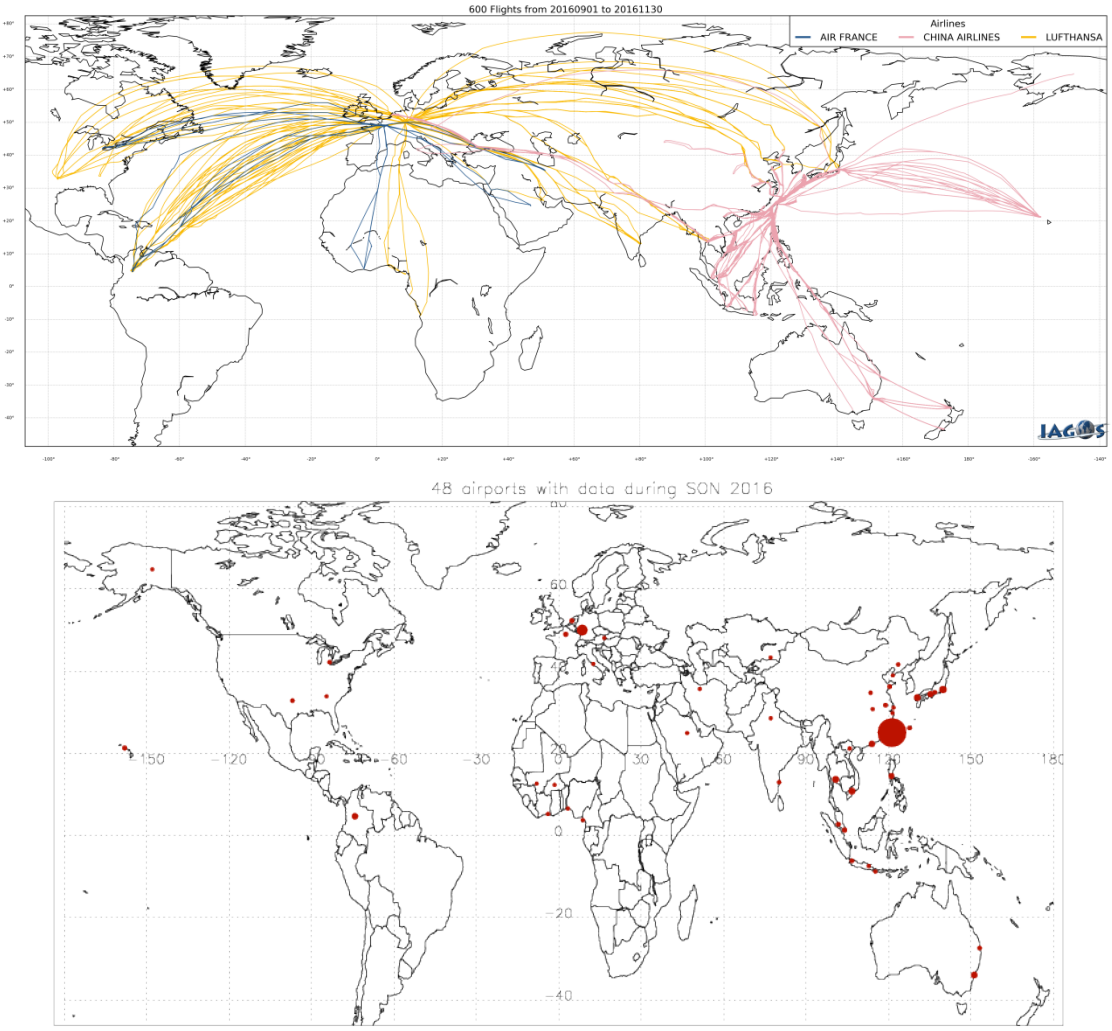

Figure 3.1.3: Map of the flights (top) and the visited airports (bottom) during the period SON 2016, by the IAGOS-equipped aircraft. The size of the plotting circle represents the number of profiles available.

two aircraft operated by Lufthansa based in Frankfurt. This report therefore displays profiles recorded by these aircraft, covering mainly the routes served by Air France to North America and West Africa and by China Airlines across South-East Asia as shown on the map in Figure 3.1.3 (with a plotting circle scaled to the highest number of flights at an airport). Data are also available in Australia and in New Zealand.

Europe

Figure 3.1.4 presents ozone at Frankfurt during September-November 2016. Ozone remains relatively elevated throughout September compared with the long term average from IAGOS. The period around September 12th saw ozone levels reach 80ppbv in the surface layer over several days. These high amounts are almost double the mean value of 40ppbv calculated from 10 years of measurements, and exceed 3-sigma from the 10-year mean (Fig. 3.1.5). At the same time surface temperatures were also about 10 degrees higher than the 10-year mean. Ozone was underestimated during this period, but otherwise for the rest of the season, the osuite does fairly well at capturing the ozone concentrations in the surface and boundary layer.

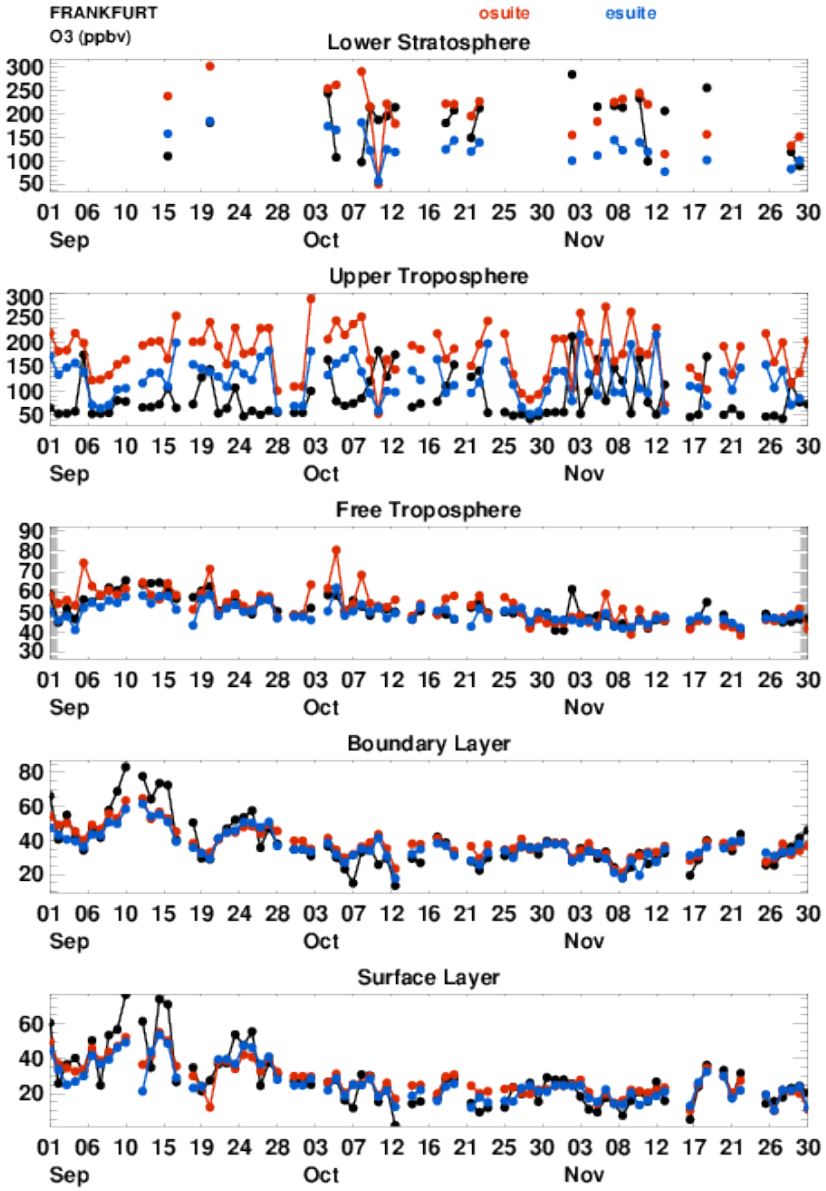

Figure 3.1.4: Time series of daily mean ozone over Frankfurt (left) and PAris (right) during September, October, November 2016 for 5 layers, Surface, Boundary layer, Free Troposphere, Upper Troposphere and Lower Stratosphere.

The depth of the ozone anomaly is evident in the vertical profiles shown in Fig. 3.1.6 on September 14th and 15th. The ozone is at elevated levels at altitudes from the surface up to 2000m. On September 17th the ozone drops back below 50ppbv in the surface and boundary layers as shown at Paris and Frankfurt and also for Amsterdam on 18th September. These three profiles also show that the control run does better than the osuite in the UTLS.

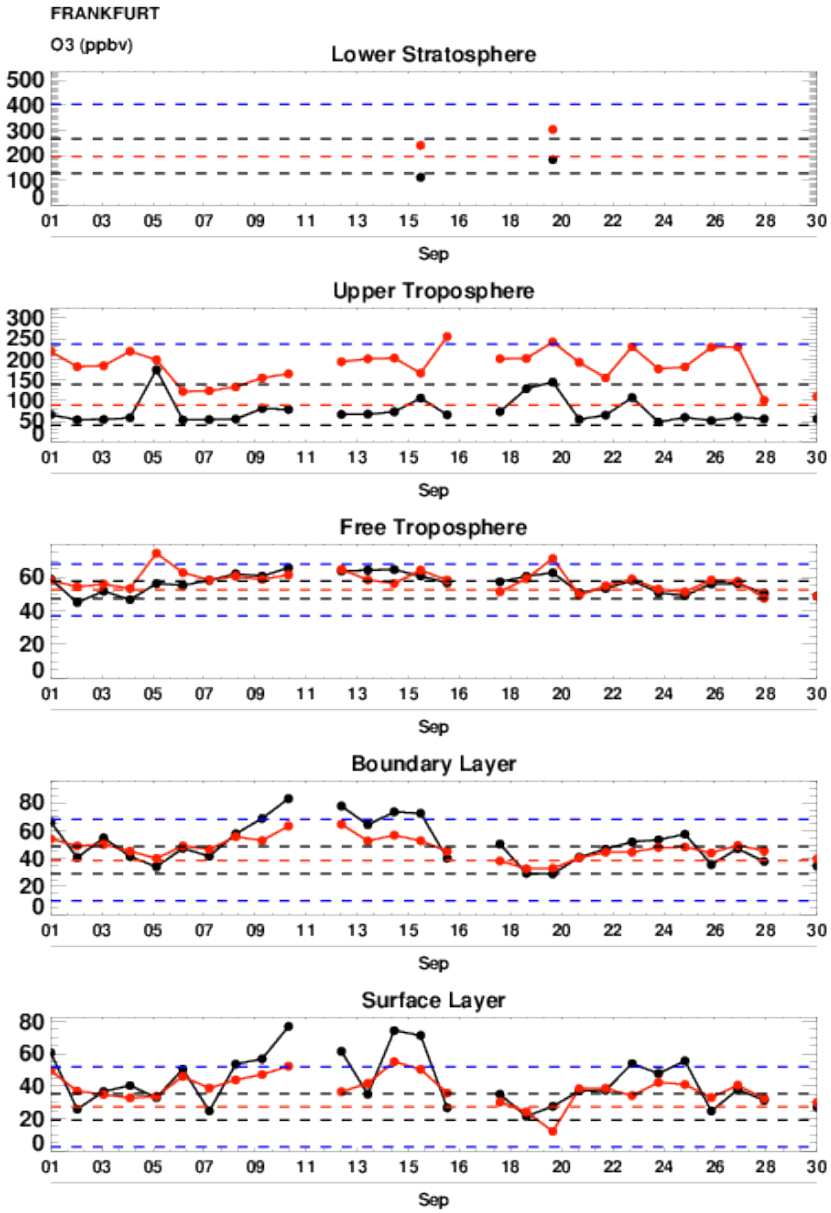

Figure 3.1.5: Time series for July 2016 of IAGOS observations (Black) and osuite (red) along with the mean Ozone calculated from 10 years of MOZAIC data (2002-2012) (red dashed line) and the standard deviation (black dashed line) and the three sigma line (blue dashed).

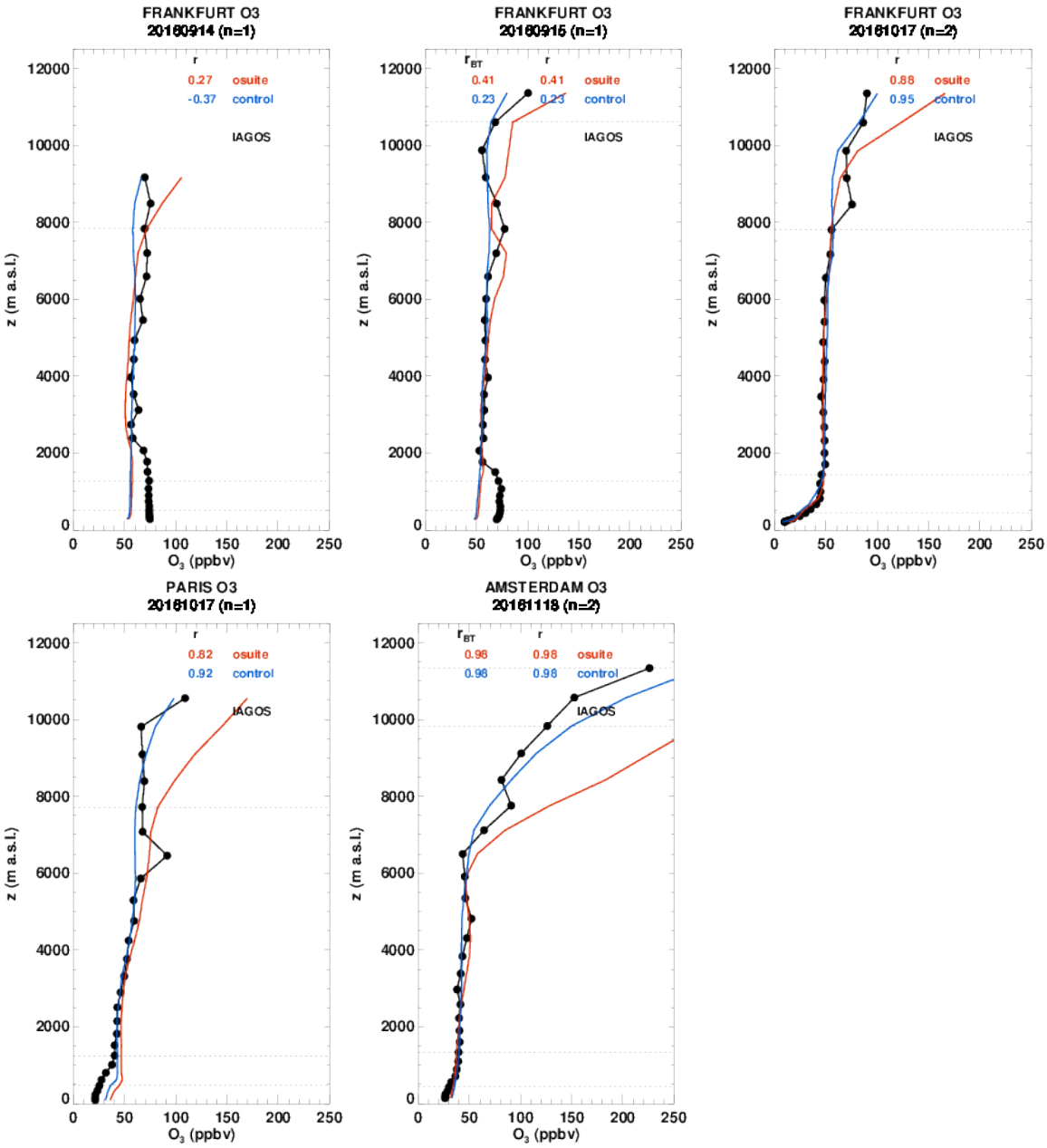

Figure 3.1.6: Selection of daily profiles of ozone from IAGOS (black) and the o-suite (red) and control (blue) over Europe (Paris, Frankfurt, Amsterdam) over the period SON 2016.

Asia

In contrast to the behaviour at Frankfurt, ozone is generally overestimated in the boundary and free troposphere (Fig. 3.1.7). The upper troposphere is markedly better represented over Taipei compared with over Frankfurt. This may be related to the more consistent height of the tropopause in the tropical region (Taipei, 25N) compared with a variable Ex-UTLS mixing zone seen at airports over Europe (Frankfurt, 50N). The period SON is dominated by Typhoons and tropical storms, which often result in the cleansing of the lower troposphere with air from the tropical Pacific Ocean.

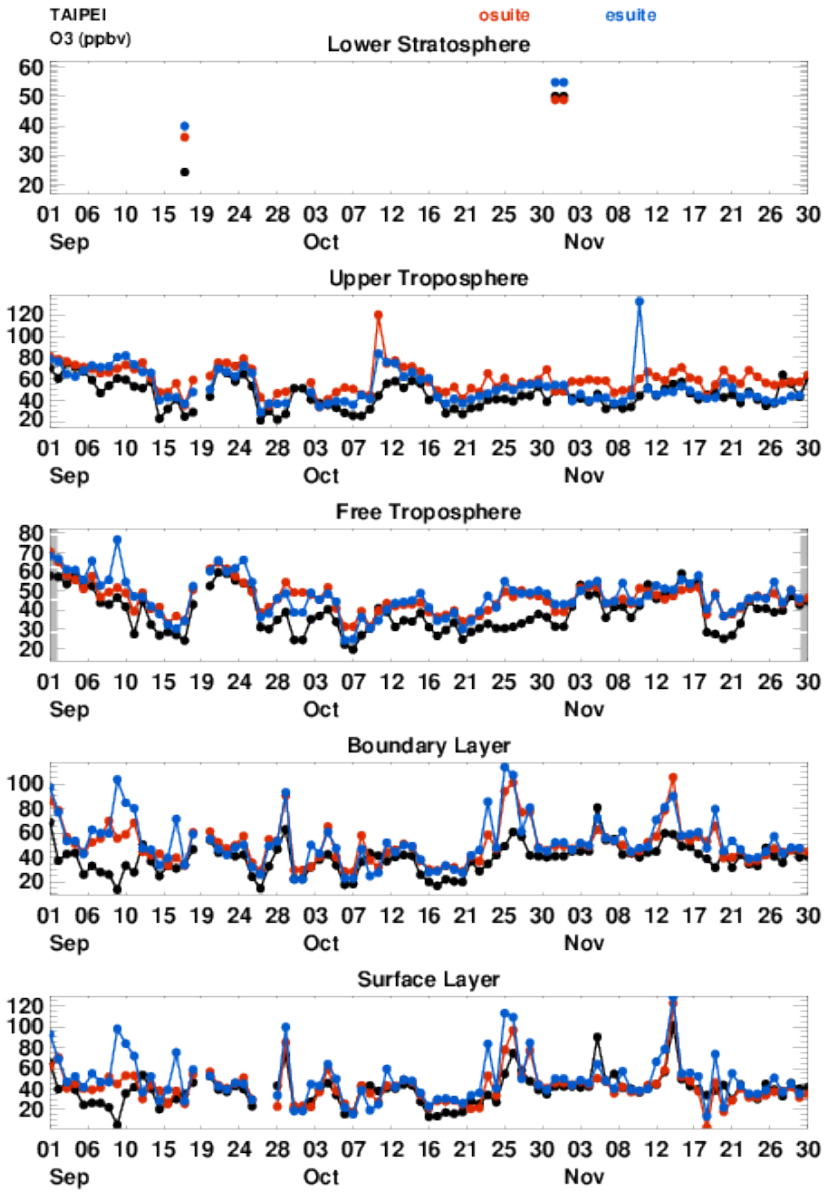

Figure 3.1.7: Time series of daily mean ozone over Taipei during JJA 2016 for 4 layers, Surface, Boundary layer, Free Troposphere, Upper Troposphere.

Typhoons Meranti, Megi and Malakas

In the JJA period we reported on the effect of typhoon Nida and Nepartak on the profiles observed at Taipei. In the SON period, three Typhoons passed close to Taiwan. Typhoon Meranti passed just to the south of Taiwan on 14th September 2016, Malakas passed to the east of Taipei on 17th September and Megi made landfall on Taiwan on 26th September 2016. Megi followed an oceanic track and in similarity with Nepartak (8th July), reduced the mixing ratios of ozone seen below 4000m to about 15ppbv and the CO to less than 80ppbv (figure 3.3.7) consistent with the arrival of clean maritime air from the tropical Pacific Ocean. Typhoon Meranti passed further from Taipei but

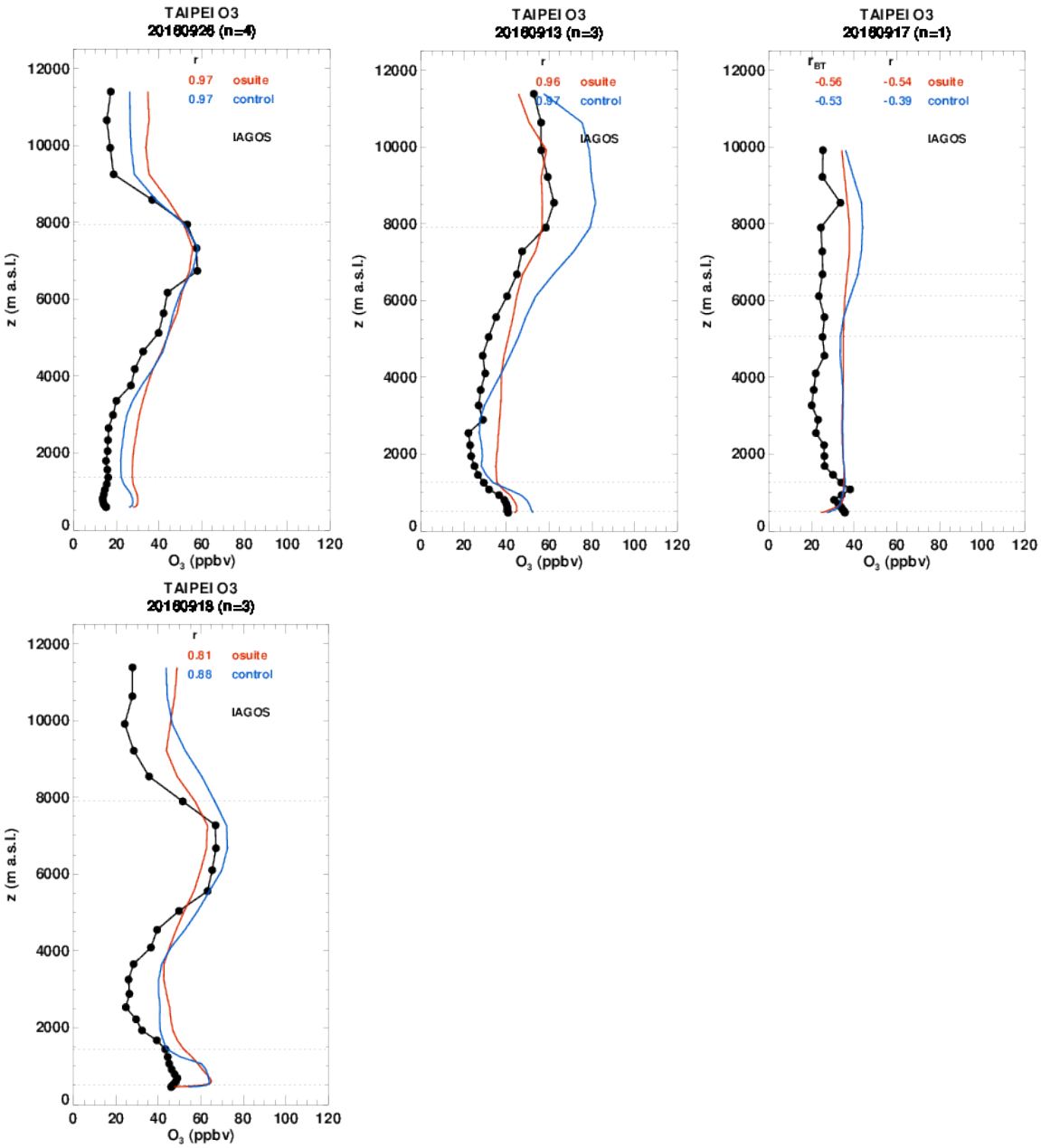

Figure 3.1.8: Profiles at Taipei during the passage of Typhoon Megi (top left) and Meranti (top middle) and Malakas (top right and bottom left).

ozone mixing ratios were reduced to about 25ppbv at altitudes around 2000m. Malakas passed to the east of Taipei on September 17 (profile shown for September 17 and 18 fig. 3.1.7 right) before heading to Japan to make landfall. Mixing ratios of ozone were similarly reduced to about 25ppbv. In all cases the osuite and control overestimate the amount of ozone in the lower troposphere, boundary layer and surface layer, whilst being better in the mid-troposphere.

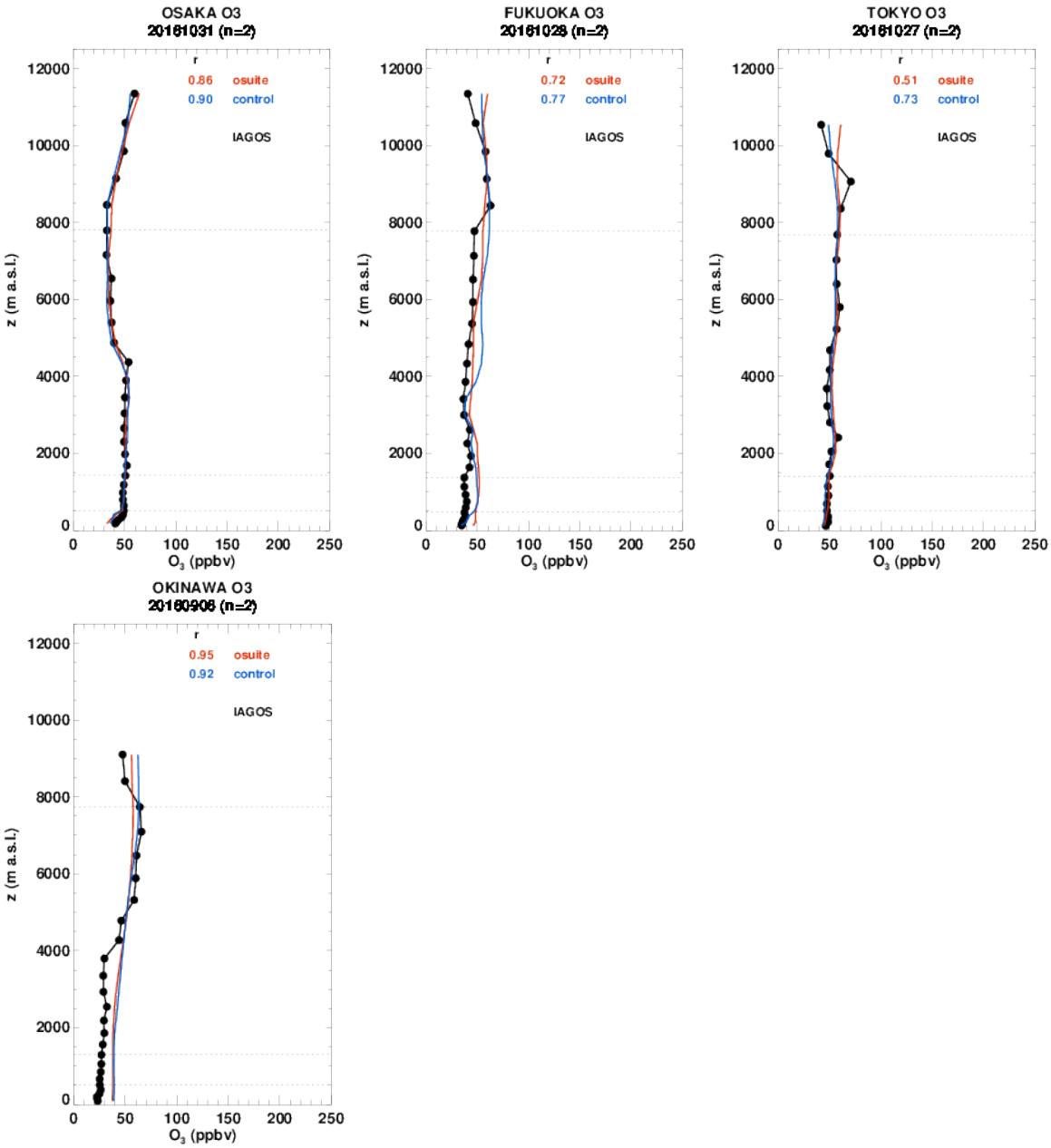

Figure 3.1.9: Profiles of ozone from IAGOS (black) and the two NRT runs over Japan.

Japan

Generally the models do very well at capturing ozone over many towns in Japan. The profile at Okinawa shows evidence of the tropical storm Malou with low mixing ratios in the lower troposphere increasing above 4000m.

Australasia

The new China Airlines aircraft has been providing profiles in Auckland (36°S, 174°E) New Zealand since August 2016. In New Zealand, we would expect the concentrations of ozone to be the closest to background concentrations due to the low population density, its remoteness from other

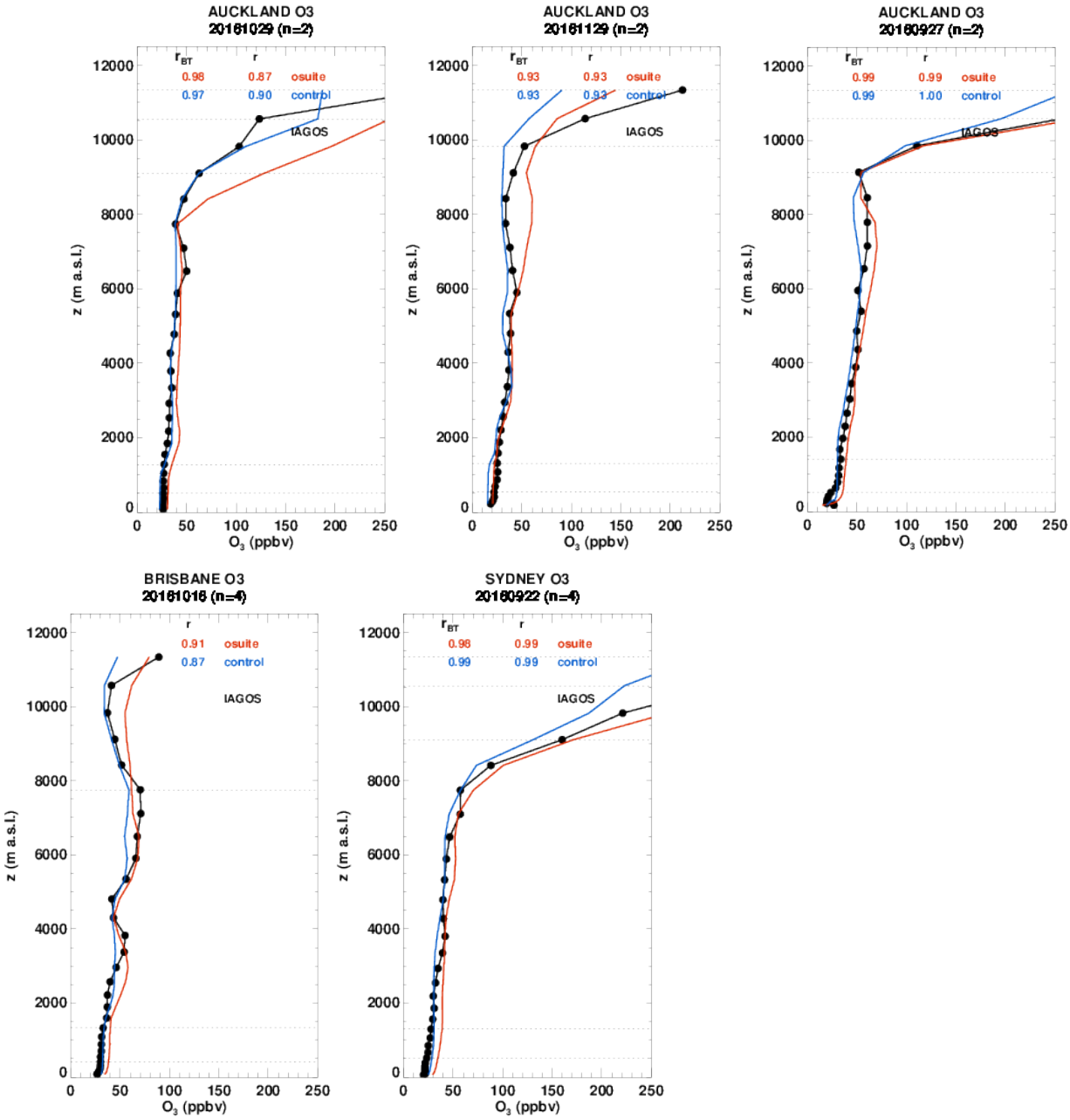

Figure 3.1.10: Profiles of ozone from IAGOS (black) and the two NRT runs over New Zealand and Australia.

continents, and the arrival of clean maritime air from the Tasman Sea and the Pacific Ocean. Figure 3.1.10 shows profiles from Auckland and also from Australia at Brisbane and Sydney. The profiles show that the models do well at capturing the profile of ozone until the UTLS region. In the UTLS, the gradients are more difficult to capture. The osuite is generally predicts a sharper gradient and a lower tropopause compared with the control. Thus, at times when the gradient is steep, it is the osuite that performs better than the control (e.g. Auckland:20160927, Sydney:20160922).

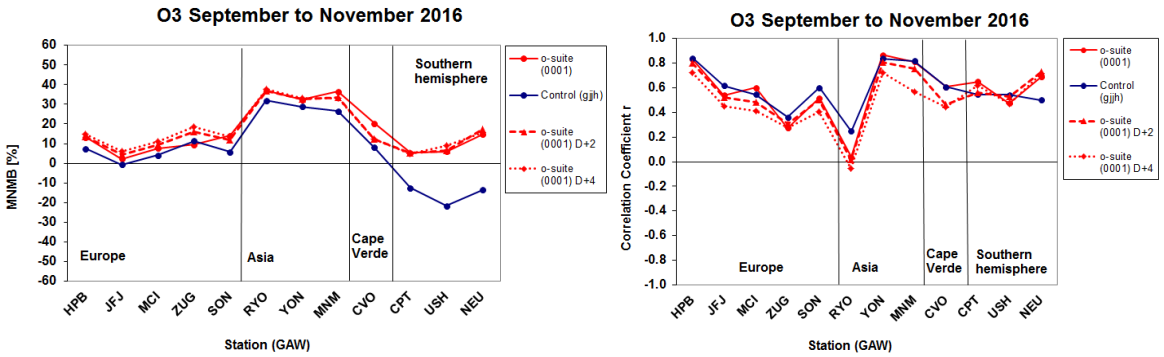

Figure 3.1.11: Modified normalized mean bias in % (left) and correlation coefficient (bottom right) of the NRT model runs compared to observational GAW data in the period March to May 2016. Circles correspond to D+0, triangles to D+2 and rhombs to D+4 metrics respectively.

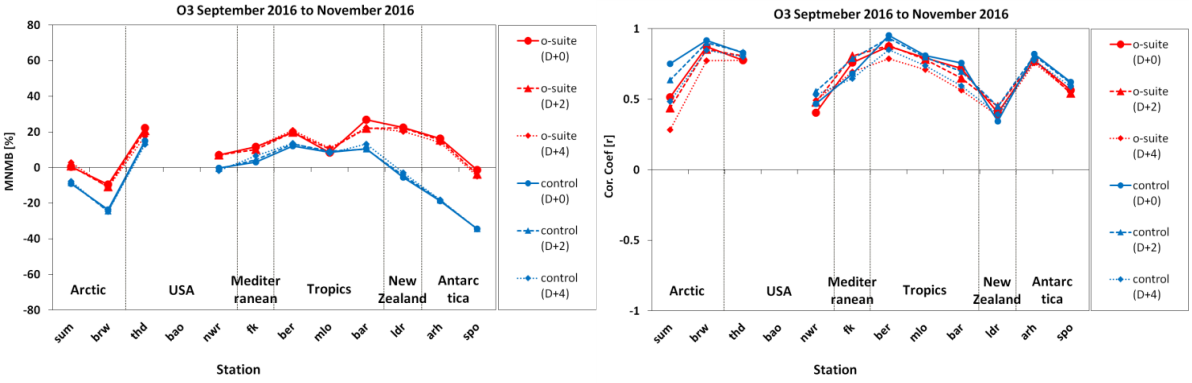

Figure 3.1.12: Modified normalized mean bias in % (left) and correlation coefficient (right) of the NRT forecast runs compared to observational ESRL data in the period September to November 2016. Circles correspond to D+0, triangles to D+2 and rhombs to D+4 metrics respectively.

3.1.3 Validation with GAW and ESRL-GMD surface observations

For the Near Real Time (NRT) validation, 13 GAW stations and 11 ESRL stations are currently delivering O_3 surface concentrations in NRT, and the data are compared to model results. In the following, a seasonal evaluation of model performance for the 2 NRT runs (o-suite and control) has been carried out for the period from September to November 2016. The latest validation results based on GAW stations can be found on the CAMS website, http://www.copernicus-atmosphere.eu/d/services/gac/verif/grg/gaw/, and based on ESRL on http://www.academyofathens.gr/kefak/cams/index.html.
Results are summarized in Figs 3.1.11 and 3.1.13.

Modified normalized mean biases in % (left, panel) and correlation coefficients (right, panel) for different forecasts days (D+2, triangles and D+4, rhombs) with respect to GAW observations are shown in Fig. 3.1.11 (left). It indicates that MNMBs for both o-suite and control run remain stable till the D+4 (forecast run from 96h to 120h). Similar results concerning MNMBs stability are found for ESRL observations (Fig. 3.1.12). Correlations between simulated and observed surface ozone values remain almost stable till D+2 (forecast run from 48h to 72h), but then drop (correlations for D+4 are

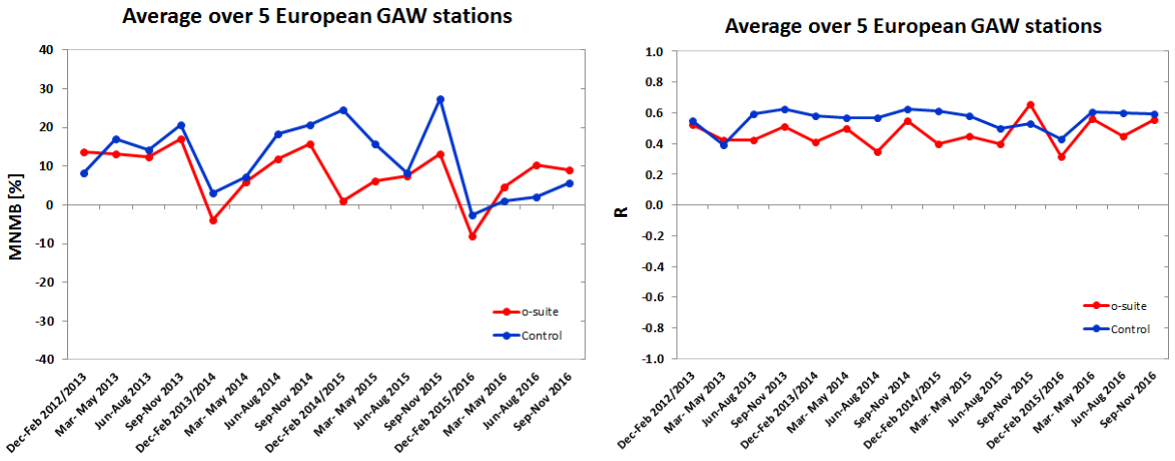

Figure 3.1.13: Long term (Dec. 2012 – Nov. 2016) evolution of seasonal mean MNMB (left) and correlation (right), as averaged over 5 GAW stations in Europe, for o-suite (red) and control (blue).

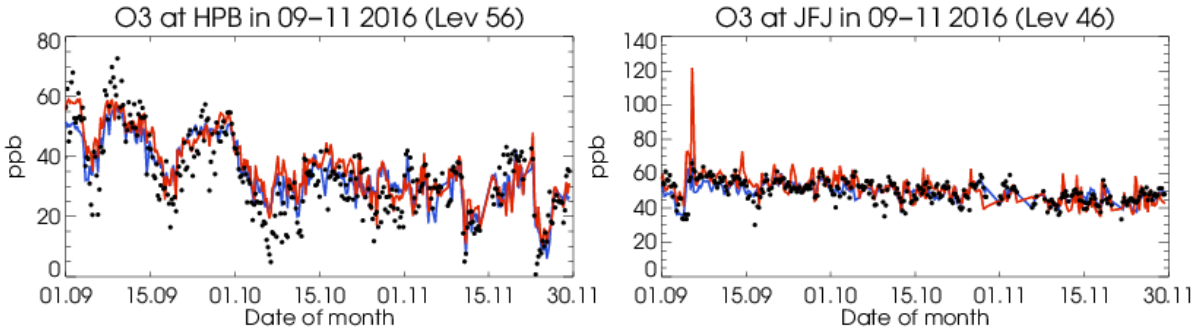

Fig. 3.1.14: Time series for the o-suite (red) and Control (blue) compared to GAW observations at Hohenpeissenberg (44.2°N, 10.7°E) and Jungfraujoch (46.55°N, 7.99°E).

lower than correlations for D+2 and D+0), except for stations in Antarctica and the see Fig. 3.1.11 and 3.1.12, right graph).

A comparison of the seasonal-mean MNMB over Europe (Fig. 3.1.13) from December 2012 to present shows that the MNMB over European GAW stations is minimal during the winter season, and tends to increase in other months. Also on average the MNMB for the o-suite shows a slight improvement over the years, while it remains higher, and more variable for the consecutive control runs. Temporal correlation is consistently better for control than for the o-suite.

Looking at different regions, for European stations (HPB, JFJ, ZUG, SON, MCI), observed O_3 surface mixing ratios are overestimated by the o-suite and the control run, with MNMBs between 2 to 14% for the o-suite and between 1 and 12% for the control run (see also Fig. 3.1.14). Correlations for the European stations are between 0.27 to 0.55 for the o-suite and between 0.36 and 0.83 for the control run. The time series plots show that especially minimum concentrations are partly not resolved by the model, see Fig. 3.1.16.

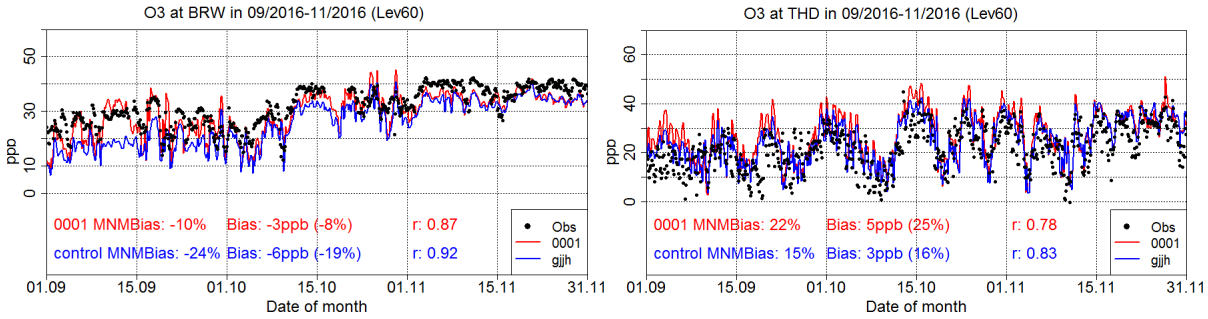

Figure 3.1.15: Time series for the o-suite (red) and control (blue) compared to ESRL observations at Point Barrow, Alaska station (71.32°N, 156.61°W, left) and Trinidad Head, California station (41.05°N, 124.15°W, right).

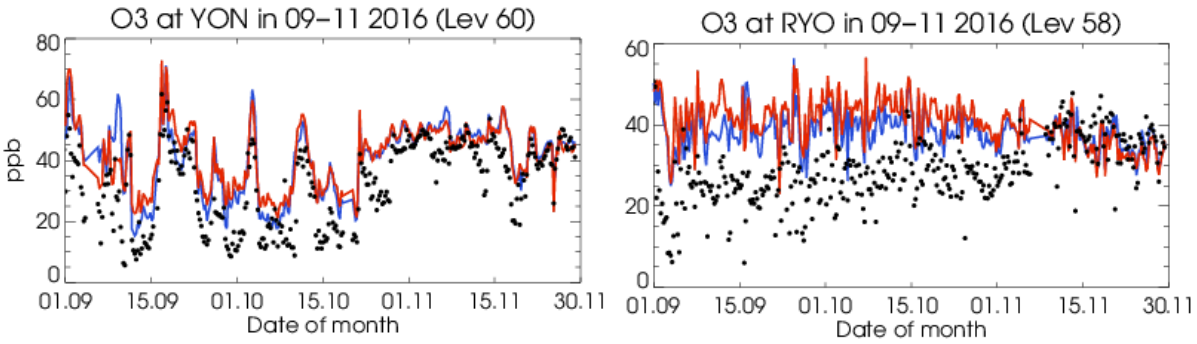

Figure 3.1.16: Time series for the o-suite (red) and Control (blue) compared to GAW observations at Yonaginijima (24.47°N, 123.02°E) and Ryori (39.03°N, 141.8°E)

In the Arctic, the o-suite reproduces well surface ozone mean concentrations over Summit (SUM, MNMBs≈0%) and Point Barrow (BRW, MNMBs≈-8%) while the control run underestimates it by -10% and -25% respectively. The control run's underestimation mostly concerns the peaks in the observations (see also Fig. 3.1.15, left). Correlations between simulated and observed surface ozone for both stations are high for the o-suite (r=0.5 over SUM and 0.85 over BRW) and even higher for the control run (r=0.75 over SUM and 0.9 over BRW).

For USA stations (THD, NWR) both runs overestimate surface ozone mean concentrations at THD (o-suite MNMBs≈20%, control MNMBs≈15%). At NWR the o-suite overestimates surface ozone by 10% while the control run reproduces well surface ozone mean. The control run reproduces slightly better the day to day surface ozone variability (r>0.8 at THD and r≈0.45 at BAO) than the o-suite (r≈0.78 at THD, r≈0.4 at NWR).

For Asian stations (RYO, YON, MNM), both runs overestimate the low observed ozone concentrations with MNMBs of up to 35%. Especially the lower values are overestimated. Concentration peaks are well reproduced, however, as can be seen in Fig. 3.1.16. Both models correlate well with the observations of two stations (YON, MNM) and show no correlation for one station (RYO).

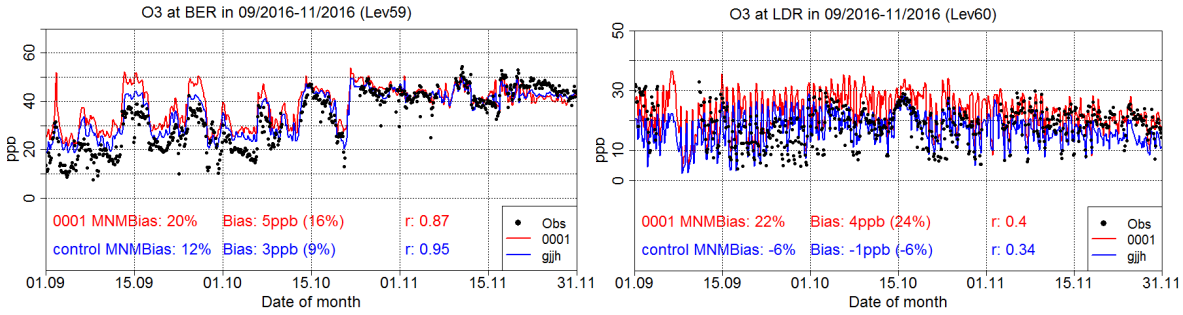

Figure 3.1.17: Time series for the o-suite (red) and control (blue) compared to ESRL observations (black dots) at Bermuda station (32.27°N, 64.88°W) and at Lauder, New Zealand station (45.04°S, 169.68°E).

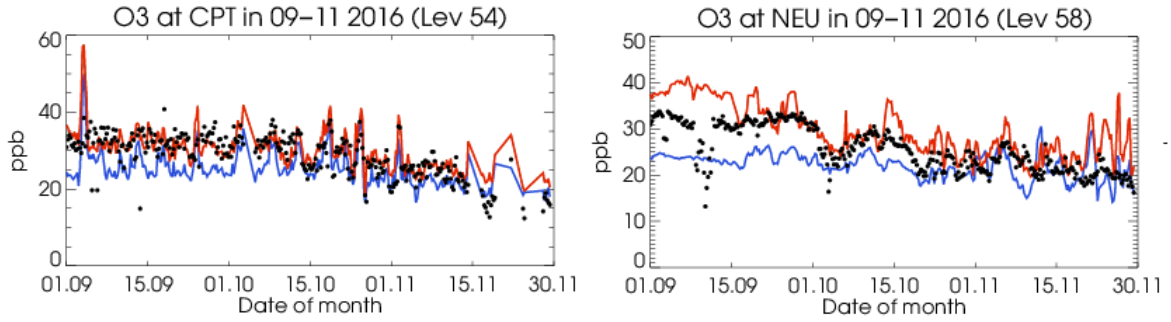

Figure 3.1.18: Time series for the o-suite (red) and control (blue) compared to GAW observations (black dots) at Cape Point (34.35°S, 18.48°E) and GAW observations at Neumayer (70.7°S, 8.3°W).

For the tropical stations (BAR, BER, MLO) both runs overestimate ozone mixing ratios and the o-suite has higher positive offset than the control run (o-suite MNMBs≈20% at BAR and BER and 10% at MLO and control MNMBs≈10% in all 3 stations). Correlations between simulated and observed surface ozone concentrations are high for all stations (r>0.8 at BAR and MLO and r>0.7 at BAR).

For the stations in the Southern Hemisphere (CPT, LDR, USH) the o-suite reproduces ozone mixing ratios well for CPT and USH with MNMBs of 6% and for LDR within 20%. The data assimilation corrects the negative offset in the control run, see Fig. 3.1.17 (right panel) and 3.1.18 (left panel). Correlation coefficients are between 0.4 and 0.7 for the o-suite.

Finally for Antarctic stations (SPO, ARH, NEU) the o-suite reproduces ozone mixing ratios with MNMBs between 15% and 0%, see Fig. 3.1.18 (right panel). The data assimilation corrects the negative offset in the control run (with MNMBs of up to-40%). Correlations between simulated and observed surface ozone over SPO and ARH stations are high for both runs (r>0.65), but for NEU correlations are very low for both runs.

3.1.4 Validation with AirBase observations in Mediterranean

The surface ozone validation analysis over the Mediterranean is based on an evaluation against station observations from the Airbase Network (http://acm.eionet.europa.eu/databases/airbase/). In addition, 3 stations from the Department of Labour Inspection - Ministry of Labour and Social Insurance, of Cyprus (http://www.airquality.dli.mlsi.gov.cy/) as well as the Navarino Environmental

Table 3.1.1: Coordinates, elevation, corresponding model level (level 60 is the surface level), as well as validation scores (MNMBs and correlations for the period SON 2016) obtained with the 2 forecast runs (o-suite and control), for each one of the selected Mediterranean stations. MNMBs and correlations with blue denote stations where control run performs better while with red are denoted stations where o-suite performs better.

						Distance from the	MNMB		Cor. Coef	
Station Name	Stat_ID	Lon	Lat	Alt (m)	Level	shore (km)	o-suite	contro	o-suite	control
Al Cornocales	ES1648A	-5.66	36.23	189	57	16	16.9	13.2	0.72	0.78
Caravaka	ES1882A	-1.87	38.12	1	60	73	-20.7	-24.9	0.61	0.61
Zarra	ES0012R	-1.10	39.08	885	56	70	-6.8	-10.5	0.83	0.84
VIillar Del Arzobispo	ES1671A	-0.83	39.71	430	60	48	-9.1	-12.3	0.78	0.83
Cirat	ES1689A	-0.47	40.05	466	60	37	3.6	-0.8	0.76	0.80
Bujaraloz	ES1400A	-0.15	41.51	327	60	60	-21.0	-23.4	0.74	0.74
Morella	ES1441A	-0.09	40.64	1150	53	51	-0.2	-4.2	0.80	0.84
Bc-La Senia	ES1754A	0.29	40.64	428	59	21	-14.2	-16.4	0.68	0.72
Ay-Gandesa	ES1379A	0.44	41.06	368	58	15	14.8	12.9	0.81	0.82
Ak-Pardines	ES1310A	2.21	42.31	1226	57	81	19.7	14.9	0.24	0.32
Hospital Joan March	ES1827A	2.69	39.68	172	57	3	15.3	13.0	0.57	0.62
Al-Agullana	ES1201A	2.84	42.39	214	60	25	-19.9	-22.7	0.63	0.61
Av-Begur	ES1311A	3.21	41.96	200	56	9	4.3	1.7	0.81	0.85
Plan Aups/Ste Baume	FR03027	5.73	43.34	675	54	21	9.8	4.7	0.72	0.72
Gharb	MT00007	14.20	36.07	114	57	31	4.0	-1.0	0.85	0.85
Aliartos	GR0001R	23.11	38.37	110	59	18	-23.5	-27.9	0.50	0.43
NEO	-	21.67	37.00	50	60	2	9.8	4.9	0.71	0.64
Finokalia	GR0002R	25.67	35.32	250	57	4	11.7	3.0	0.76	0.68
Ineia	-	32.37	34.96	672	52	5	2.7	-2.3	0.49	0.55
Oros Troodos	-	32.86	34.95	1819	49	11	0.1	-3.5	0.80	0.74
Agia Marina	CY0002R	33.06	35.04	532	55	14	3.1	-1.7	0.62	0.67

Observatory (http://www.navarinoneo.gr/index.php/en/) station in Messene Greece are used in the validation analysis. For the validation analysis, stations in the Mediterranean located within about 100 km from the shoreline of the Mediterranean shore are used. Table 3.1.1 shows the names, coordinates, elevation and the MNMBs and correlations obtained with the 2 forecast runs (o-suite and control). It indicates that the variance explained by each station of both the o-suite and control is high and correlations are highly significant over Western, Central and Eastern Mediterranean, with the exception of Ak-Pardines station in Spain. It should be noted that the control run mostly reproduces slightly better the day to day variability than the o-suite run over the Mediterranean shore of Spain while the o-suite reproduces slightly better the day to day variability over Greek stations (see Table 3.1.1).

In terms of biases, both runs' MNMBs vary between -20% and 20% over Spain (for Stations Caravaka and Bujaraloz MNMBs exceed -20%). Over the Mediterranean shore of Spain data assimilation seems to improve slightly the biases. In all other Mediterranean stations (Plan Aups/Ste Baume in France, Gharb in Malta, Aliartos, NEO and Finokalia in Greece, Ineia, Oros Troodos and Agia Marina in Cyprus) both, the o-suite and control run, reproduce well surface ozone mean concentrations (-10%<MNMBs<10%; see also Fig. 3.1.19, central and lower graphs) with the only exception of Aliartos station (MNMB≈-25).

The spatial distribution of MNMBs and correlations of the o-suite over the Mediterranean is shown in 3.1.20, with highly significant correlations over the entire Mediterranean from Gibraltar to Cyprus. On the other hand it clearly shows the slightly better o-suite performance over the Central and Eastern Mediterranean compared to the Mediterranean shore of Spain in terms of biases.

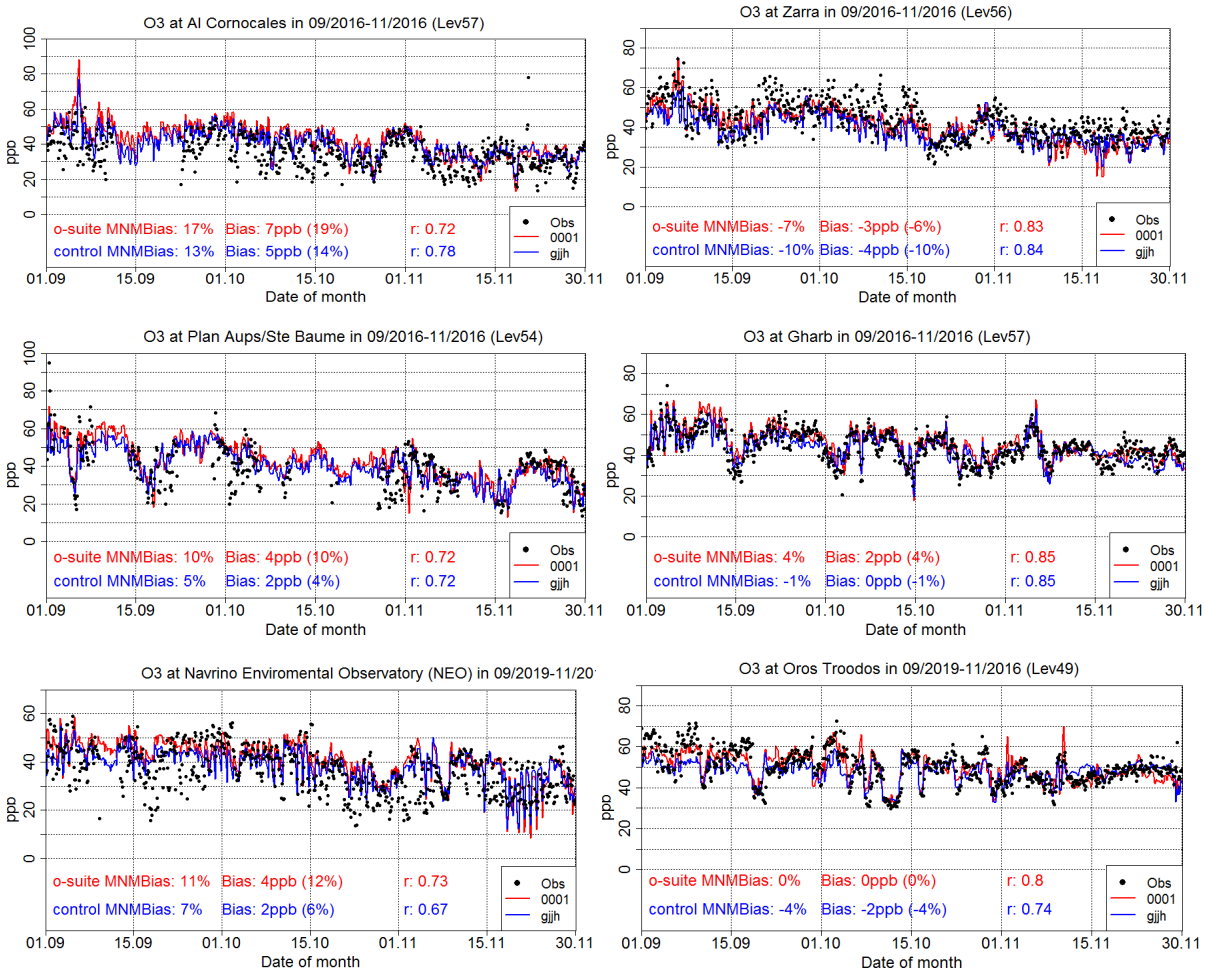

Figure 3.1.19: Time series for the o-suite (red) and Control (blue) compared to Airbase observations at Al Cornocales, Spain station (36.23°N, 5.66 °W, top left), at Morella, Spain station (40.64°N, 0.09°W, top right), at Plan Aups/Ste Baume, France station (43.34°N, 5.73°E, center left), at Gharb, Malta station (36.07°N, 14.20°E, center right) and at Finokalia, Crete station (35.32°N, 25.67°E, low left), and compared to observations provided by the Department of Labour Inspection - Ministry of Labour and Social Insurance of Cyprus, at Troodos Mountain station (34.95°N, 32.86 °E, low right).

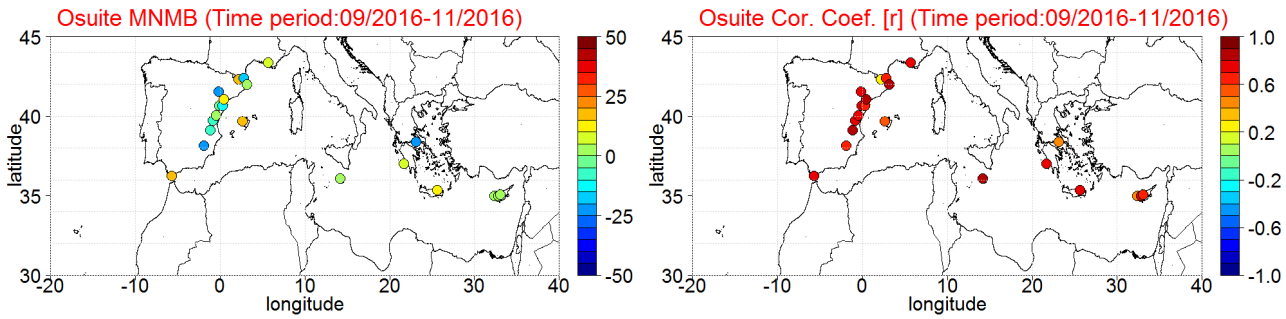

Figure 3.1.20: Spatial distribution of MNMB in % (left) and correlation coefficient (right) of the o-suite run compared to observational data during the period from 1 September 2016 to 30 November 2016.

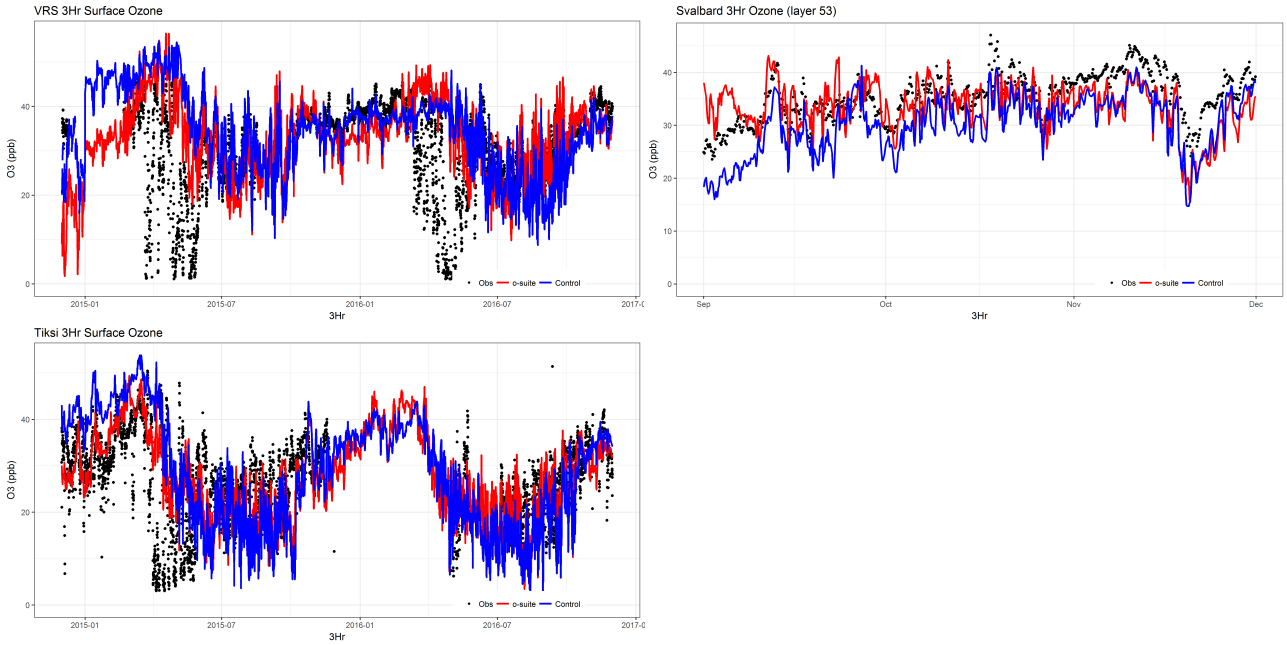

Figure 3.1.21: Time series for o-suite (red) and Control (blue) compared to observations (black dots) at the Villum Research Station, Station Nord, Greenland (top left), Zeppelin Mountain, Svalbard (top right) and Tiksi, Russia (bottom left).

3.1.5 Validation with IASOA surface observations

Model results were compared to O_3 observations from the Villum Research Station, Station Nord in north Greenland (81.6°N 16.7°W), from the Zeppelin mountain, Svalbard (78.9°N 11.9°E) and Tiksi, Russia (71.6°N 128.9°E) from the IASOA network, Fig. 3.1.21.

The measurement time series for VRS and Tiksi covers the period from December 2014 to November 2016. Data from Svalbard covers the period September – November 2016. Ozone depletion events in March – June in 2015 and 2016 are not captured by the model simulations during spring for the sites. These events are related to halogen chemistry reactions that are not represented in the model simulations. The simulations are on average in good agreement with the observations apart from the spring depletion events.

For the period September 2016 – November 2016 the measurements are not quality controlled. The model simulations underestimate the observed concentrations at all three sites. The levels predicted by the o-suite run is in better agreement with the observations with a normalized mean bias of -5% for the period compared to the normalized mean bias of -8 – -15% for the control run. The short-term variability is captured slightly better by the control run with r = 0.40 – 0.86, while it is r = 0.28 – 0.61 for the o-suite (Table 3.1.2).

Table 3.1.2. Normalised Mean Bias (NMB) and correlation coefficient (r) of the Control and the O-suite simulations for the three sites Zeppelin mountain, Svalbard, Villum Research Station, Greenland (VRS) and Tiksi, Russia for the period September – November 2016.

		NMB	R
Svalbard	o-suite	-0.05	0.47
	control	-0.15	0.86
VRS	o-suite	-0.05	0.61
	control	-0.17	0.87
Tiksi	o-suite	-0.05	0.28
	control	-0.08	0.40

3.2 Tropospheric nitrogen dioxide

3.2.1 Evaluation against GOME-2 retrievals

In this section, model columns of tropospheric NO_2 are compared to SCIAMACHY/Envisat NO_2 satellite retrievals (IUP-UB v0.7) [Richter et al., 2005] for model data before April 2012, and to GOME-2/MetOp-A NO2 satellite retrievals (IUP-UB v1.0) [Richter et al., 2011] for more recent simulations. This satellite data provides excellent coverage in space and time and very good statistics. However, only integrated tropospheric columns are available and the satellite data is always taken at the same local time, roughly 10:00 LT for SCIAMACHY and 09:30 LT for GOME-2, and at clear sky only. Therefore, model data are vertically integrated, interpolated in time and then sampled to match the satellite data. GOME-2 data were gridded to model resolution (i.e. 0.4° deg x 0.4° deg). Model data were treated with the same reference sector subtraction approach as the satellite data. Uncertainties in NO_2 satellite retrievals are large and depend on the region and season. Winter values in mid and high latitudes are usually associated with larger error margins. As a rough estimate, systematic uncertainties in regions with significant pollution are on the order of 20% – 30%.

Figure 3.2.1 shows global maps of GOME-2 and model monthly mean tropospheric NO_2 columns as well as differences between retrievals and simulations for November 2016. The overall spatial distribution and magnitude of tropospheric NO_2 is well reproduced by both model runs, indicating that emission patterns and NO_x photochemistry are reasonably represented. Some differences are apparent between observations and simulations, with generally larger shipping signals simulated by the models. For example, shipping signals are largely overestimated to the south of India. Compared to satellite data, all model runs underestimate tropospheric background values over Europe, Africa and South America, while background values are overestimated over the US. Local maxima of values observed over anthropogenic emission hotspots in East Asia (e.g. over the heavily populated Sichuan Basin; 30°N, 105°E), India, North America and others such as Teheran, Mekka, Bagdad are overestimated. Both runs overestimate fire emissions over Central Africa, while fire emissions over South Africa are underestimated.

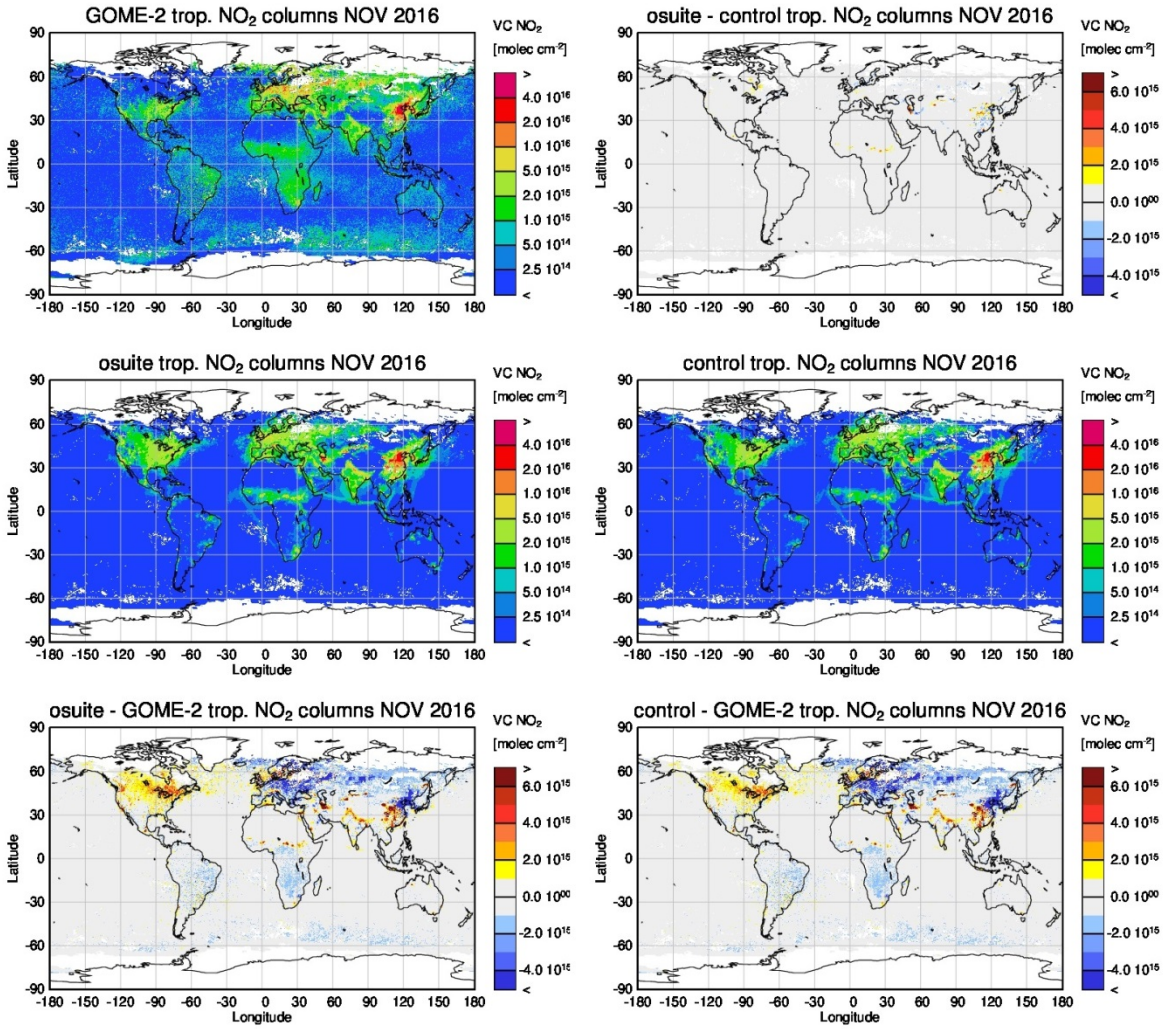

Figure 3.2.1: Global map comparisons of satellite retrieved and model simulated tropospheric NO_2 columns [molec cm^{-2}] for November 2016. The top row shows monthly mean tropospheric NO_2 columns retrieved by GOME-2 as well as the difference between osuite and control, the second row shows the corresponding tropospheric NO_2 columns for model simulated averages. The third row shows differences of monthly means between models and GOME-2. GOME-2 data were gridded to model resolution (i.e. 0.4° deg x 0.4° deg). Model data were treated with the same reference sector subtraction approach as the satellite data.

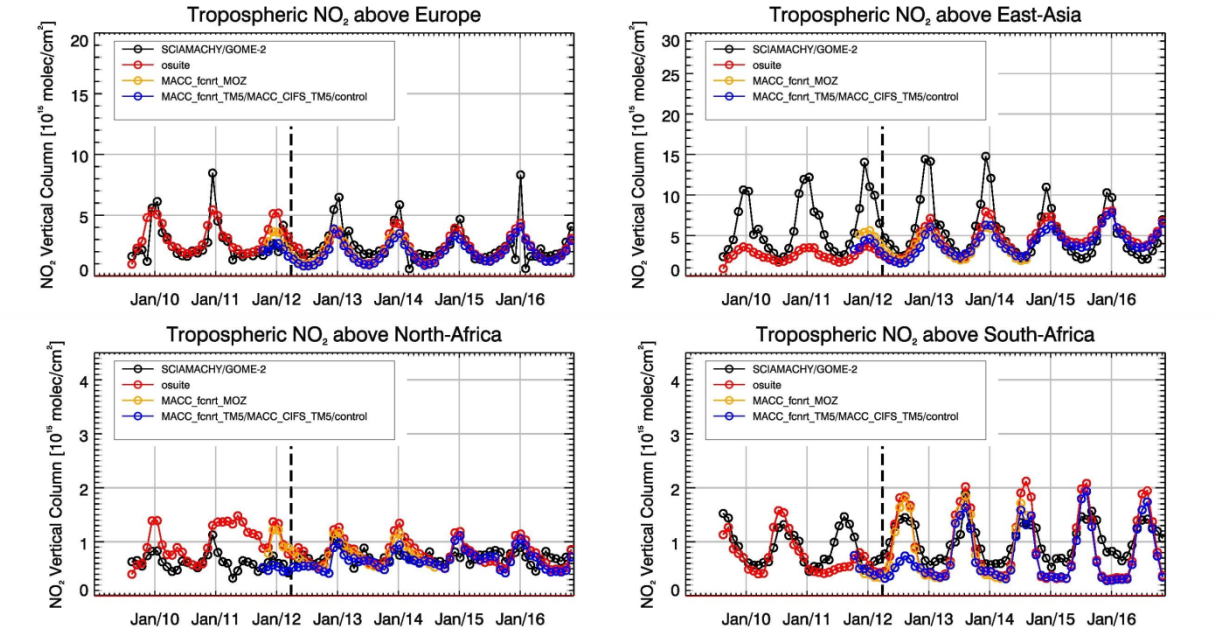

Figure 3.2.2: Time series of average tropospheric NO_2 columns [10^{15} molec cm^{-2}] from SCIAMACHY (up to March 2012) and GOME-2 (from April 2012 onwards) compared to model results for different regions (see Annex 2 for definition of regions). Upper panels represent regions dominated by anthropogenic emissions, lower panels represent those dominated by biomass burning. The blue line shows MACC_fcnrt_TM5 from November 2011 to November 2012, MACC_CIFS_TM5 results from December 2012 to August 2014 and control results from September 2014 onwards. Vertical dashed black lines mark the change from SCIAMACHY to GOME-2 based comparisons in April 2012.

Closer inspection of the seasonal variation of tropospheric NO_2 in some selected regions (Fig. 3.2.2) reveals significant differences between the models and points to some simulation problems. Over regions where anthropogenic emissions are major contributors to NO_x emissions, models catch the shape of the satellite time series rather well. However, over East-Asia absolute values and seasonality are in general strongly underestimated by all model runs (most likely due to an underestimation of anthropogenic emissions), with the o-suite showing the best results since the upgrade in July 2012. As NO_2 column retrievals decreased since 2014, model simulated values are in better agreement with the satellite retrieved ones for recent years. However, this decrease in values is not reproduced by the simulations and as such, the better agreement for more recent years cannot be attributed to an improvement of the simulations. Springtime and summertime model values increased in 2015 compared to previous years, which is in contrast to the satellite retrievals, so that the simulated values for the summers 2015 and 2016 are about 50% larger than satellite retrieved ones. As for East-Asia, a decrease in satellite retrieved values also occurs for Europe where a peak is usually found around January, which is, as a result, only slightly underestimated by the models for January 2015. The underestimation of tropospheric NO_2 columns over Europe may be caused to some extent by a change of emission inventories in 2012. However, the situation changed for winter 2015/2016, for which GOME-2 shows (compared to previous years) a strong increase in January peak values, combined with a decrease in values for December 2015 and February 2016, which is not reproduced by the models. It is not clear if the GOME-2 observations are realistic here, although a first inspection of daily GOME-2 satellite images did not point to any problems regarding the retrieval.

Over regions where biomass burning is the major contributor to NO_x emissions, seasonality and amplitude of model columns are determined by fire emissions. The seasonality for the two regions in Africa is simulated reasonably well for 2010 and after October 2011. In the time period in between, a bug in reading fire emissions lead to simulation errors for all MOZART runs. Over North-Africa, the o-suite shows improved results since the update in July 2012 and the change to CIFS-CB05 in September 2014. However, tropospheric NO_2 columns around December are still overestimated by the models. Summertime NO_2 columns over North-Africa are underestimated compared to the satellite data for 2015 and 2016. The models strongly overestimates the seasonal cycle for South-Africa since 2014 with an overestimation of the seasonal maximum which usually occurs around August of each year (e.g. by a factor of 1.4 larger compared to GOME-2 retrievals in August 2016). For 2014 model runs without data assimilation agree much better with satellite observations, in contrast to more recent CB05-based o-suite runs since 2015. For November 2015 and November 2016, satellite retrieved values over South-Africa do not decrease below $1x10^{15}$ molec/cm^2, a feature which did not show up in the time series before. While wintertime values over South-Africa were also underestimated by the models for previous years, the underestimation is now even stronger given the comparatively large satellite retrieved NO_2 columns since November 2015.

Details on the NO_2 evaluation can be found at:
http://www.doas-bremen.de/macc/macc_veri_iup_home.html.

3.2.2 Evaluation against ground-based DOAS observations

In this section, we compare the NO_2 profiles of the CAMS models with UVVIS DOAS measurements at Xianghe (39.8°N, 117°E, station near Beijing, altitude 92m) and Haute Provence (43.9°N, 5.71°E, rural station, altitude 650m).[1] This ground-based, remote-sensing instrument is sensitive to the NO_2 abundance in the lower troposphere, up to 1km altitude with an estimated uncertainty of 8%. Tropospheric NO_2 profiles and columns are validated (up to 3.5km). A description of the instruments and applied methodologies is the same all DOAS OFFAXIS measurements, see http://nors.aeronomie.be. It is important to mention here that the model partial column values between the surface and 3.5 km are calculated for the smoothed model profiles (see Fig. 3.2.3). This guarantees that the model levels where the measurement is not sensitive do not contribute to the observed bias. We should mention that the measurement data is still catalogued as rapid delivery and not in the consolidated NDACC database.

From Figs. 3.2.3 and the below table, we see the assimilation has a positive effect OHP during SON 2016. The osuite performs better during the winter months at Xianghe when the background NO_2 concentrations are higher.

[1] No contribution from UCCLE due to instrument failure.

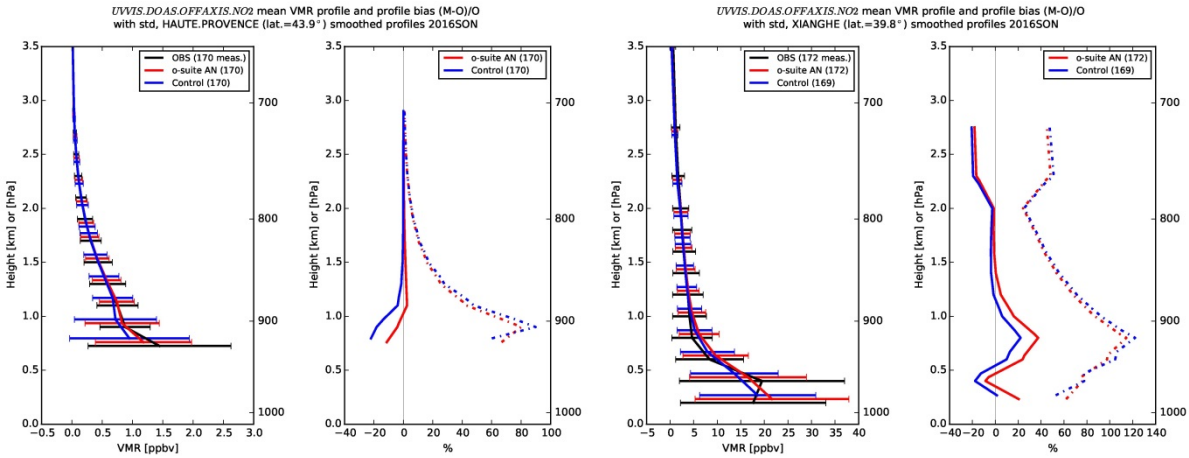

Figure 3.2.3: Seasonal mean tropospheric NO2 profiles by o-suite (red) and Control (blue) compared to NDACC UVVIS DOAS data at Haute Provence (43.9°N, 5.71°E, left top) and Xianghe (39.8°N, 117°E, right) for SON 2016.

Table 3.2.1: Seasonal relative mean bias (MB, %), standard deviation (STD, %) for the considered period and number of observations used (NOBS), compared to NDACC UVVIS OFFAXIS observations at Haute Provence and Xianghe (mean bias and stddev in %). The overall mean uncertainty for the NO_2 measurements is 5%. Colored numbers indicate best performance (osuite or control).

		DJF			MAM			JJA			SON		
		MB	stddev	nobs	MB	stddev	nobs	MB	stddev	nobs	MB	stddev	nobs
osuite	ohp	35.13	96.22	115	-6.08	48.27	353	13.28	55.57	204	4.66	40.95	170
control	ohp	21.16	84.90	115	-20.36	33.14	353	2.46	51.24	204	-7.74	35.79	170
osuite	xianghe	11.73	77.38	103	23.50	74.65	216	76.55	106	270	43.14	110	172
control	xianghe	24.63	105.46	103	5.21	63.77	216	42.74	74.95	270	34.09	103.7	169

3.3 Carbon monoxide

3.3.1 Validation with Global Atmosphere Watch (GAW) Surface Observations

For the Near-Real-Time (NRT) validation, 11 GAW stations have delivered CO surface mixing ratios in NRT and data is compared to model results as described in Eskes et al (2016) and is used for CAMS model evaluation for September – November 2016. The latest validation results can be found on the CAMS website: http://www.copernicus-atmosphere.eu/d/services/gac/verif/grg/gaw/

For stations in Europe and the Southern hemisphere, the MNMBs and correlation coefficients indicate that the forecast remains stable till the D+4 (forecast run from 96h to 120h). For stations in Japan, results show differences in MNMBs compared to the analysis but also lower correlation for the forecasts D+2 and D+4.

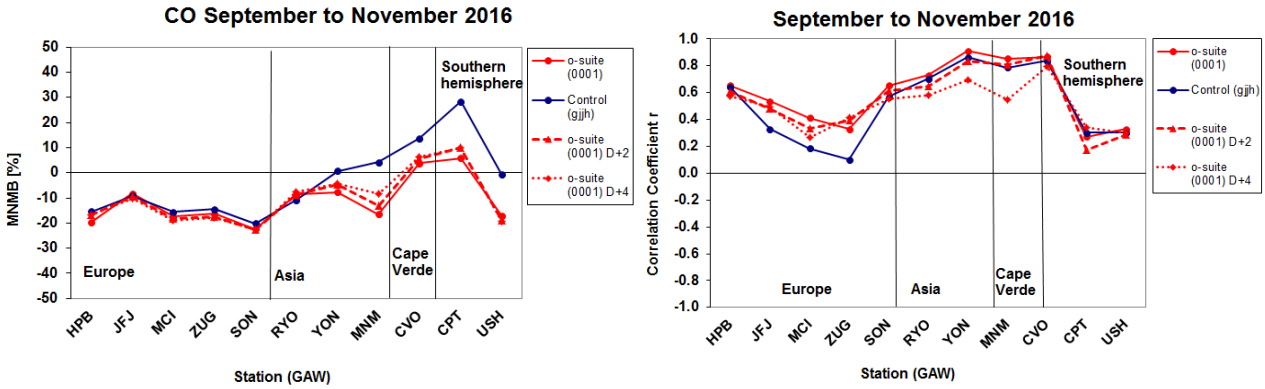

Figure 3.3.1: Modified normalized mean bias in % (left) and correlation coefficient (right) of the NRT model runs compared to observational GAW data in the period September to November 2016. Circles correspond to D+0, triangles to D+2 and rhombs to D+4 metrics respectively.

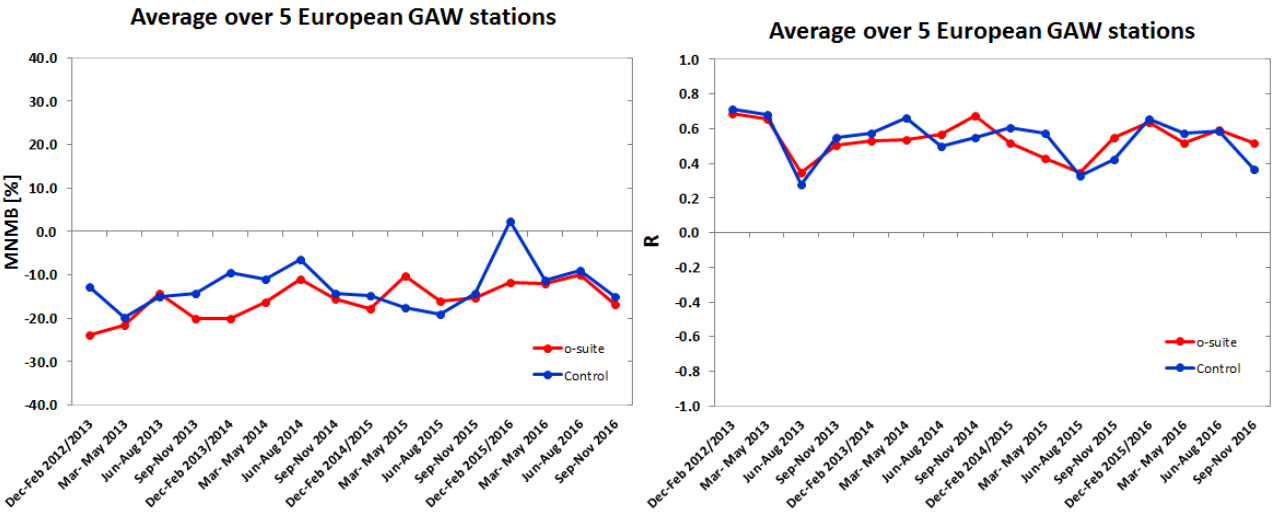

Figure 3.3.2: Long term (Dec. 2012 – November 2016) evolution of seasonal mean MNMB (left) and correlation (right), as averaged over 5 GAW stations in Europe, for o-suite (red) and control (blue).

A comparison of the seasonal-mean MNMB over Europe (Fig. 3.3.2) from December 2012 to present shows a slowly improving MNMB from about -20% in 2013 to -10% for more recent periods. Temporal correlation remains relatively constant at r=0.5 on average.

For European stations, both analyses runs show an underestimation of observed CO mixing ratios, with MNMBs between -9% and -22%. Correlation coefficients are between 0.32 and 0.65 for the o-suite and between 0.10 and 0.63 for the control run.

For Asian stations, the control run corresponds well to the observations, with MNMBs between 4 and -10% whereas the o-suite shows partly a larger negative offset (up to -15%), see Fig. 3.3.4. Correlation coefficients are high between 0.70 and 0.91 for both runs.

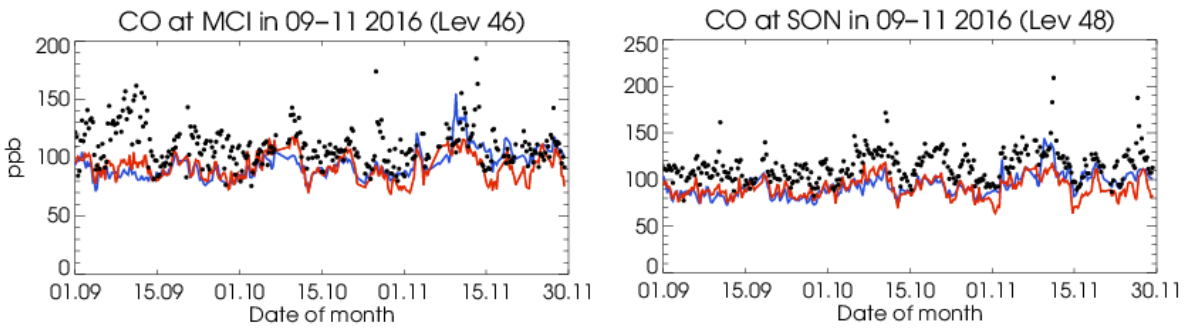

Figure 3.3.3: Time series for the o-suite (red) and control (blue) compared to GAW observations at Hohenpeissenberg (47.8°N, 11.0°E) and Jungfraujoch (46.5°N, 7.9°E).

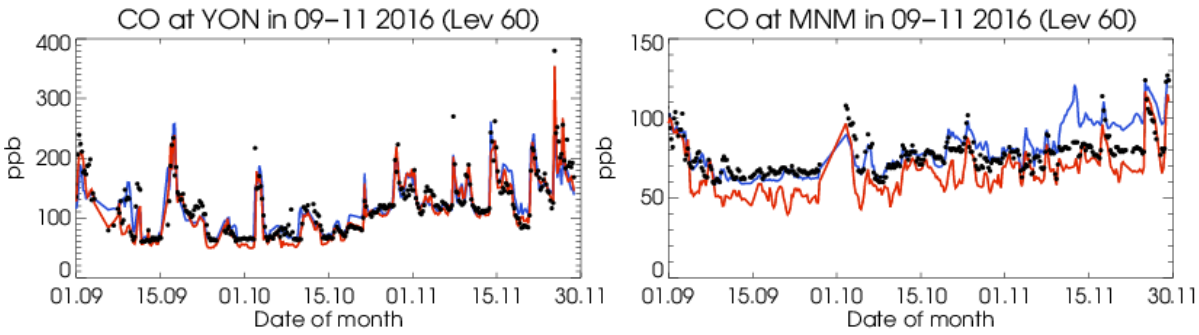

Figure 3.3.4: Time series for the o-suite (red) and control (blue) compared to GAW observations at Yonagunijima (24.47°N, 123.0°E) and Minamitorishima (24.3°N, 123.9°E).

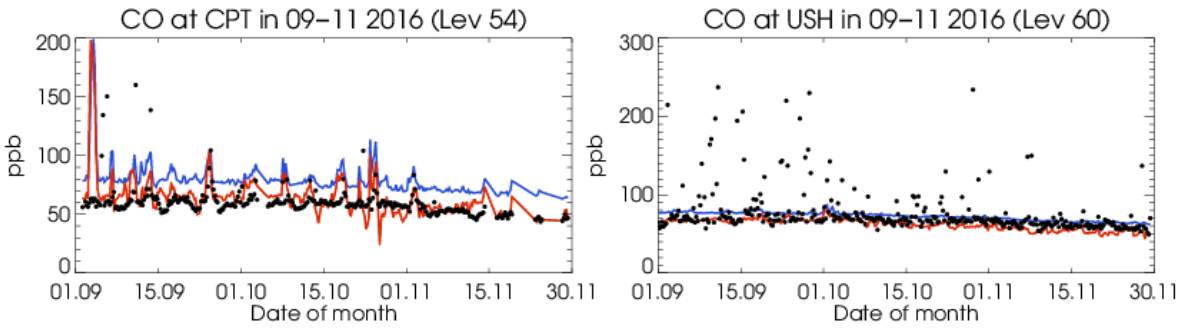

Figure 3.3.5: Time series for the o-suite (red) and control (blue) compared to GAW observations at Cape Point (34.35°S, 18.5°E) and Cape Verde (16.9°N, 24.9°W).

For the two stations in the Southern Hemisphere (CPT, USH), the positive offset visible for the control run is corrected by the data assimilation for the o-suite, see Fig. 3.3.5 (left panel).

3.3.2 Validation with IAGOS Data

The daily profiles of ozone and CO measured at airports around the world are shown on the website at http://www.iagos.fr/macc/nrt_day_profiles.php. For the period September-November 2016, data from several aircraft have been validated, as discussed in Sec. 3.1.2.

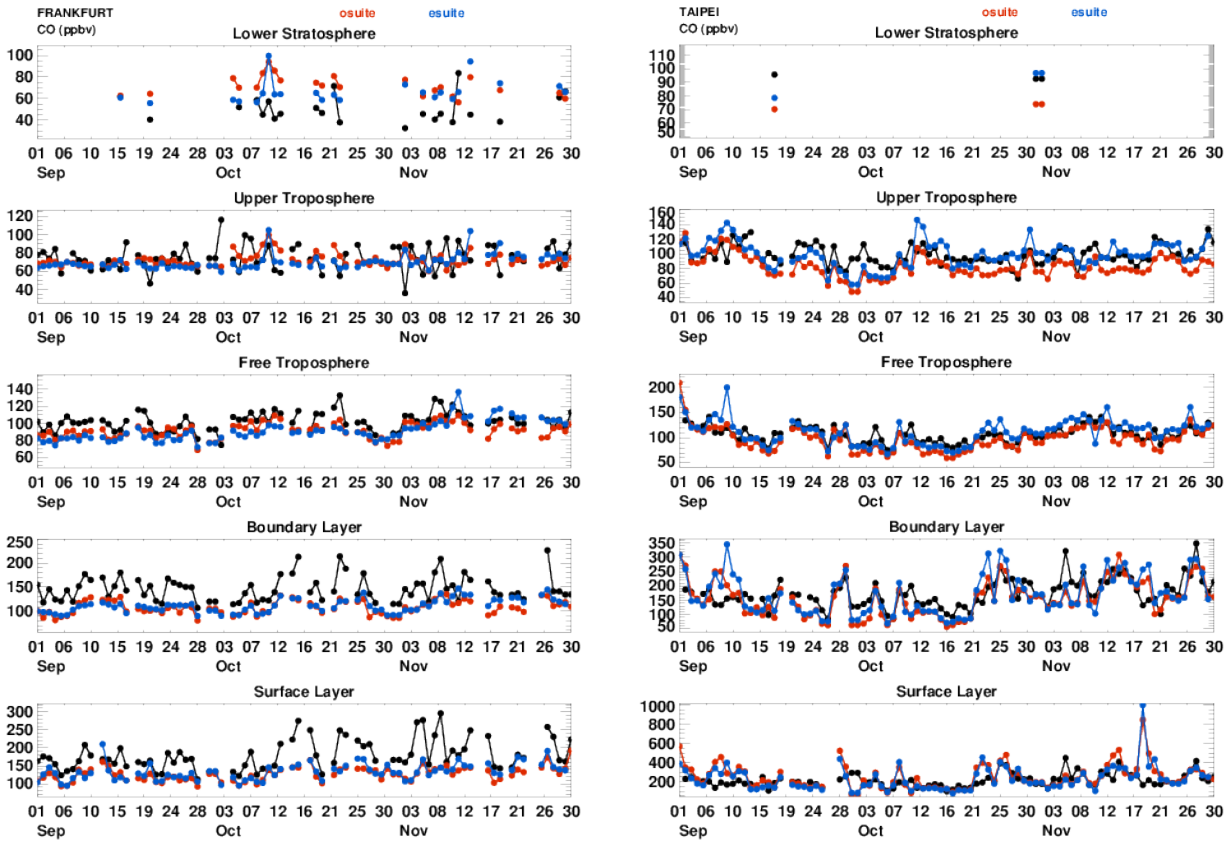

Figure 3.3.6: Time series of daily mean CO at Frankfurt and Taipei during SON 2016 for 5 layers, Surface, Boundary layer, Free Troposphere, Upper Troposphere and Lower Stratosphere.

Figure 3.3.6 shows the time series of CO over Frankfurt and Taipei for the 5 different layers throughout the troposphere. Over Taipei the models reproduce CO quite well in all atmospheric layers. However, over Frankfurt, we can see an underestimation of CO in the surface and boundary layers as seen in previous seasons and as described by Stein et al. (2014).

Europe

Figure 3.3.7 gives examples of the CO profiles over Frankfurt, Amsterdam, Paris and Rome. CO in the boundary and surface layers is systematically underestimated, but CO in the free-troposphere is generally well estimated by the models. In the upper troposphere, the models overestimate the CO. The profiles on 18 October at Paris and Frankfurt are very similar but taken by two different aircraft.

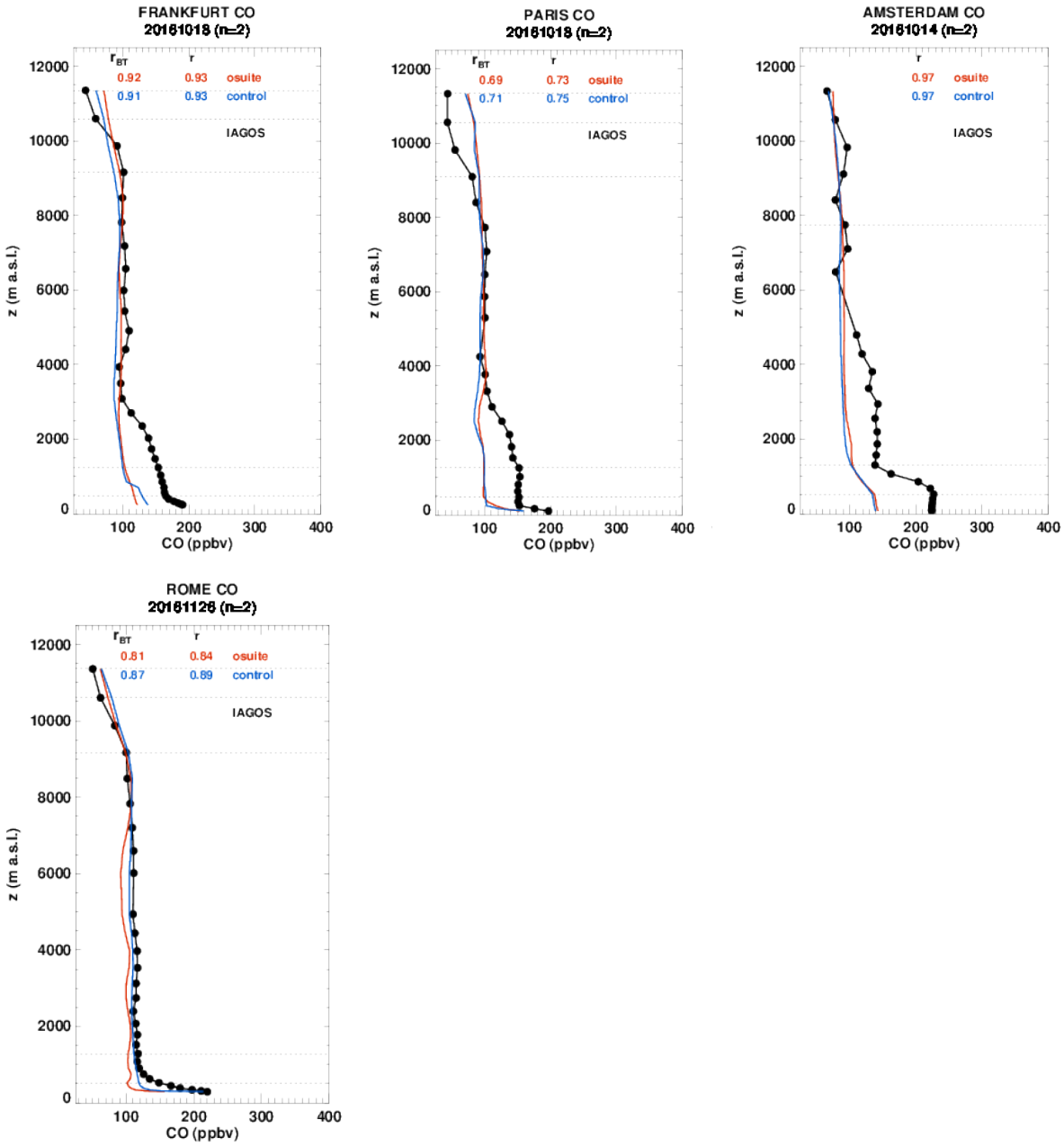

Figure 3.3.7: Selection of profiles of CO from IAGOS (black) and the two NRT runs over Europe in SON 2016.

Asia

The time series at Taipei (Fig. 3.3.6) showed that the CO from the model versions showed good correspondence to the observations in the free troposphere and upper troposphere. In general, this is the case in many locations across Asia and South-east Asia as the profiles from a range of airports show (Fig 3.3.8). The underestimation of CO in the boundary and surface layers which is so prominent in Europe, is often absent on profiles over Asia.

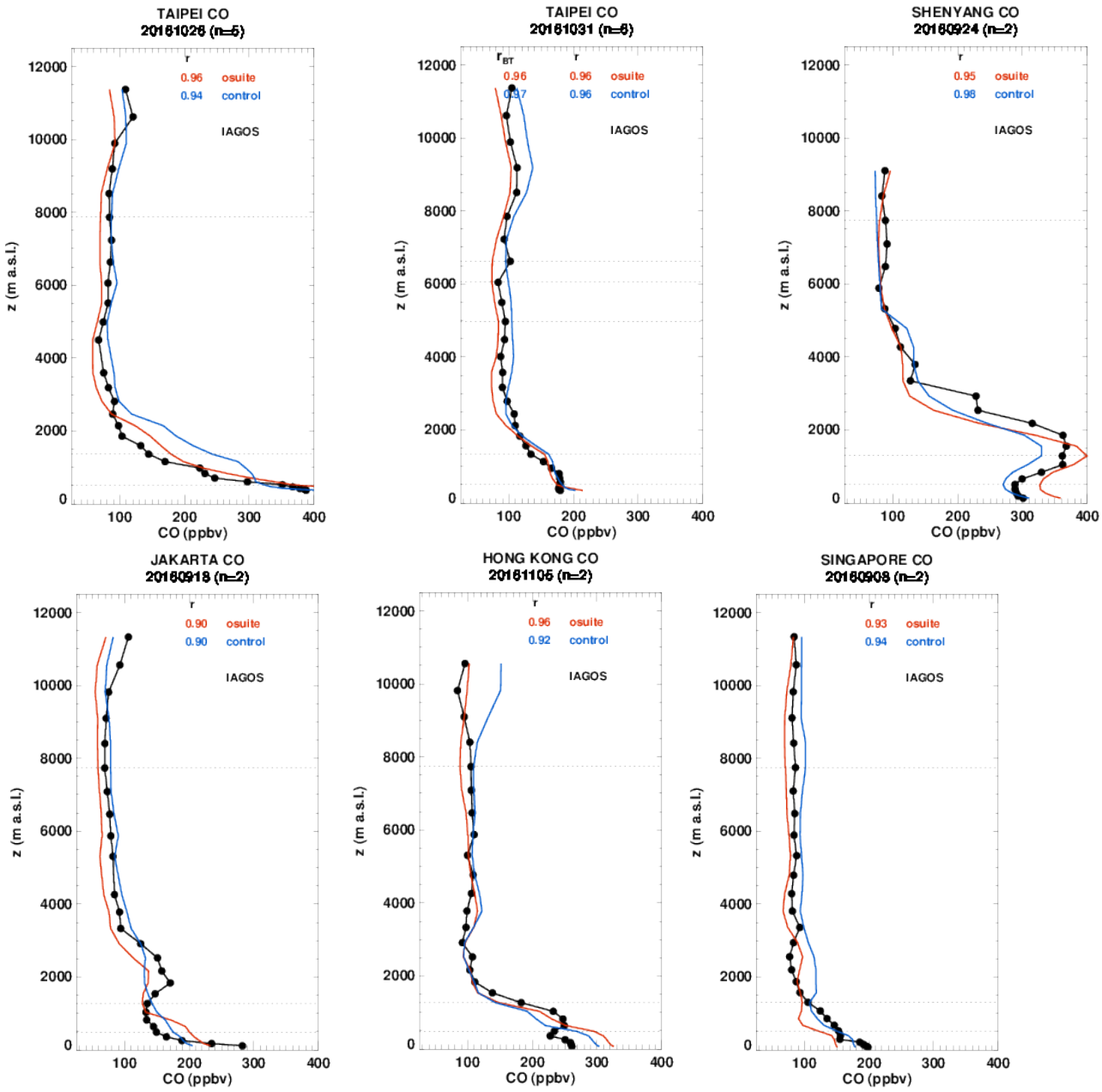

Figure 3.3.8: Profiles of CO from IAGOS (black) and the two NRT runs in China and South East Asia during the period September to November 2016.

Typhoons

The effect of the passage of typhoons or tropical storms can be seen on the profiles of CO in Fig. 3.3.9, where the mixing ratios in the boundary layer are reduced from around 200ppbv to less than 100ppbv. It is possible that the high CO mixing ratios at Busan are the result of the passage of Typhoon Chaba which hit Busan a few days before and may have dumped polluted air from the surface into the upper troposphere. The magnitude of this feature is overestimated by the control and improved after assimilation, but the depth of the anomaly remains too shallow.

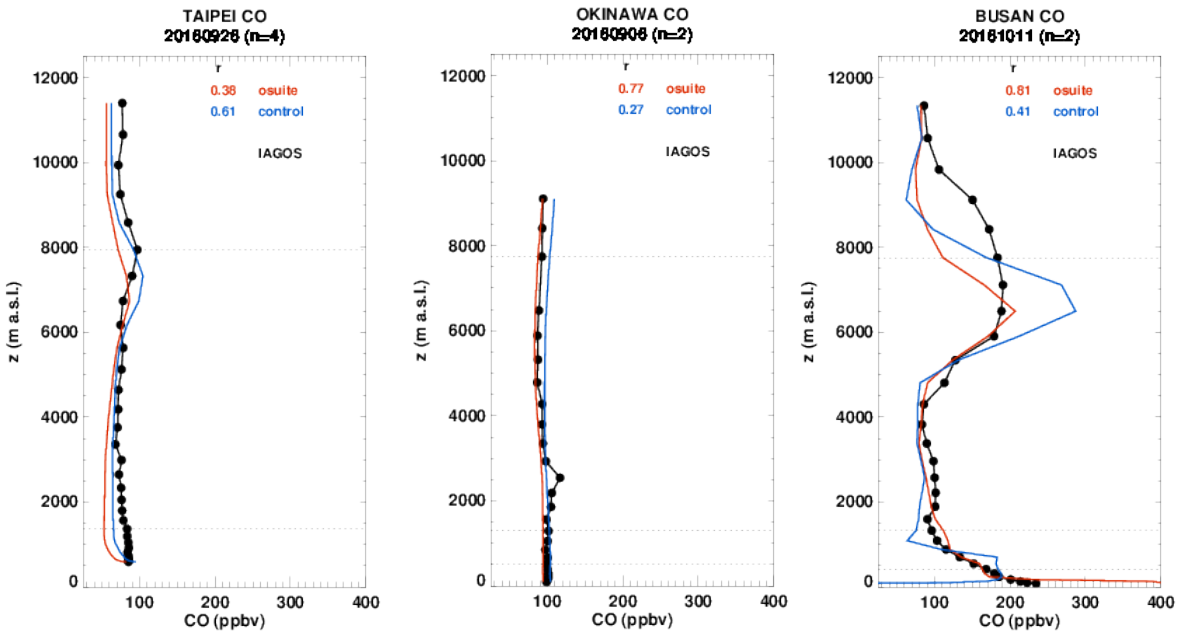

Figure 3.3.9: Profiles of CO from IAGOS (black) and the two NRT runs in China and South East Asia during the period September to November 2016.

Japan

The models perform well over many different cities in Japan (Fig. 3.3.10) although there is often an underestimation of the CO in the surface layer. Generally the osuite makes an improvement over the control such as over Osaka (20161007) or at Fukuoka (20161130) where a mid-tropospheric peak in CO was indicated by the control and corrected after assimilation. The mid-tropospheric maximum at Fukuoka may be a plume exported from China.

Australasia

The new China Airlines aircraft has been providing profiles in Auckland (36°S, 174°E) New Zealand since August 2016. In New Zealand, we would expect the concentrations of ozone to be the closest to background concentrations due to the low population density, its remoteness from other continents, and the arrival of clean maritime air from the Tasman Sea and the Pacific Ocean.

The profiles (Fig. 3.3.11) show that the models do well at capturing the profile of CO over the entire height range, except when CO in the surface layer is higher than normal (Auckland: 20160927). In the UTLS, CO is also well captured, in contrast to ozone for the same days. Profiles at Sydney and Brisbane in Australia show that the control run does better throughout the troposphere with the osuite underestimating the amount of CO.

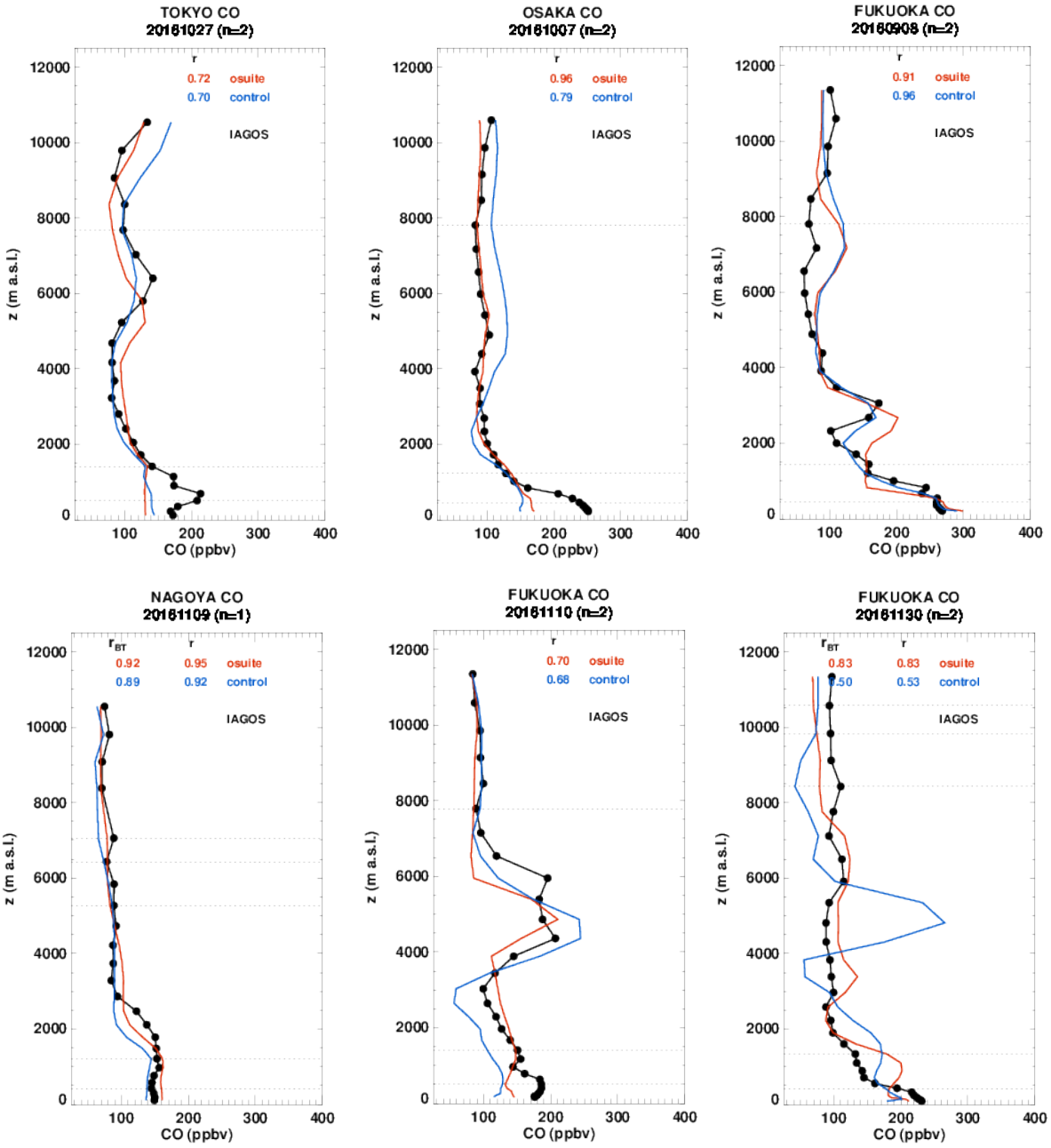

Figure 3.3.10: Profiles of CO from IAGOS (black) and the two NRT runs in China and South East Asia during the period SON 2016.

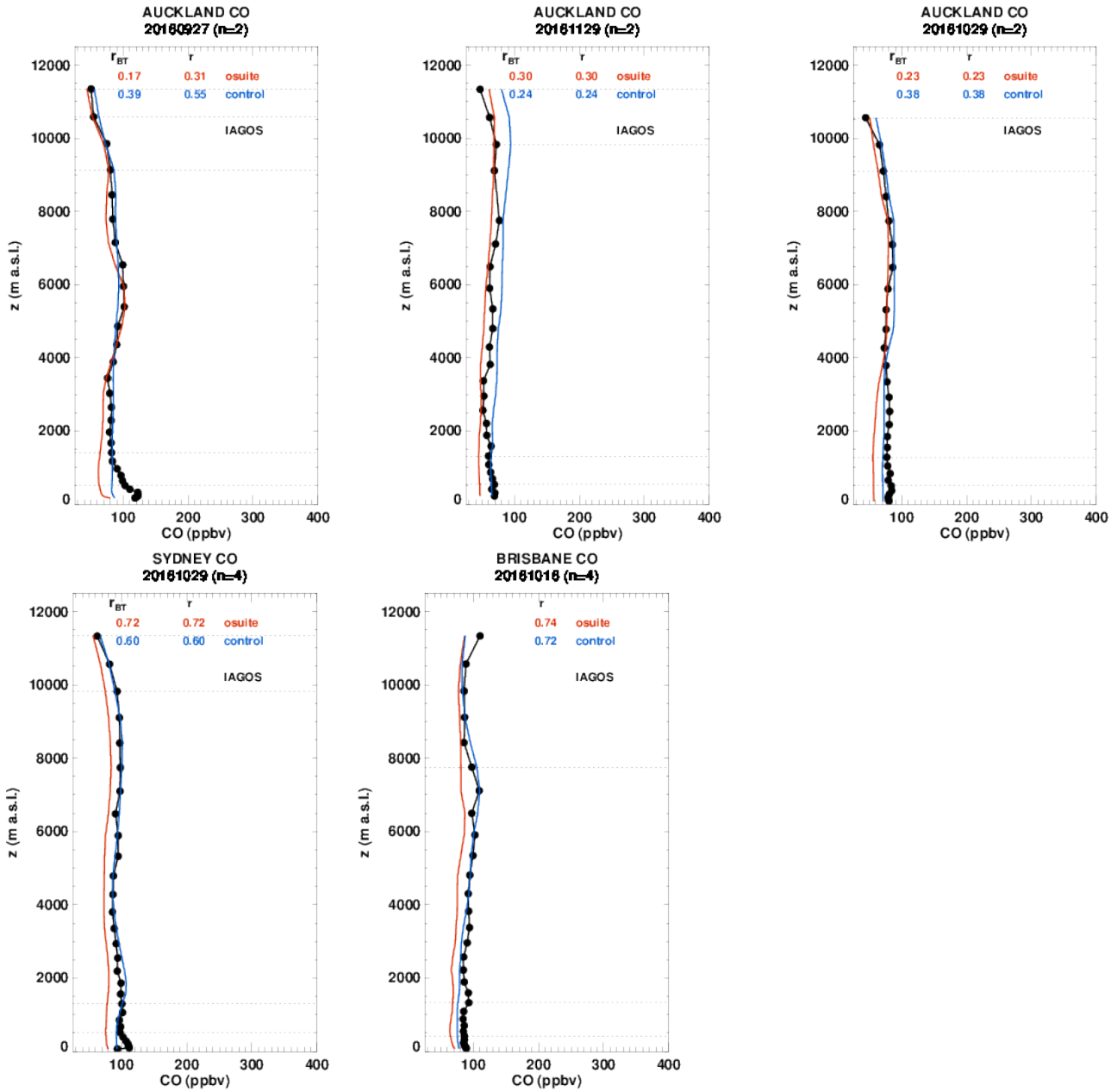

Figure 3.3.11: Profiles of CO from IAGOS (black) and the two NRT runs in New Zealand and Australia during the period SON 2016.

3.3.3 Validation against FTIR observations from the NDACC network

In this section, we compare the CO profiles of the CAMS models with FTIR measurements at Maido (21°S, 55°E, i.e. southern tropics, altitude 2.2km) and Lauder (46°S, 169.7°E, altitude 370m. These ground-based, remote-sensing instruments are sensitive to the CO abundance

in the troposphere and lower stratosphere, i.e. between the surface and up to 20 km altitude. Tropospheric CO profiles and columns are validated (up to 10km). A description of the instruments and applied methodologies can be found at http://nors.aeronomie.be.

Table 3.3.1: Seasonal relative mean bias (MB, %), standard deviation (STD, %) for the considered period and number of observations used (NOBS), compared to NDACC FTIR observations at Lauder and Maido (mean bias and stddev in %). The overall uncertainty for the CO measurements at Lauder and Maido is approximately 5%.

		SON			DJF			MAM			JJA		
		MB	stddev	nobs	MB	stddev	nobs	MB	stddev	nobs	MB	stddev	nobs
o-suite	Lauder	-8.53	5.27	93	-1.71	5.66	150	6.65	23.35	150	-2.36	4.00	126
control	Lauder	36.82	12.21	93	45.87	5.17	150	33.25	12.23	148	17.44	7.18	126
o-suite	Maido	-8.60	3.34	290	-5.30	3.34	527	-6.59	3.55	822	-5.49	3.74	852
control	Maido	34.00	6.14	290	30.70	5.29	527	21.77	8.28	822	3.21	8.42	832

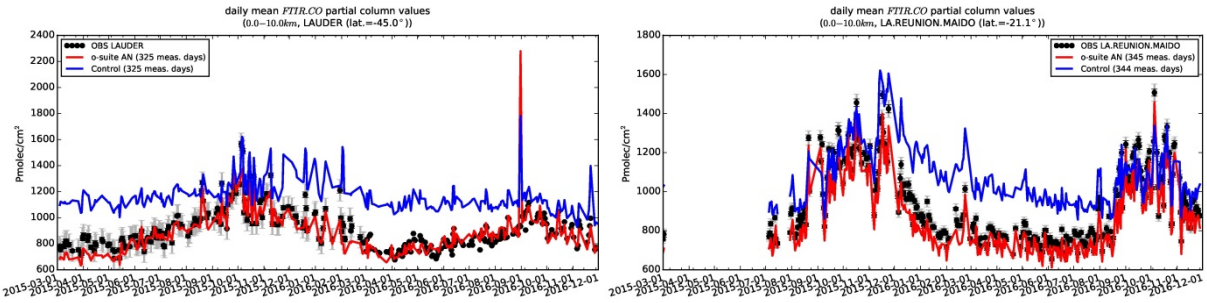

Figure 3.3.12: Daily mean values of tropospheric CO columns (till 10km) by the o-suite (red) and the Control run (blue) compared to NDACC FTIR data at Lauder, New Zeeland (45°S, 169.7°E) (left) and Maido (21°S, 55°E) (right) for the period March 2015-November 2016. The number of measurement days is indicated in the legend. In Lauder a spike is seen at the end of August 2016. This is caused by a drifting fire source in the model, as discussed in the previous report.

Table 3.3.1 and Fig. 3.3.12 show that the tropospheric columns of CO agree well. The o-suite underestimates CO at Lauder with values around 2%, which is within the measurements uncertainty range (6%). At Maido the o-suite underestimates the CO abundance (approx. -6%, underestimation seems to decrease in time). The mean uncertainty on these measurements is 5%, so the observed o-suite biases are now only slightly larger than the measurement uncertainty). For both stations, the control run overestimates the background CO with MBs between 20%-30%, clearly showing the positive effect of assimilation.

3.3.4 Evaluation with MOPITT and IASI data

In this section, model CO total columns are compared to MOPITT versions 5 and 6 (thermal infrared radiances) (Emmons et. al., 2009, Deeter et al., 2010) and IASI satellite retrievals (Clerbaux et al., 2009). Figure 3.3.13 shows the global distribution of CO total columns retrieved from MOPITT (top left) and IASI (top right) and the relative bias of model runs with respect to MOPITT V5, averaged for November 2016. MOPITT and IASI show relatively high values over east China and biomass burning areas in Africa. IASI also has high CO values over South America in Brazil, which is not the case with the MOPITT data. IASI values are much higher in biomass burning areas in Africa, compared to MOPITT, while MOPITT data are higher for East Asia.

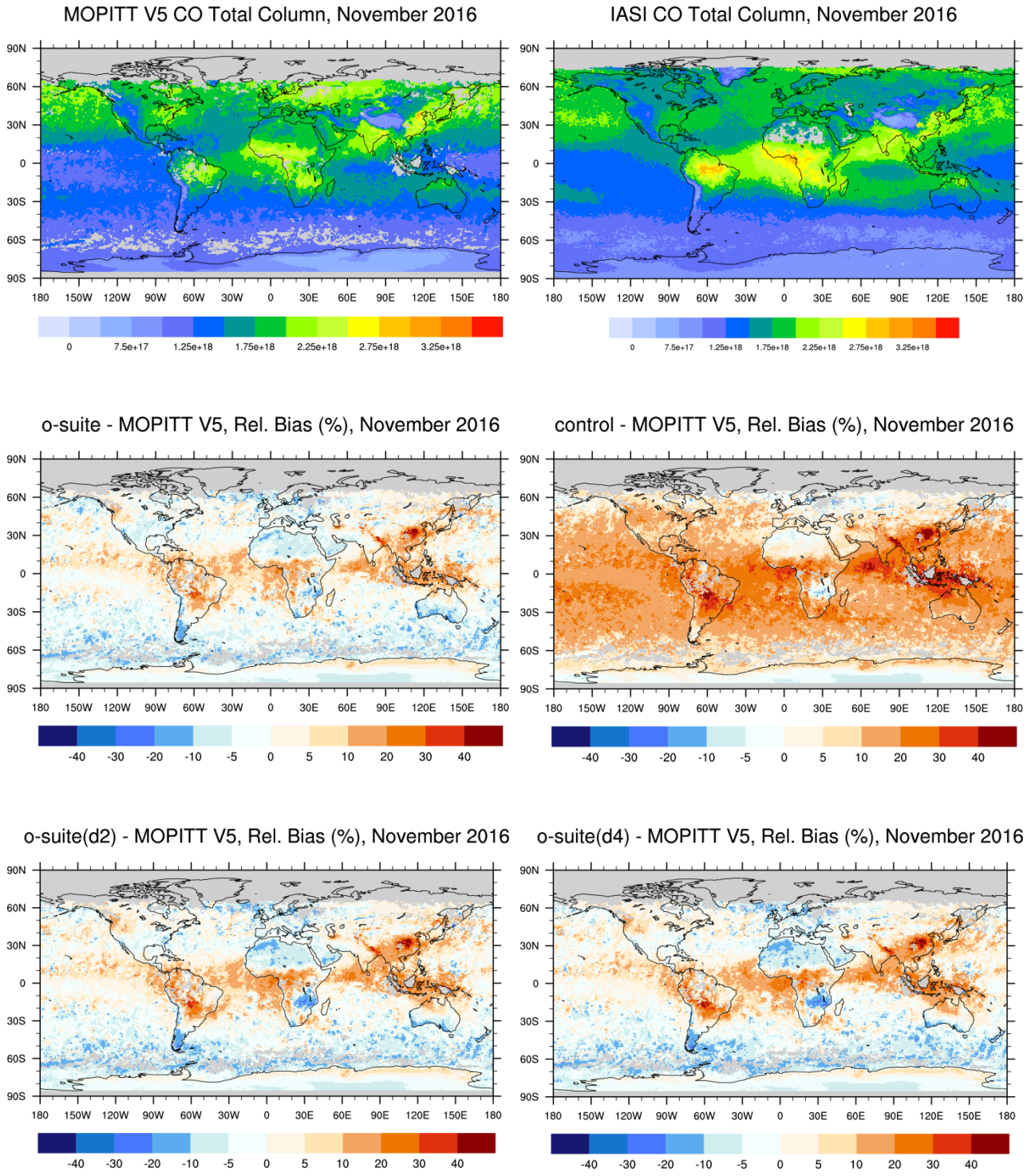

Fig. 3.3.13: CO total column for MOPITT V5 (top left) and IASI (top right) satellite retrievals and relative difference between the model runs and MOPITT for November 2016: o-suite (middle left), control run (middle right), o-suite 2nd forecast day (bottom left), o-suite 4th forecast day (bottom right). Grey color indicates missing values.

The modeled CO geographical distribution and magnitude values show that the model performs reasonably (not shown). The relative difference between the model runs and MOPITT shows that both model runs overestimate CO total column over the Himalaya region, east of China and South America by up to 40 %. In general, the o-suite performs better than the control run without data assimilation, with some overestimation in the tropics and underestimations in the mid-latitudes up to 20 %. The control run overestimates CO total columns over the entire globe by about 20-30 % with regional exceptions over the western part of Eurasia and parts of southern Africa. Figure 3.3.14 shows no significant difference between o-suite analysis and 2nd and 4th forecast days.

Figure 3.3.14 shows the time series of CO total columns for MOPITT V5 and V6, IASI and the model runs over the eight selected regions. For the comparison with MOPITT, the modelled CO concentrations were transformed using MOPITT V5 averaging kernels (Deeter, 2004). Both, MOPITT and IASI CO total column are assimilated in the o-suite run, while a bias correction scheme is applied to IASI data to bring it in line with MOPITT. MOPITT and IASI CO total columns show a relatively similar variability over different regions. In general, IASI CO values are lower compared to MOPITT over most regions with some seasonal exceptions. Significant difference between MOPITT and IASI are observed over the Alaskan and Siberian fire regions in winter seasons, with IASI CO total column values lower up to 30 %. The modelled seasonality of CO total columns is in relatively good agreement with the retrievals. In general, the comparison between o-suite and control run shows that assimilation of satellite CO has a more positive, pronounced impact on model results over East and South Asia and North and South Africa and smaller impact over other regions.

Since September 2014 the o-suite shows better agreement with the satellite retrievals over Europe and the US, especially during the seasonal maximum in spring. Improvements can also be seen in Siberian fire regions and North Africa.

In autumn 2016 both model runs show good agreement with the observations over Europe with biases of about 5%. CO values in South and East Asian regions in autumn 2016 for both, observations and model runs, are significantly smaller compared to autumn 2015.

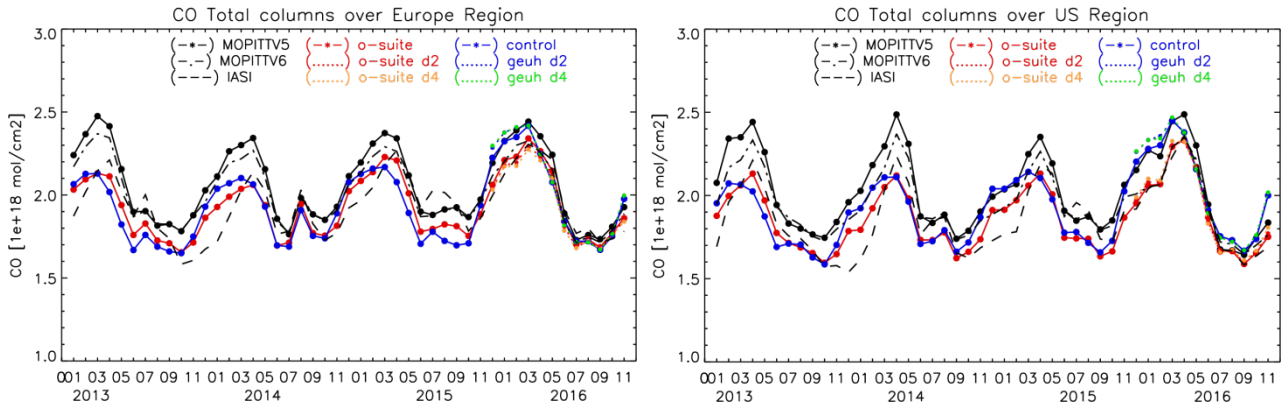

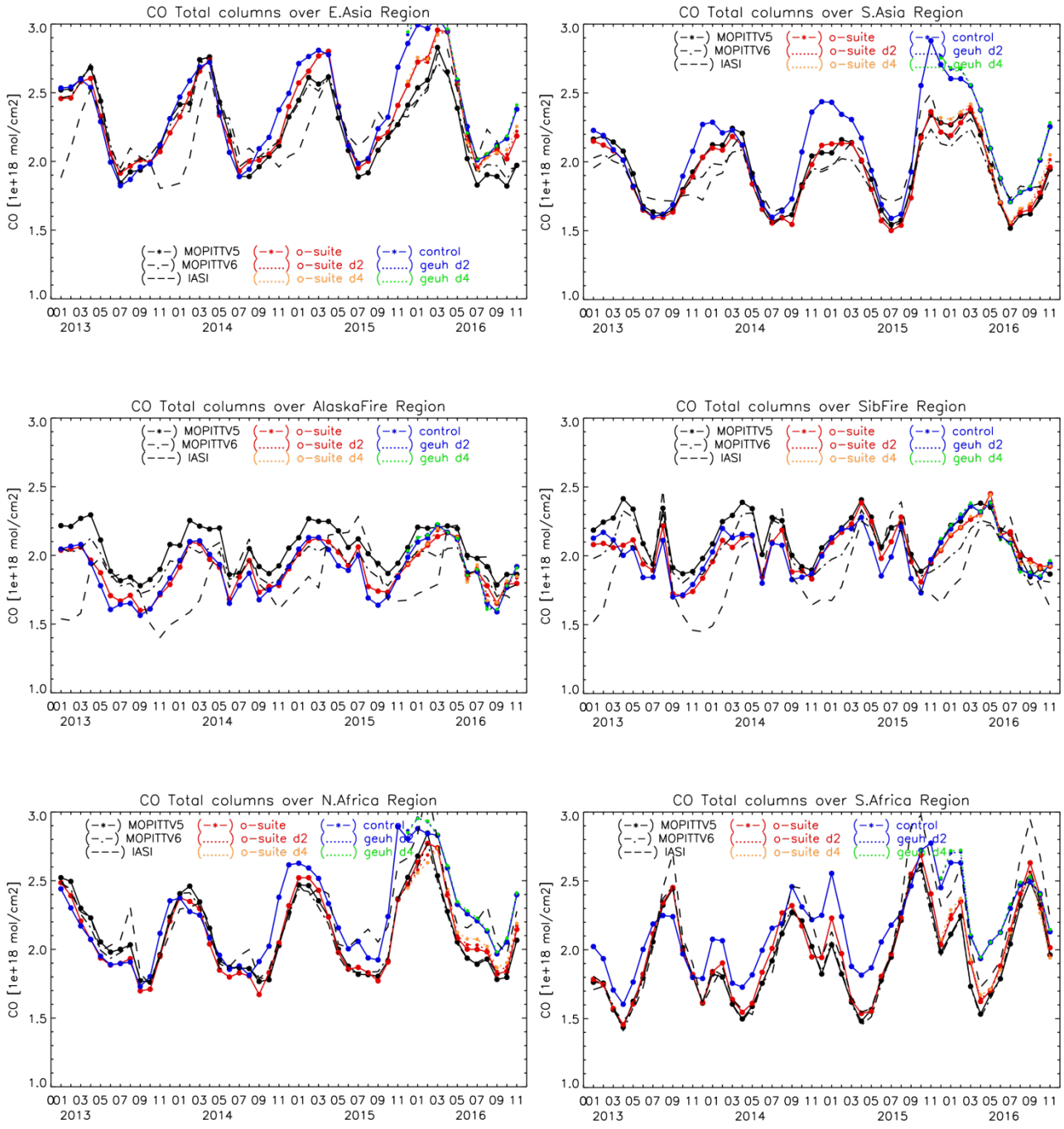

Fig. 3.3.14: Time series of CO total column for satellite retrievals MOPIT V5 and V6, IASI (black) and the model runs over the selected regions: o-suite (red, solid), control (blue, solid), o-suite 2nd forecast day (red, dotted), o-suite 4th forecast day (orange, dotted), control 2nd forecast day (blue, dotted), control 4th forecast day (green, dotted).

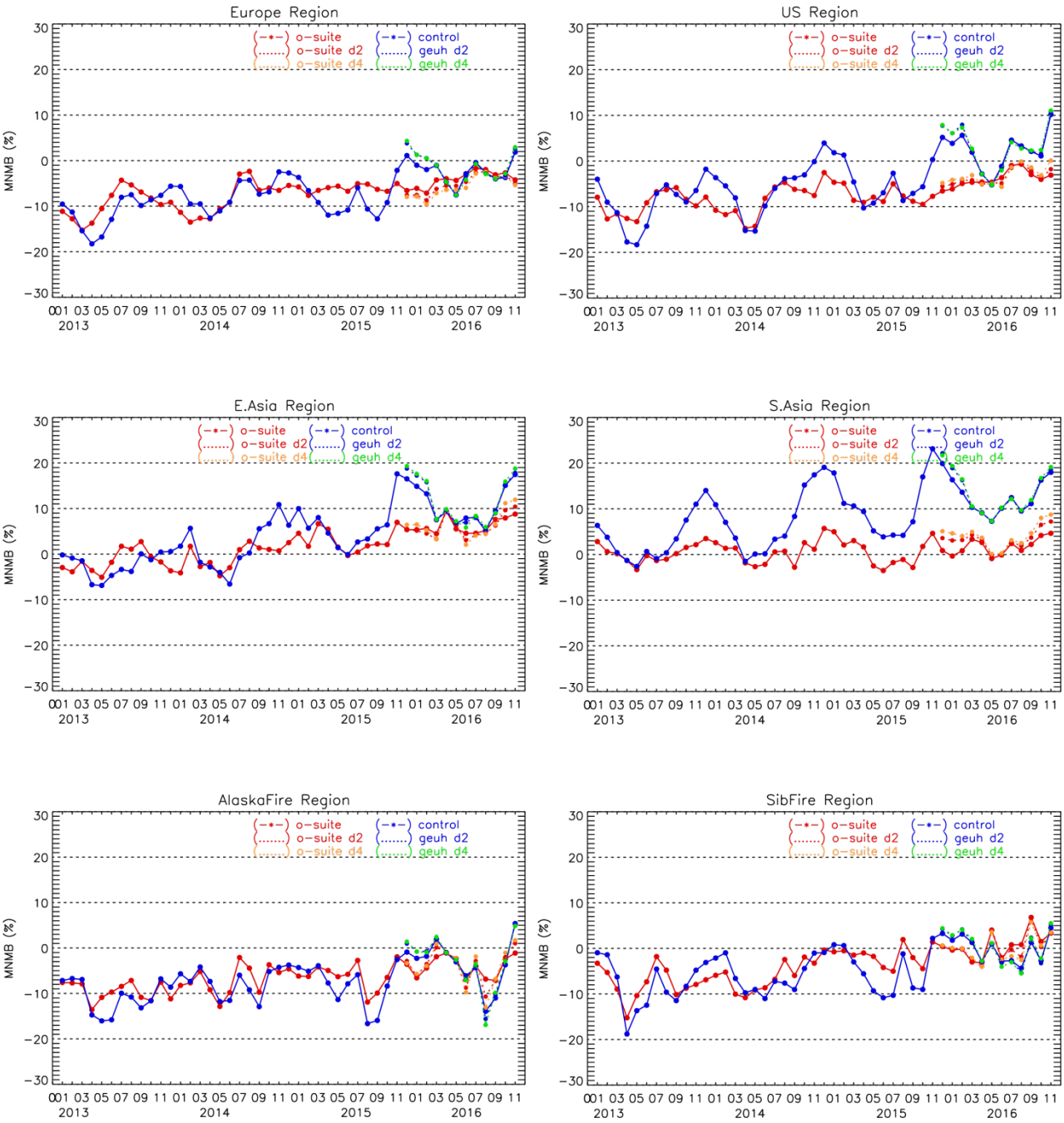
Europe Region
US Region
E.Asia Region
S.Asia Region
AlaskaFire Region
SibFire Region
(-*-) o-suite
(.....) o-suite d2
(.....) o-suite d4
(-*-) control
(.....) geuh d2
(.....) geuh d4
MNMB (%)
30
20
10
0
-10
-20
-30
0 01 03 05 07 09 11 01 03 05 07 09 11 01 03 05 07 09 11 01 03 05 07 09 11
2013
2014
2015
2016

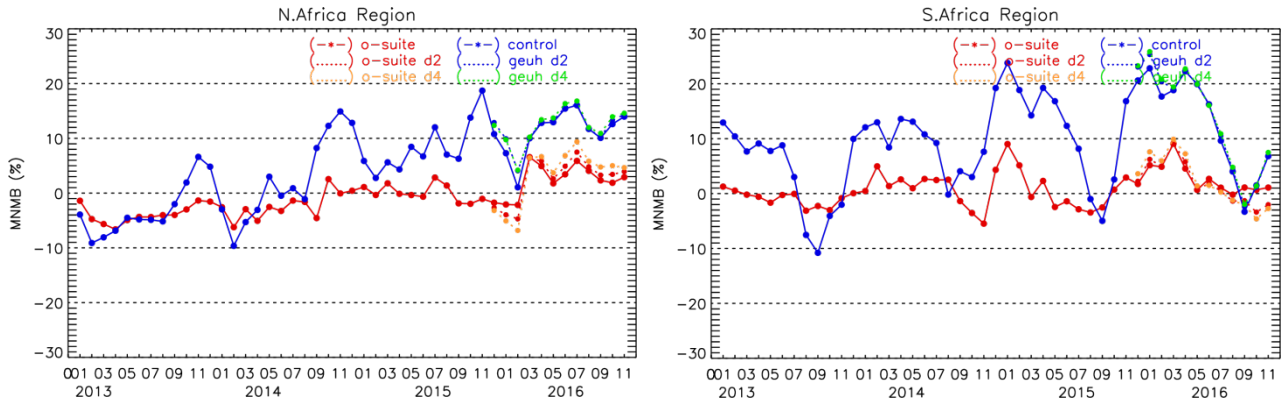

Fig. 3.3.15: Modified normalized mean bias (%) for CO total column from the model simulations vs MOPITT V5 retrievals over selected regions. O-suite (red, solid), control run (blue, solid), o-suite 2nd forecast day (red, dotted), o-suite 4th forecast day (orange, dotted), control 2nd forecast day (blue, dotted), control 4th forecast day (green, dotted).

The modified normalized mean bias (MNMB) of the model runs compared to MOPITT V5 (Fig. 3.3.16) allows quantifying the impact of assimilation on the model performance. All model runs show negative bias over Europe and Alaskan fire regions with some seasonal exceptions. The control run shows systematic positive bias up to 20% over South Asia in November-December 2014, 2015, 2016. Over the southern Africa the control run overestimates satellite retrieved values up to 25% in the seasonal maximums in winter and spring 2015, 2016.

In autumn 2016 the o-suite shows better agreement with the satellite observations than control run over US, Asian and African regions with bias within 10 %. In Asian regions the control run has a systematic positive bias up to 20 % in November. In general, in year 2016 o-suite shows growing positive bias in East Asia within 10 %. The o-suite 2nd and 4th forecast days show growing positive bias up to 5% compared to analysis in Asian and North African regions and negative bias up to 5% in South African region.

3.3.5 Evaluation against TCCON CO

For the validation column averaged mole fractions of CO (denoted as XCO) from the Total Carbon Column Observing Network (TCCON) are used. Column averaged mole fractions provide different information content than the in situ measurements and are therefore complementary to the in situ data. The observations are compared with the high-resolution CO simulations, the o-suite, as well as the control run. At Bialystok and Orleans all model simulations overestimate the XCO (Fig. 3.3.16 and 3.3.17). At Orleans all three models represent the seasonality equally well. At Bialystok the representation of seasonality is worse for the o-suite than for the control run and the high resolution model.

At Reunion (3.3.18) the o-suite captures the seasonality and agrees with the measurements within 5%. The control run as well as the high resolution FC CO model simulations show strong deviations from the measurements. The difference between these two models (control, high resolution) and the measurements show a clear seasonal pattern, which is very similar for the years 2015 and 2016.

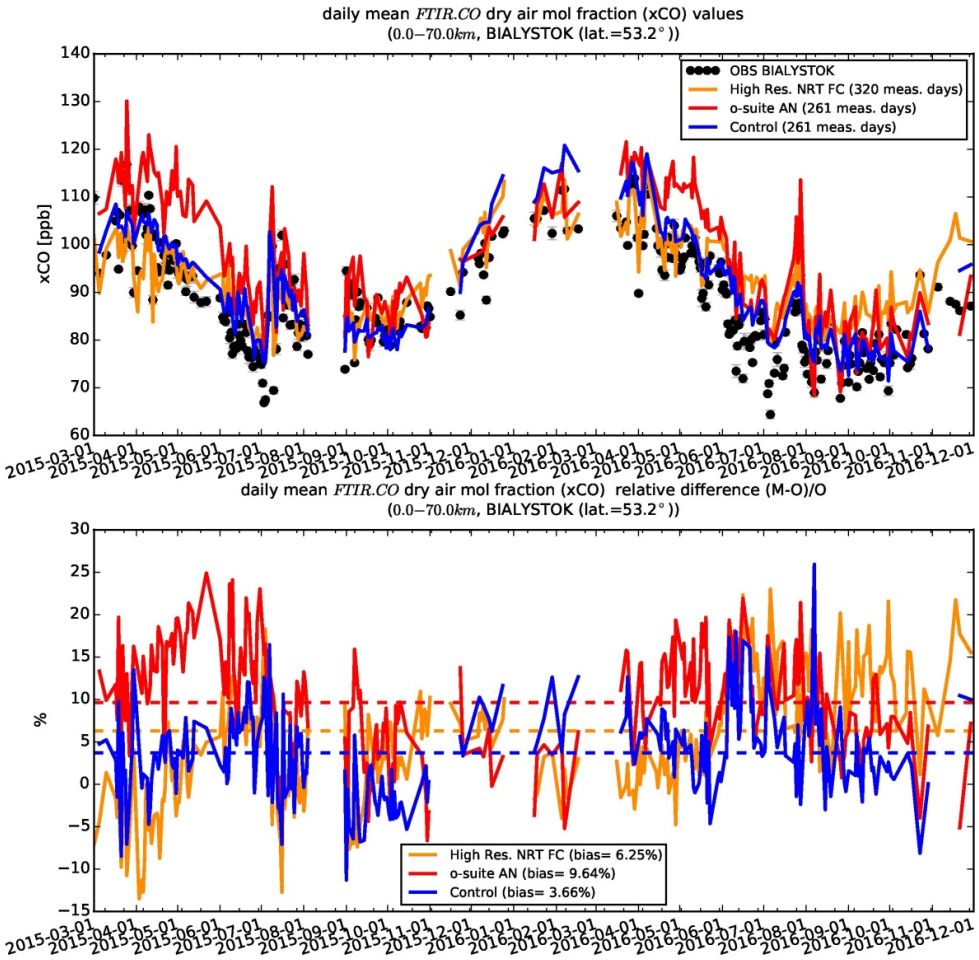

Figure 3.3.16: Time series and relative difference of column averaged mole fractions of carbon monoxide (CO) at the TCCON site Bialystok compared to the o-suite (red), control (blue) and the high resolution NRT FC model (yellow).

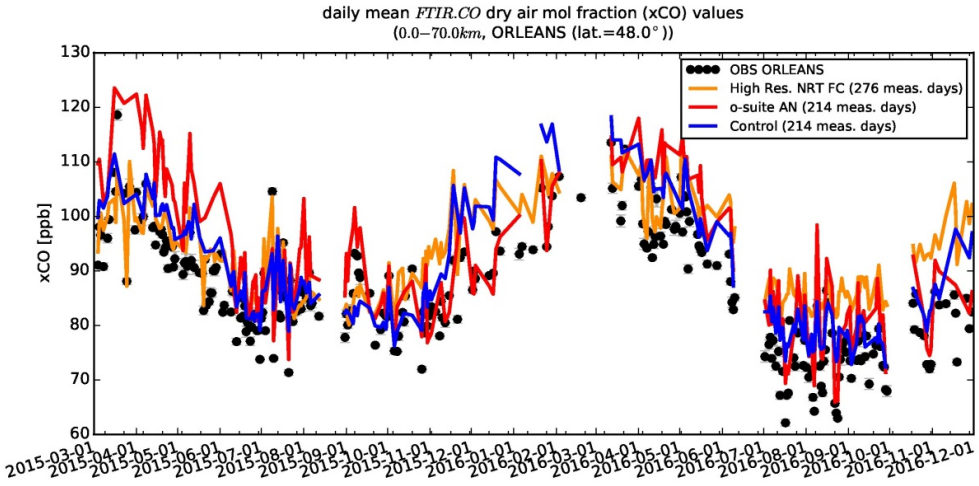

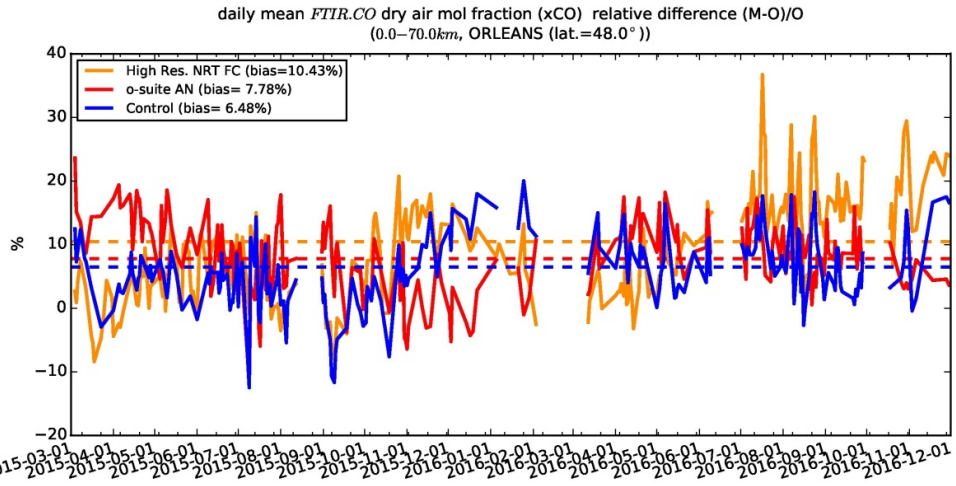

Figure 3.3.17: Time series and relative difference of column averaged mole fractions of carbon monoxide (CO) at the TCCON site Orleans compared to the o-suite (red), control (blue) and the high resolution NRT FC model (yellow).

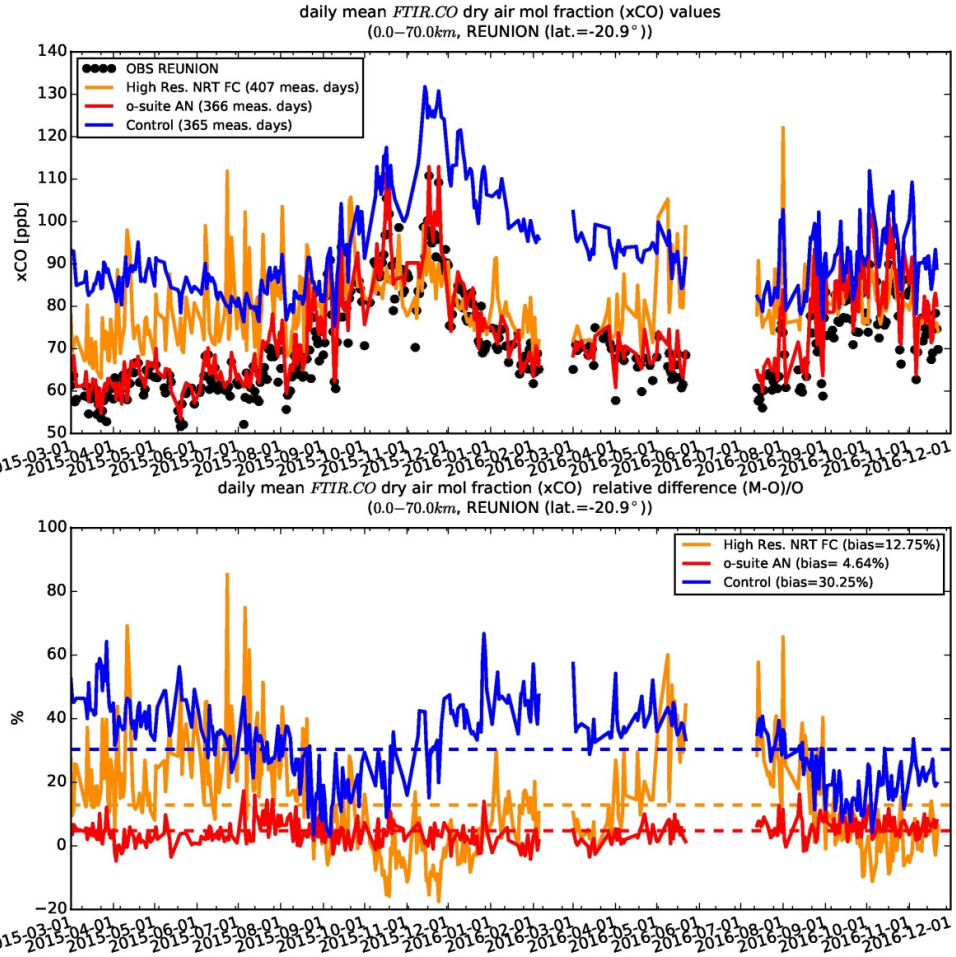

Figure 3.3.18: Time series and relative difference of column averaged mole fractions of carbon monoxide (CO) at the TCCON site Reunion compared to the o-suite (red), control (blue) and the high resolution NRT FC model (yellow).

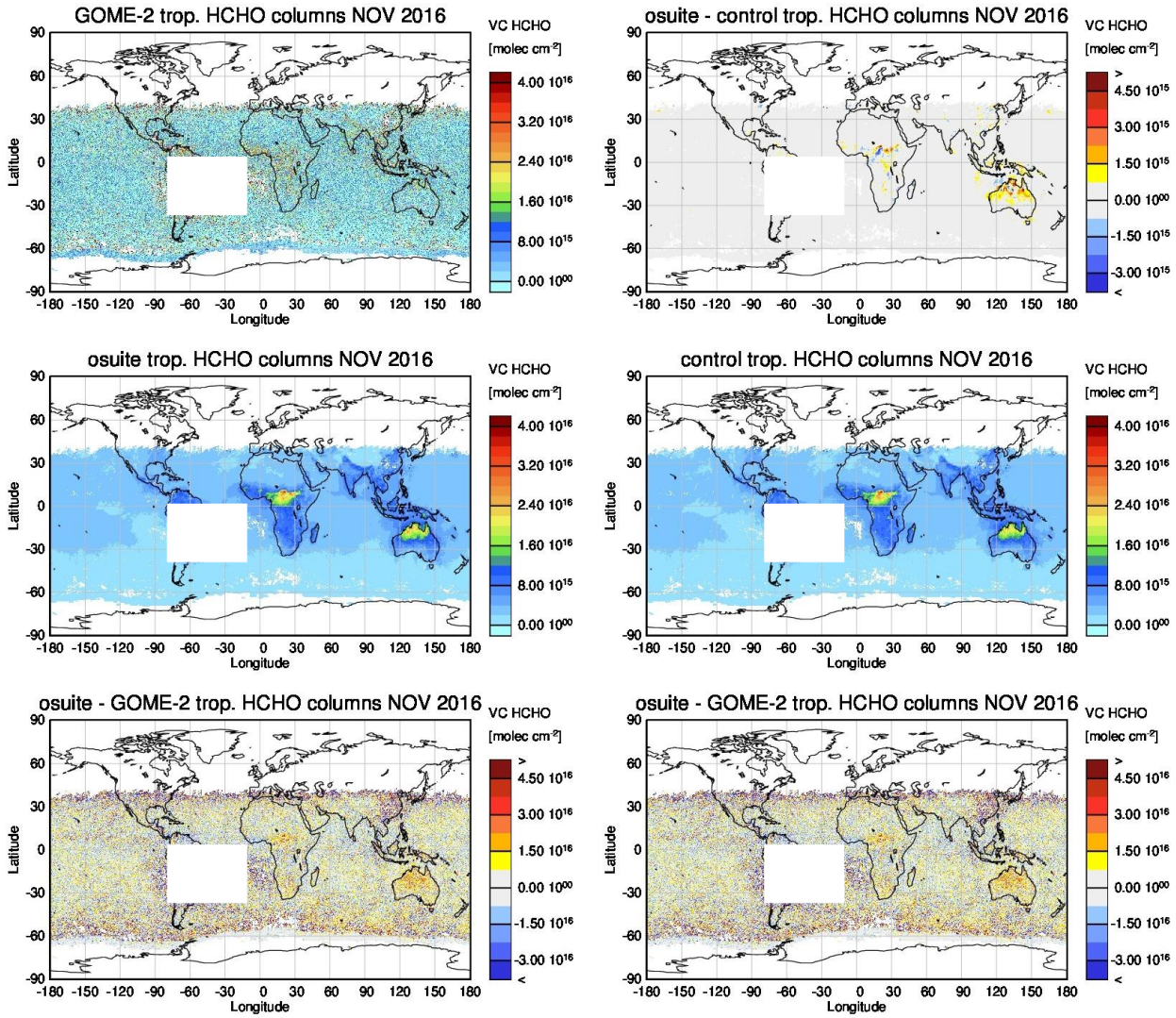

Figure 3.4.1: Global map comparisons of satellite retrieved and model simulated tropospheric HCHO columns [molec cm^{-2}] for November 2016. The top row shows monthly mean tropospheric HCHO columns retrieved by GOME-2, the second row shows the same but for model simulated averages. The third row shows differences of monthly means between models and GOME-2. GOME-2 data were gridded to model resolution (i.e. 0.4° deg x 0.4° deg). Model data were treated with the same reference sector subtraction approach as the satellite data. Satellite retrieved values in the region of the South Atlantic anomaly are not valid and therefore masked out (white boxes in all images except those which show model results only).

3.4 Formaldehyde

3.4.1 Validation against satellite data

In this section, simulations of tropospheric formaldehyde are compared to SCIAMACHY/Envisat HCHO satellite retrievals (IUP-UB v1.0) [Wittrock et al., 2006] for model data before April 2012 and to GOME-2/MetOp-A HCHO data (IUP-UB v1.0) [Vrekoussis et al., 2010] afterwards. As the retrieval is performed in the UV part of the spectrum where less light is available and the HCHO absorption signal is smaller than that of NO_2, the uncertainty of monthly mean HCHO columns is relatively large

(20% – 40%) and both noise and systematic offsets have an influence on the results. However, absolute values and seasonality are retrieved more accurately over HCHO hotspots.

In Figure 3.4.1, monthly mean satellite HCHO columns are compared to model results for November 2016. The magnitude of oceanic and continental background values and the overall spatial distribution are well represented by o-suite and control. Compared to GOME-2 satellite retrievals, there is an overestimation of values for Central Africa which may be due to an overestimation of fire emissions in this region (as for tropospheric NO_2, see section 3.2). There also is an overestimation over North and Central Australia.

Time series in Fig. 3.4.2 highlight three cases:

- East-Asia and the Eastern US, where HCHO is dominated by biogenic emissions. Model results and measurements generally agree rather well. However, all model runs underestimate the yearly cycle over East-Asia since 2012. In contrast to MOZART runs, MACC_CIFS_TM5 overestimates satellite values for the Eastern US since the middle of 2013. However, the newer CIFS-CB05 runs perform well for Eastern US since 2015. For recent years and both regions, there is virtually no difference between the most recent o-suite run with CIFS-CB05 chemistry and the corresponding control runs without data assimilation. The variability or “ups and downs” in HCHO columns observed by GOME-2 since December 2014 is due to the lack of data (caused by instrument degradation) for these regions during Northern Hemisphere winter months (see Figure 3.4.1 for an example). This also explains the negative values in the GOME-2 time series for Eastern US in December 2015 and January 2016. Summertime maxima are still underestimated by the now, higher resolution runs for both regions in 2016.

- North-Africa, where biomass burning as well as biogenic sources largely contribute to HCHO and its precursors. Satellite observations over North-Africa are generally overestimated by CIFS-CB05 chemistry model runs but are in good agreement with the retrievals for the latest higher resolution model versions since July 2016.

- Indonesia, where HCHO is also dominated by biogenic sources and biomass burning. Models generally overestimate satellite values here (by a factor of 3 – 4 in the second half of 2010) and fail to reproduce the observed seasonality. This may be due to the use of fire emissions including El Nino years which experience much larger fire activities. MOZART simulations and observations agree much better since late 2012. CIFS-CB05 runs agree very well with satellite retrieved ones for December 2014 to August 2015. For September and October 2015, satellite retrieved HCHO columns show a pronounced maximum. 2015 was a strong El Nino year, which caused droughts and higher fire activity in Indonesia. As for previous El Nino years, fire emissions used by CIFS-CB05 seem to be largely overestimated, resulting in model simulated HCHO columns which are almost twice as large as those retrieved by GOME-2. Further investigations (see previous reports) show that this is not caused by cloud flagging applied to the satellite and model data. The recent higher resolution runs overestimate values over Indonesia as well.

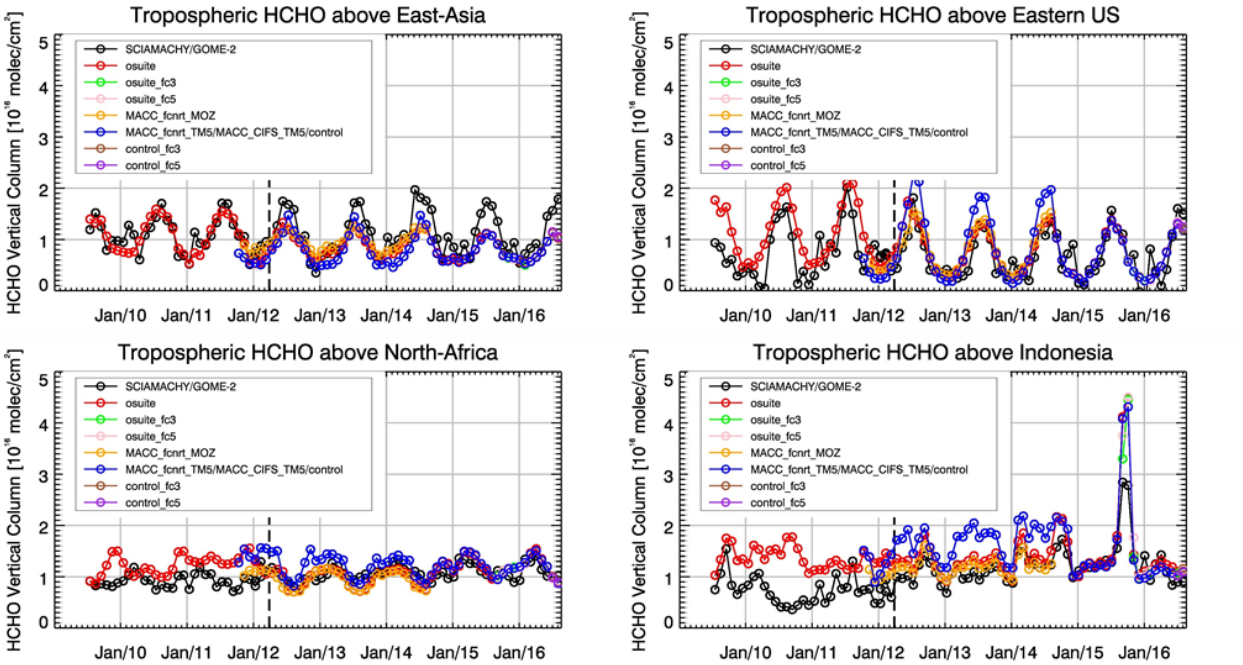

Figure 3.4.2: Time series of average tropospheric HCHO columns [10^{16} molec cm^{-2}] from SCIAMACHY (up to March 2012) and GOME-2 (from April 2012 onwards) compared to model results for different regions. The blue line shows MACC_fcnrt_TM5 from November 2011 to November 2012, MACC_CIFS_TM5 results from December 2012 to August 2014 and control results from September 2014 onwards. The regions differ from those used for NO2 to better focus on HCHO hotspots: East-Asia (25-40°N, 110-125°E), Eastern US (30-40°N, 75-90°W), Northern Africa (0-15°N, 15°W-25°E) and Indonesia (5°S-5°N, 100-120°E). Negative satellite retrieved values over Eastern US are due to a lack of data (caused by instrument degradation) during Northern Hemisphere winter months for this region. Vertical dashed black lines mark the change from SCIAMACHY to GOME-2 based comparisons in April 2012.

Details on the HCHO evaluation can be found at:
http://www.doas-bremen.de/macc/macc_veri_iup_home.html.

3.4.2 Validation against UVVIS DOAS observations from the NDACC network

In this section, we compare the HCHO profiles of the CAMS models with UVVIS DOAS measurements at Haute Provence (43.9°N, 5.71°E, rural station, altitude 650m) and Xianghe (39.8°N, 117°E, station near Beijing, altitude 92m). Due to instrument failure, the Uccle (50.8°N, 4.36°E, urban) measurements are not displayed. These ground-based, remote-sensing instruments are sensitive to the HCHO abundance in the lower troposphere, up to 1km altitude. Tropospheric HCHO profiles and columns are validated (up to 3.5km). A description of the instruments and applied methodologies is the same as for the MWR O_3 and FTIR O_3 and CO validations see http://nors.aeronomie.be. It is important to mention here that the model partial column values between the surface and 3.5 km are calculated for the smoothed model profiles (see Figure 3.4.3, left). This guarantees that the model levels where the measurement is not sensitive do not contribute to the observed bias. In this specific situation the smoothing of the model profiles implies a strong increase of the model column data by the MAXDOAS apriori (and only the relative difference plots should be considered). We should mention that the measurement data is still catalogued as rapid delivery and not in the consolidated NDACC database. The measurements have

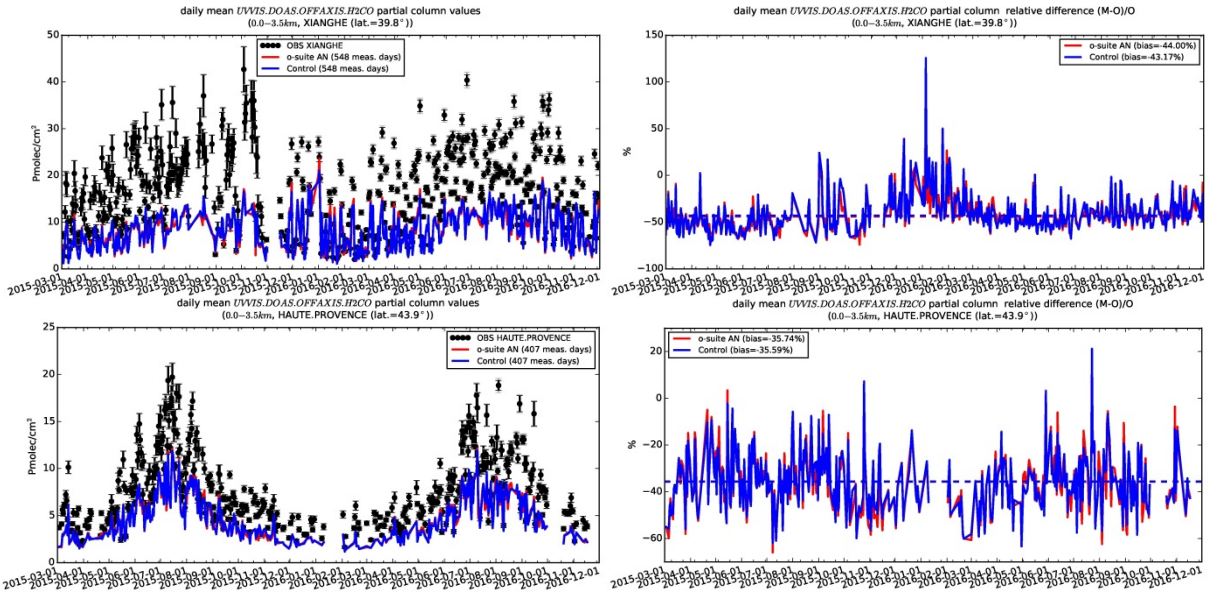

Figure 3.4.3: Daily mean relative differences of tropospheric HCHO columns (till 3.5km) by the o-suite (red) and the control run (blue) compared to NDACC UVVIS DOAS data at at Xianghe (39.8°N, 117°E, station near Beijing, altitude 92m) and Haute Provence (43.9°N, 5.71°E, rural station, altitude 650m, bottom) for the period March. 2015 –November 2016. The number of measurements and median of differences is indicated in the legend (the overall measurement uncertainty is 10%).

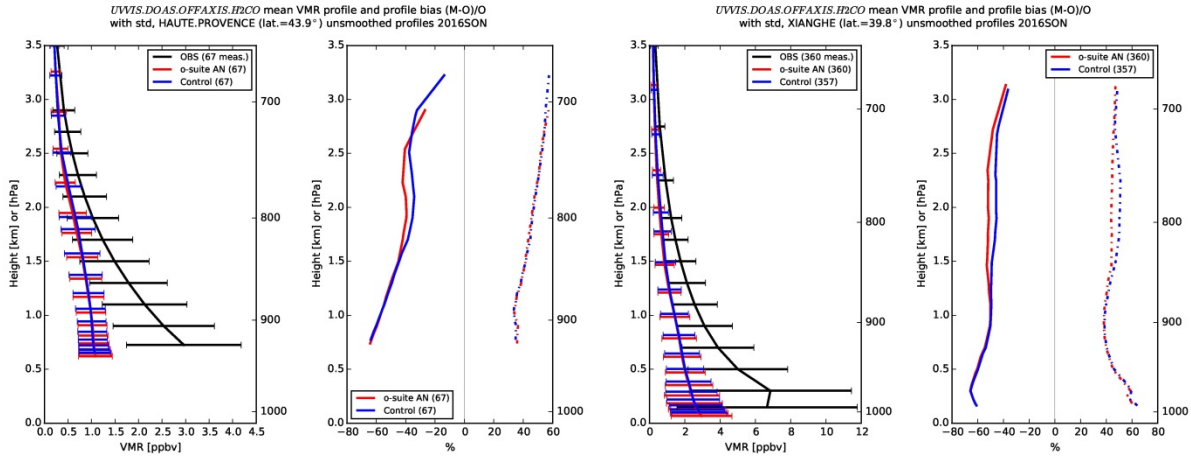

Figure 3.4.4: Mean tropospheric HCHO profiles by the o-suite (red) and the control run (blue) compared to NDACC UVVIS DOAS data at Haute Provence (43.9°N, 5.71°E, left) and at Xianghe (39.8°N, 117°E, right) for the period SON 2016.

been quality filtered on cloud conditions: only measurements under “clear sky” and “thin clouds” are used (see Gielen et al., 2014).

From Fig. 3.4.3 and 3.4.4 we see little difference between the o-suite and the control run. Both models underestimate the observations below 1km. Although the background column values are well captured by the models, the high emission events are not (see Fig. 3.4.4).

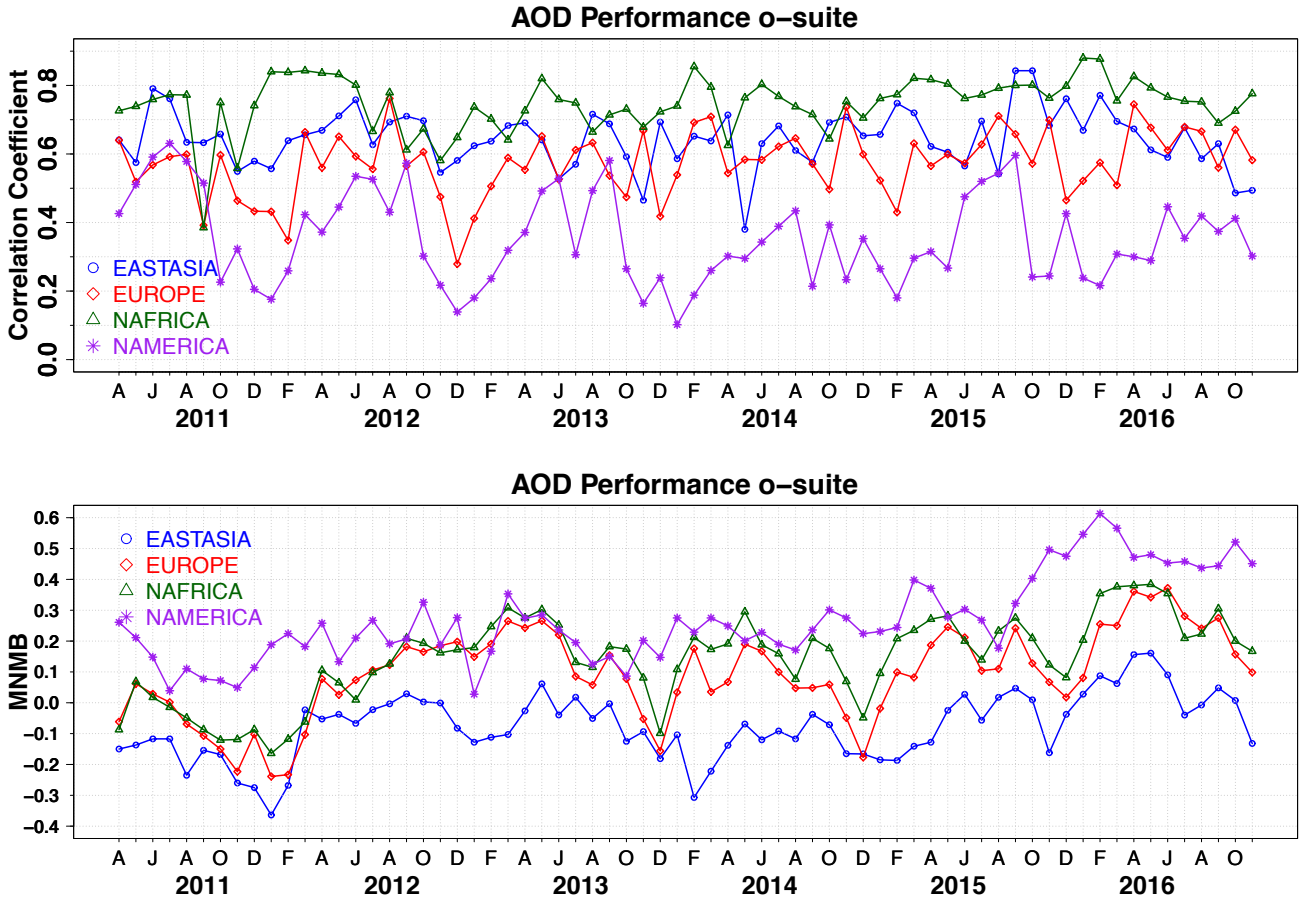

Figure 3.5.1 a) Correlation coefficient and b) modified normalized mean bias (MNMB) in AOD, since 2011, based on daily AOD comparison in four world regions [Eastasia(blue); Europe(red); NAfrica(green); NAmercia(purple)] for the o-suite.

3.5 Aerosol

3.5.1 Global comparisons with Aeronet and PM

Standard scores, maps, scatterplots, bias maps, time series comparison and histograms illustrating the performance of the aerosol simulation in the IFS system are made available through the AeroCom web interface:
http://aerocom.met.no/cgi-bin/aerocom/surfobs_annualrs.pl?PROJECT=CAMS&MODELLIST=CAMS-VALreports . The model run can be compared to the MACC reanalysis (available until Dec 2012) and the AeroCom Median model. A daily updated comparison against 30 selected Aeronet stations is available via the ECMWF CAMS service website:
http://www.copernicus-atmosphere.eu/d/services/gac/verif/aer/nrt/.

Correlation, based on daily aerosol optical depth and NRT Aeronet observations, is rather stable since 2011, exhibits significant variation and seems to have increased recently. The o-suite forecast at +3 days shows slightly lower correlation, as expected. See figure S3. Part of the month-to-month variation in correlation is due to the limited quality of the NRT Aeronet data, which are of preliminary nature. Retrospective analysis since the year 2011 shows that this level 1.5 NRT AOD

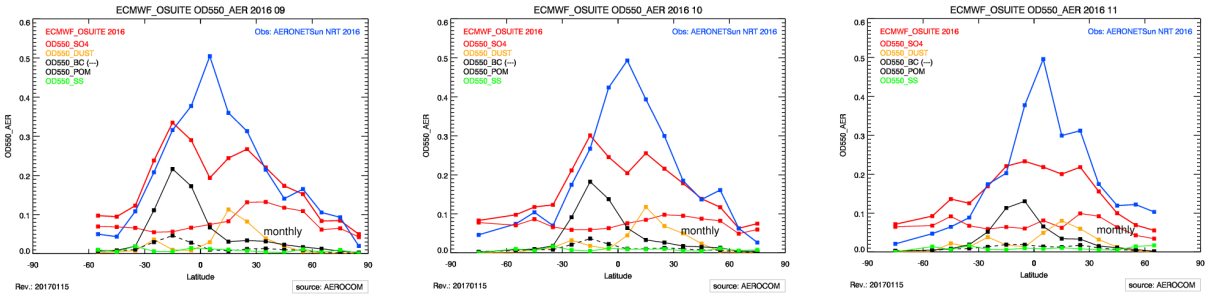

Figure 3.5.2: Aerosol optical depth of o-suite (red) compared to latitudinally aggregated NRT Aeronet level 1.5 data (blue) for the three months covered by this report.

Aeronet data, due to undetected cloud contamination and any uncorrected drift, are on global average +20% higher than quality assured level 2.0 data. However, using the MNMB bias score such bias is not as visible, because outliers have less impact. Since 2014 the CAMS model MNMB type of bias against level 2.0 data was +5-10% higher than that against level 1.5 data (see figure S3). Figure S3 also shows the evaluation against level 2.0 data for the whole time period. Note that an establishment of a more precise correction of bias in the most recent months is rather difficult because of few level 2.0 data being available.

The regional performance of the o-suite model exhibits some seasonal cycle in AOD depending on region (Fig. 3.5.1 a). For instance, the model performance in the North American winter season with respect to correlation seemed to be worst in 2011-2013 but seems to be more balanced now. Noteworthy is the persistent AOD overestimation over North America (Fig. 3.5.1 b). The latitudinal display of model and Aeronet AOD in the period investigated here (Fig. 3.5.2) shows the negative bias against Aeronet NRT in tropical and sub-tropical regions.

The simulated aerosol size distribution may be validated to first order using the wavelength dependent variation in AOD, computed as Ångström exponent, with higher Ångström exponents indicative of smaller particles. Figure 3.5.3 a) shows the temporal evolution of simulated and observed mean Ångström exponent, while the correlation is found in figure 3.5.3 b). We find in SON 2016 a positive bias of +22% (against -5% before October 2013). Temporal and spatial variability is rather high and correlation is lower than for AOD (Figure 3.5.3 b). Figure 3.5.4 shows that the Oct 2013 model changes are responsible for this shift in Ångström exponent. Less sea salt and more sulphate shift the size distribution to smaller sizes. AOD due to sea salt decreased by 50%, that to due organics decreased by 25%, while that of sulphate increased by 40%.

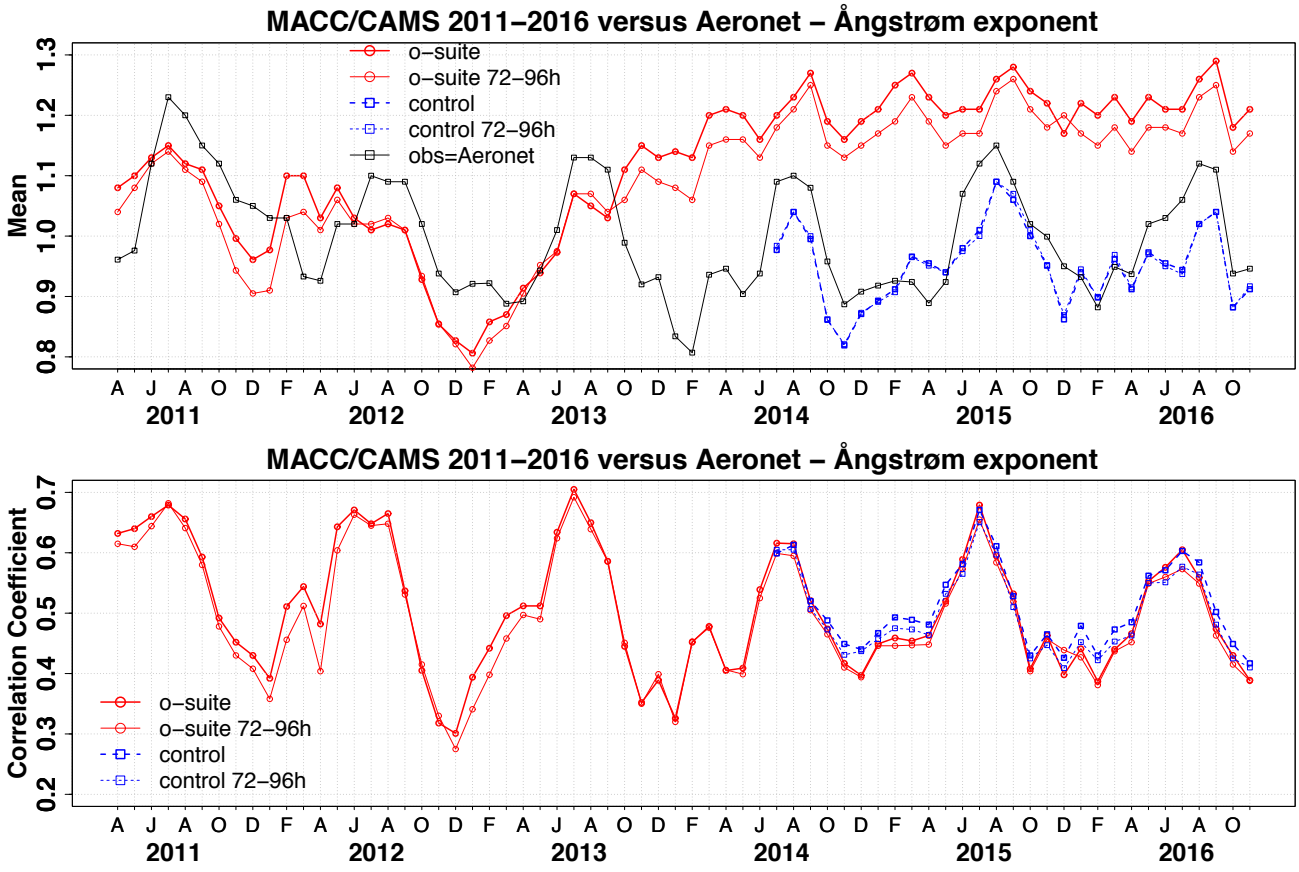

Figure 3.5.3 a) Evolution of mean Ångström exponent in o-suite and control at Aeronet sites, based on matching monthly mean values. o-suite (thick red curve); o-suite at last forecast day (light red curve); control (blue dashed curve); control at last forecast day (light blue dashed curve). b) Correlation using daily matching Ångström exponent.

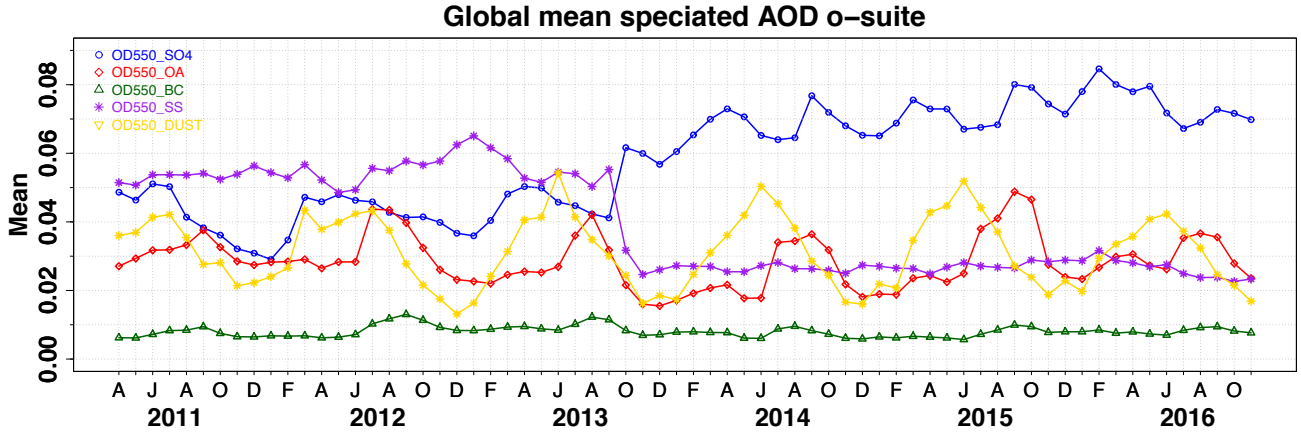

Figure 3.5.4: Evolution of aerosol component's AOD@550nm [OD550_SO4 = sulphate(blue); OD550_OA = organics(red); OD550_BC = black carbon(green); OD550_SS = sea salt(purple); OD550_DUST = dust(yellow)].

Table 3.5.1: Mean global total and speciated AOD in the o-suite for the last two periods covered by the VAL report and change after 3 forecast days.

	o-suite		o-suite	
	Mean JJA 2016 0-24h	Change wrt to first day on day 4	Mean SON 2016 0-24h	Change wrt to first day on day 4
AOD@550	0.173	-12%	0.153	-6%
BC-OD@550	0.008	-21%	0.008	-15%
Dust-OD@550	0.037	8%	0.021	38%
OA-OD@550	0.033	-15%	0.029	3%
SO4-OD@550	0.069	-22%	0.071	-25%
SS-OD@550	0.025	-4%	0.023	8%

The o-suite uses data assimilation to obtain a first guess aerosol field. In the forecast period, however, a-priori model parameterisations and emissions (except fire emissions, which are kept in the forecast equal to the latest GFAS emission values) determine more and more the shape and amplitude of the aerosol fields. The performance of the day three forecasted AOD fields as compared to the first guess is shown in Figure S3 in the summary of this report. Table 3.5.1 shows an average global decrease in total aerosol optical depth of 12% during the first four forecast days, dominated by sulphate and organics. Against Aeronet the o-suite forecast for day three has little overall positive bias in AOD. The control run with no assimilation shows significant less AOD (-50% compared to o-suite, see figure S3). All this supports the conclusion that either a-priori IFS aerosol and aerosol precursor sources are too small or sinks are to effective in the IFS model.

Surface concentration of particulate matter below 10 µm (PM10) from the o-suite experiment have been validated against data from 150 background IMPROVE and EMEP stations (figure 3.5.5). A climatological average has been constructed from data in the period 2000-2009 as available in the EBAS database hold at NILU. The data coverage is not the same at all stations, and sometimes covers only a few years. All used time series used are documented via the CAMS-AeroCom web interface.

In contrast to earlier validation reports we have taken since 2016 the PM10 concentrations as diagnosed by the IFS model in the mars archive, while before we have constructed a high-biased “PM10” concentration using all available IFS aerosol mass. This changes the bias evaluation considerably. The bias maps show that both in North America and Europe still some high bias appears at few stations located in regions close to the coastlines. This is an indication that simulated PM10 concentrations may be high due to sea salt aerosols. Regional models using the sea salt concentrations as boundary condition should take over the PM10 definition as used in IFS. Inner-continental sites indicate a negative MNMB bias of -30% both in Europe and North America.

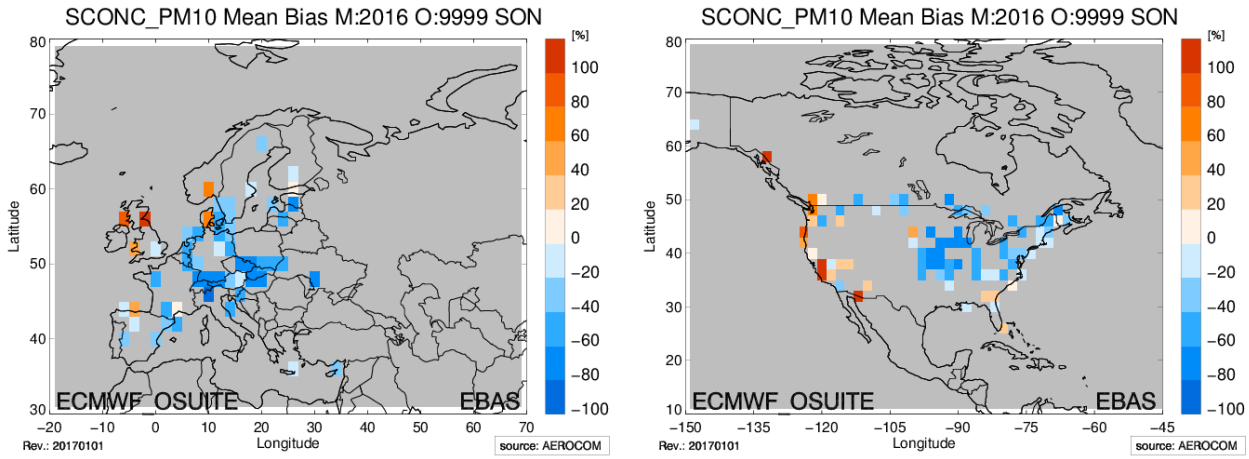

Figure 3.5.5: Bias [%] map of September/October/November mean PM 10 concentrations at EMEP (Europe) and IMPROVE sites (North America); simulated o-suite versus climatological average (2000-2009).

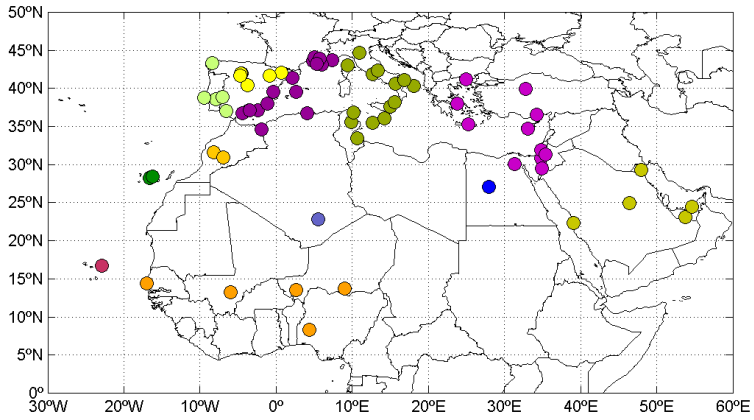

Figure 3.5.6: Map of 71 AERONET level-1.5 stations used in this analysis. The twelve regions considered in the analysis are shown by different colours.

3.5.2 Dust forecast model intercomparison: Validation of DOD against AERONET, and comparisons with Multimodel Median from SDS-WAS

72 hour forecasts (on 3-hourly basis) dust aerosol optical depth (DOD) from CAMS o-suite and control experiments have been validated for the period 1 September – 30 November 2016 against 71 AERONET stations grouped in twelve regions (Fig. 3.5.6), MODIS aerosol product available through the NASA's EOSDIS system (MCDAODHD files) and compare with the SDS-WAS Multi-model Median DOD. The SDS-WAS Multi-model Median DOD is obtained from twelve dust prediction models participating in the Sand and Dust Storm Warning Advisory and Assessment System (SDS-WAS) Regional Center for Northern Africa, Middle East and Europe (http://sds-was.aemet.es/).

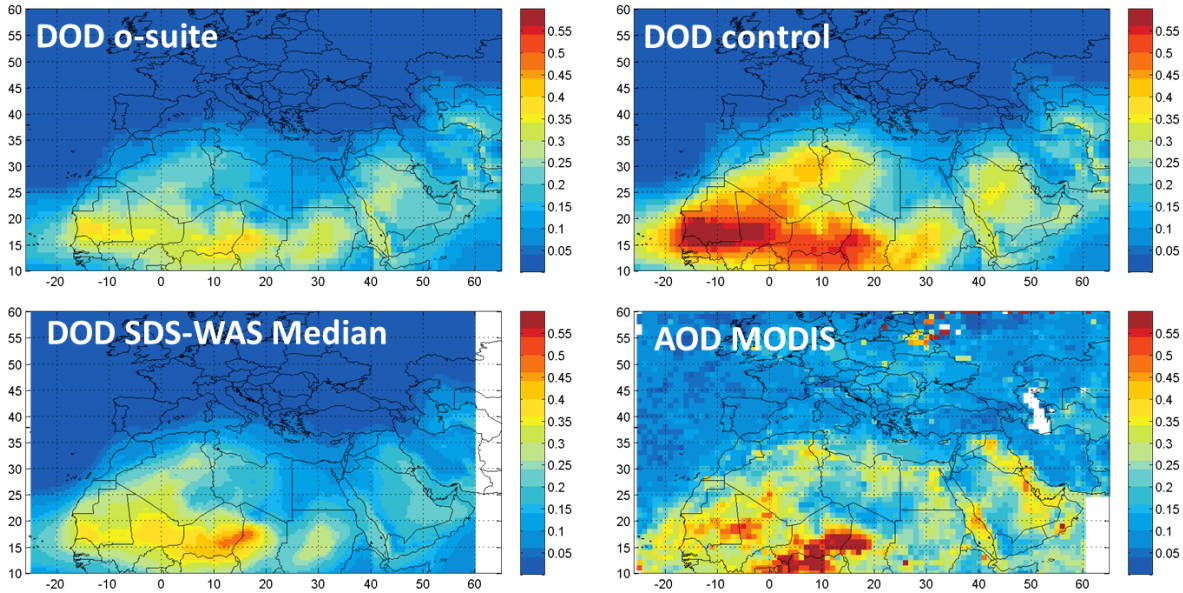

Figure 3.5.7: Averaged DOD 24h forecast from o-suite (top left) and control (top right) as well as DOD of the multi-model SDS-WAS Median product (bottom left) and AOD from MODIS combined Dark target and Deep Blue product (bottom right) from September 1 to November 30, 2016.

During the period of analysis, during this period dust activity is low in comparison the previous season. Satellites (see MODIS in Fig. 3.5.7) show that major dust activity is concentrated over the Sahara (in the Bodelé Basin and the Mali/Mauritania border), the dust corridor of North Western Maghreb and Iraq. CAMS model can simulate the main areas of dust activity in comparison with MODIS, although o-suite reduces the strong overestimations observed in control, some important dust sources (as the Bodélé and Iraq) appear underestimates.

Table 3.5.2: Skill scores (MB, FGE, RMSE and r) of 24h forecasts for CAMS o-suite, CAMS control and SDS-WAS Multi-model Median for the study period, and the number of data (NDATA) used. Dust AOD (DOD) from AERONET is the reference.

		control				o-suite DOD				SDS-WAS Median DOD			
	NDATA	MB	FGE	RMSE	r	MB	FGE	RMSE	r	MB	FGE	RMSE	r
Western Mediterranean	1919	-0.02	1.64	0.16	0.49	-0.05	1.70	0.17	0.51	-0.04	1.68	0.16	0.49
Tropical North Atlantic	198	0.05	0.38	0.28	0.44	-0.15	0.47	0.29	0.56	-0.16	0.47	0.30	0.48
Eastern Mediterranean	1200	0.02	1.42	0.14	0.61	-0.02	1.44	0.13	0.62	-0.03	1.45	0.13	0.63
Sahel	1236	-0.04	0.43	0.44	0.23	-0.23	0.50	0.48	0.41	-0.18	0.38	0.44	0.45
Subtropical North Atlantic	417	0.02	1.29	0.10	0.53	-0.01	1.26	0.07	0.53	-0.02	1.26	0.06	0.56
Central Mediterranean	1685	0.02	1.36	0.22	0.60	-0.06	1.41	0.20	0.61	-0.05	1.34	0.20	0.59
Middle East	662	-0.03	0.97	0.31	0.38	-0.05	1.03	0.32	0.35	-0.08	1.02	0.31	0.48
Iberian Peninsula	871	-0.03	1.83	0.15	0.38	-0.04	1.86	0.15	0.38	-0.04	1.85	0.15	0.36
Western Iberian Peninsula	598	-0.04	1.65	0.17	0.48	-0.06	1.69	0.18	0.47	-0.06	1.70	0.18	0.46
North Western Maghreb	419	0.00	0.80	0.22	0.38	-0.10	0.91	0.22	0.44	-0.09	0.81	0.22	0.44
Sahara	307	0.10	0.48	0.18	0.46	-0.07	0.39	0.14	0.57	-0.06	0.34	0.14	0.55
Eastern Sahara	207	0.06	1.01	0.15	0.44	-0.01	0.91	0.11	0.53	0.00	0.87	0.12	0.50

From September to November, o-suite is the model that best reproduces the daily variability of AERONET observations with a correlation coefficient of 0.64 in average for all the AERONET sites. The performance of o-suite is particularly good over Sahel and Sahara regions (with correlation values of 0.41 and 0.57, respectively, see Table 3.5.2 as well as Tamanrasset and Banizoumbou AERONET sites in Fig. 3.5.8) achieving close values similar to the SDS-WAS Median Multimodel (with correlation values of 0.45 and 0.55, respectively for Sahel and Sahara). Furthermore, over Sahara with a decrease of MB from 0.10 to -0.07 for control and o-suite respectively. Otherwise, in the Middle East, controls shows slightly better performance scores than o-suite with a decrease of the correlation coefficient from 0.38 to 0.35 and an increase of MB from -0.03 to -0.05 (see Table 3.5.2 and in Mezaira AERONET site in Fig. 3.5.9).

Over long-range transport regions, o-suite shows the best correlations in all the regions (with correlations between 0.38 in Iberian Peninsula to 0.62 in Eastern Mediterranean, see Table 3.5.2 and Forth Crete and Tunis Carthage in Fig. 3.5.9) in comparison with control. The skill scores of the o-suite in the Mediterranean are slightly better to those obtained by the SDS-WAS Median Multimodel (see Table 3.5.2). The lower performance scores observed in Iberian Peninsula and Western Mediterranean are linked to the low dust activity observed during the period of analysis (see Granada in Fig. 3.5.8)

Table 3.5.3: Skill scores (MB, FGE, RMSE and r) of 48h and 72h forecasts for CAMS o-suite and CAMS control for the study period, and the number of data (NDATA) used. Dust AOD (DOD) from AERONET is the reference.

		48h control				48h o-suite				72h control				72h o-suite			
	NDATA	MB	FGE	RMSE	r	MB	FGE	RMSE	r	MB	FGE	RMSE	r	MB	FGE	RMSE	r
Western Mediterranean	1919	-0.02	1.68	0.17	0.41	-0.05	1.74	0.17	0.40	-0.02	1.73	0.19	0.25	-0.04	1.78	0.18	0.23
Tropical North Atlantic	198	0.02	0.49	0.32	0.28	-0.16	0.57	0.32	0.33	-0.02	0.59	0.34	0.13	-0.16	0.69	0.35	0.18
Eastern Mediterranean	1200	0.02	1.49	0.17	0.35	-0.02	1.51	0.15	0.39	0.02	1.57	0.20	0.15	-0.02	1.60	0.17	0.19
Sahel	1236	-0.05	0.43	0.45	0.20	-0.23	0.50	0.49	0.28	-0.05	0.46	0.46	0.16	-0.21	0.53	0.49	0.20
Subtropical North Atlantic	417	0.01	1.37	0.11	0.30	-0.02	1.36	0.08	0.26	0.02	1.47	0.13	0.15	-0.02	1.45	0.10	0.09
Central Mediterranean	1685	0.03	1.44	0.25	0.49	-0.05	1.46	0.21	0.48	0.03	1.51	0.29	0.31	-0.04	1.54	0.25	0.27
Middle East	662	-0.04	0.99	0.32	0.33	-0.06	1.05	0.32	0.35	-0.03	1.03	0.33	0.25	-0.06	1.07	0.33	0.26
Iberian Peninsula	871	-0.03	1.84	0.15	0.40	-0.04	1.88	0.16	0.38	-0.03	1.88	0.16	0.26	-0.04	1.91	0.16	0.26
Western Iberian Peninsula	598	-0.04	1.71	0.18	0.40	-0.06	1.75	0.19	0.39	-0.05	1.76	0.20	0.24	-0.07	1.79	0.20	0.26
North Western Maghreb	419	-0.02	0.86	0.22	0.38	-0.10	1.01	0.23	0.37	-0.03	0.91	0.23	0.31	-0.10	1.06	0.24	0.31
Sahara	307	0.09	0.51	0.19	0.34	-0.04	0.40	0.15	0.39	0.08	0.55	0.20	0.21	-0.02	0.44	0.16	0.28
Eastern Sahara	207	0.05	1.02	0.17	0.26	-0.01	1.03	0.14	0.21	0.03	1.03	0.16	0.20	-0.02	1.06	0.14	0.20

Finally, the comparison of 48h and 72h forecasts for both CAMS experiments shows that meanwhile the MB, RMSE and FGE is stable during the 3-days forecasts, the correlation is reduced drastically from 24h to 72h in all the regions (see Table 3.5.2 and Table 3.5.3). It is worthy to highlight the slightly higher correlation values of o-suite respect control for 48h and 72h forecast in Sahara and Sahel (see Table 3.5.3).

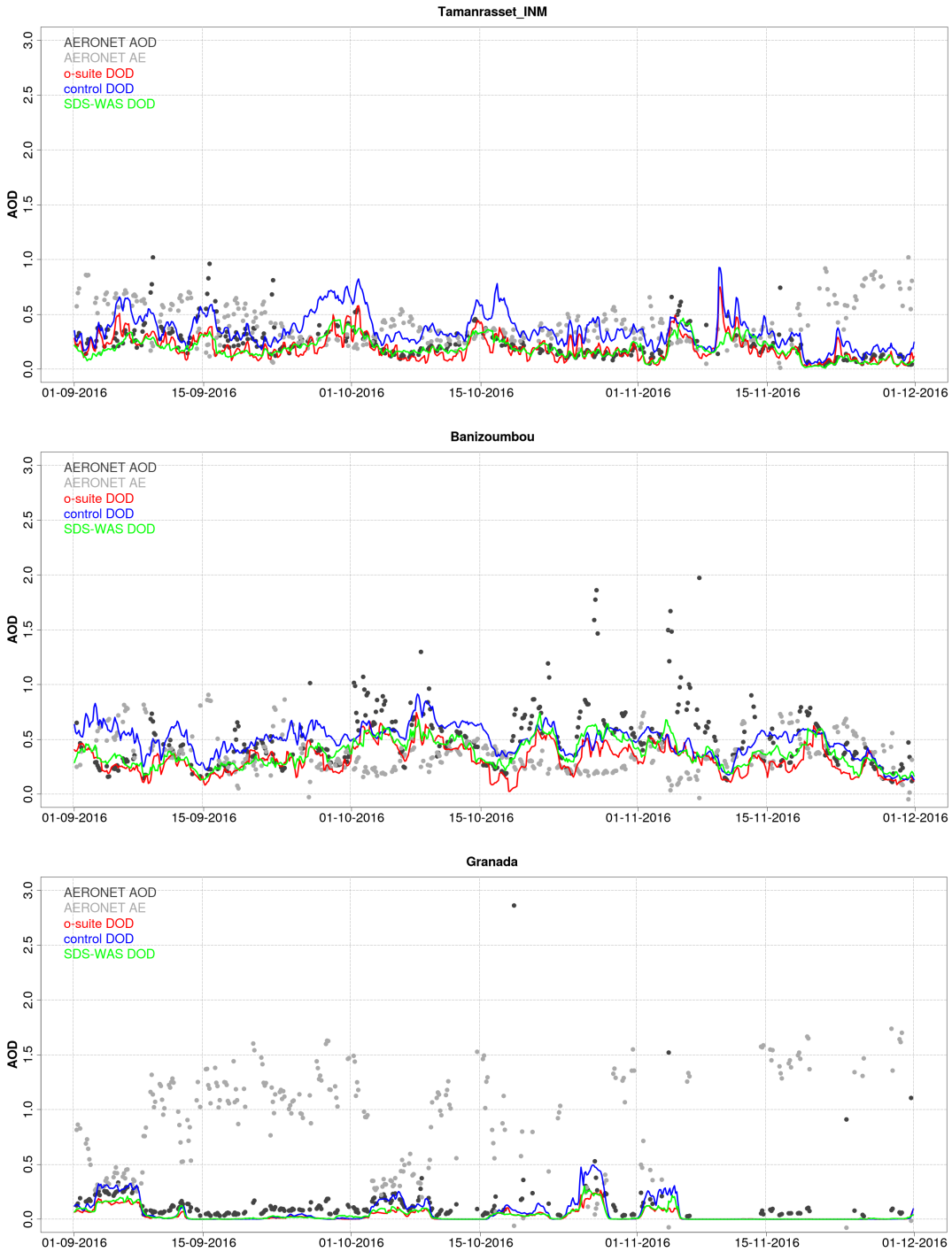

Figure 3.5.8: AOD from AERONET (black dots), DOD o-suite (red line), DOD control (blue line) and DOD Multimodel SDS-WAS Median (green line) for the study period over Tamanrasset (Sahara), Banizoumbou (Sahel) and Granada (Western Mediterranean).

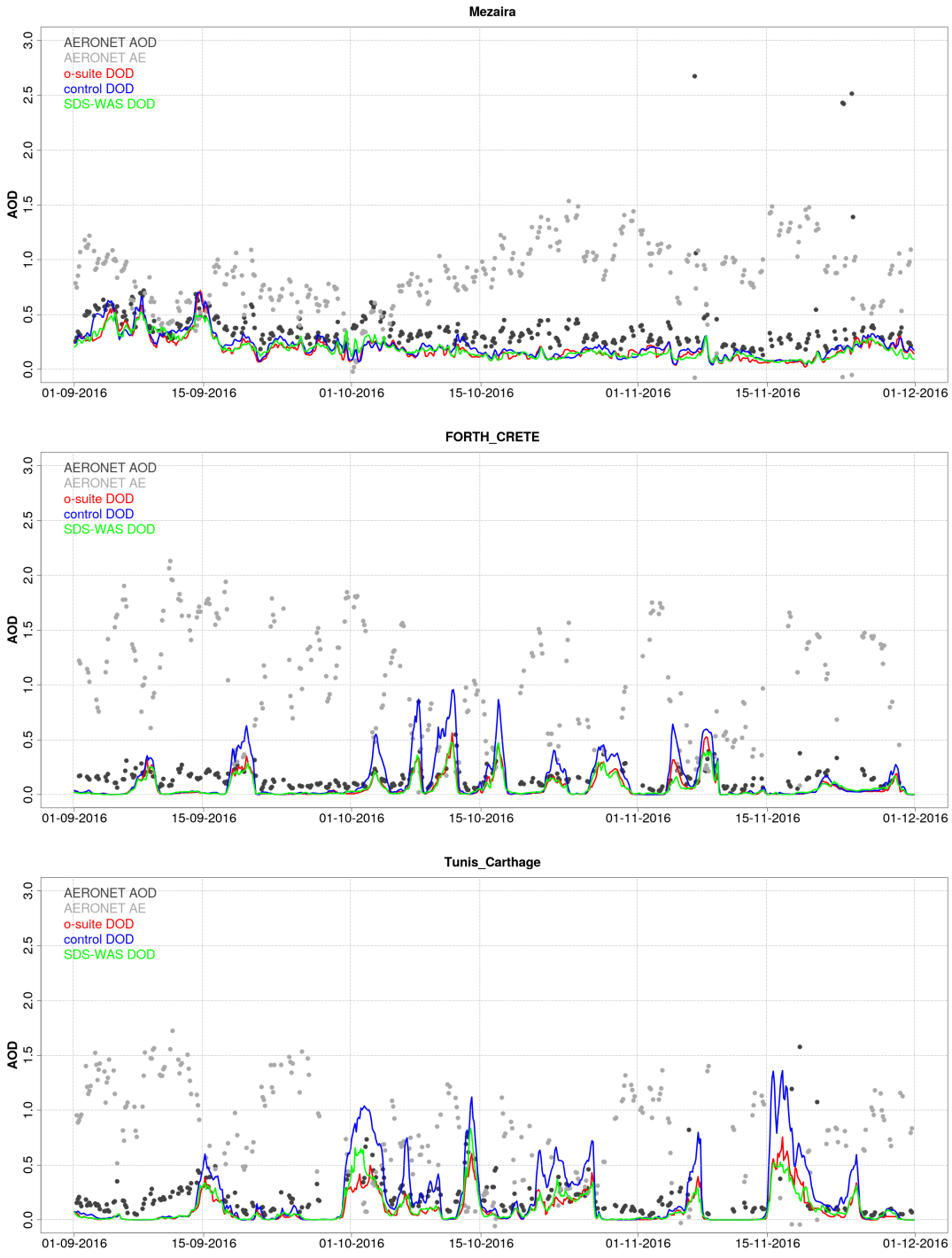

Figure 3.5.9: AOD from AERONET (black dots), DOD o-suite (red line), DOD control (blue line) and DOD Multimodel SDS-WAS Median (green line) for the study period over Mezaira (Middle East), Forth Crete (E. Mediterranean) and Tunis-Carthage (Central Mediterranean).

3.5.3 Aerosol validation over the Mediterranean

Daily aerosol optical depth (AOD) and surface concentration (PM10 and PM2.5) from o-suite experiment (Morcrette et al., 2009; Benedetti et al., 2009) and control experiment have been validated against 37 AERONET and 18 Airbase stations in the Mediterranean region for the period 1 September – 30 November 2016. The main goal is to know the behaviour of AOD and surface concentration (PM2.5 and PM10) from o-suite and control over the Mediterranean. In this report, we validate CAMS o-suite and control experiments using AERONET and Airbase observations as the reference.

Aerosol optical depth

3-hourly values of AOD from AERONET, o-suite and control for the period 1 September – 30 November 2016 over selected sites are shown in Fig. 3.5.10 and Fig. 3.5.11. For this period, CAMS o-suite is the model that best reproduces the daily variability of AERONET observations (see the correlation coefficient in Fig. 3.5.10). In average for all the sites, MB decreases from -0.00 for control to -0.01 for o-suite; and correlation increases from 0.58 for control to 0.62 for o-suite. The highest peaks on CAMS AOD simulations are linked to natural sources (see Fig. 3.5.11). Overestimations in Central Mediterranean observed in control are reduced in o-suite, although, o-suite shows overestimations in Western and Central Mediterranean. This is in agreement with the FGE values (see Fig. 3.5.10). Poor scores are observed in o-suite in Northwestern Mediterranean are linked to overestimations the observed AERONET values (see Fig. 3.5.10). These overestimations are systematically observed during background situations (see Toulon in Fig. 3.5.11).

Surface aerosol concentrations

3-hourly values of PM10/PM2.5 from Airbase, o-suite and control for the period 1 September – 30 November 2016 over selected sites are shown in Fig. 3.5.12. In general, CAMS o-suite presents better results regarding load concentrations reducing the observed overestimations both PM10 and PM2.5 (see Fig. 3.5.12). In average for all the sites, PM10 2.27 µg/m3 for control to -0.01 µg/m3 for o-suite. From September to November 2016, CAMS experiments reproduce the daily variability of the most intense aerosol events observed by Airbase sites (see Hospital Joan March, Venaco and Gharb stations in Fig. 3.5.13) although both CAMS experiments tend to overestimate the observed values. Like previous seasons, CAMS model reproduces extreme peaks particularly over maritime sites that are not observed in the Airbase stations. These peaks are reduced in CAMS o-suite providing better results than control.

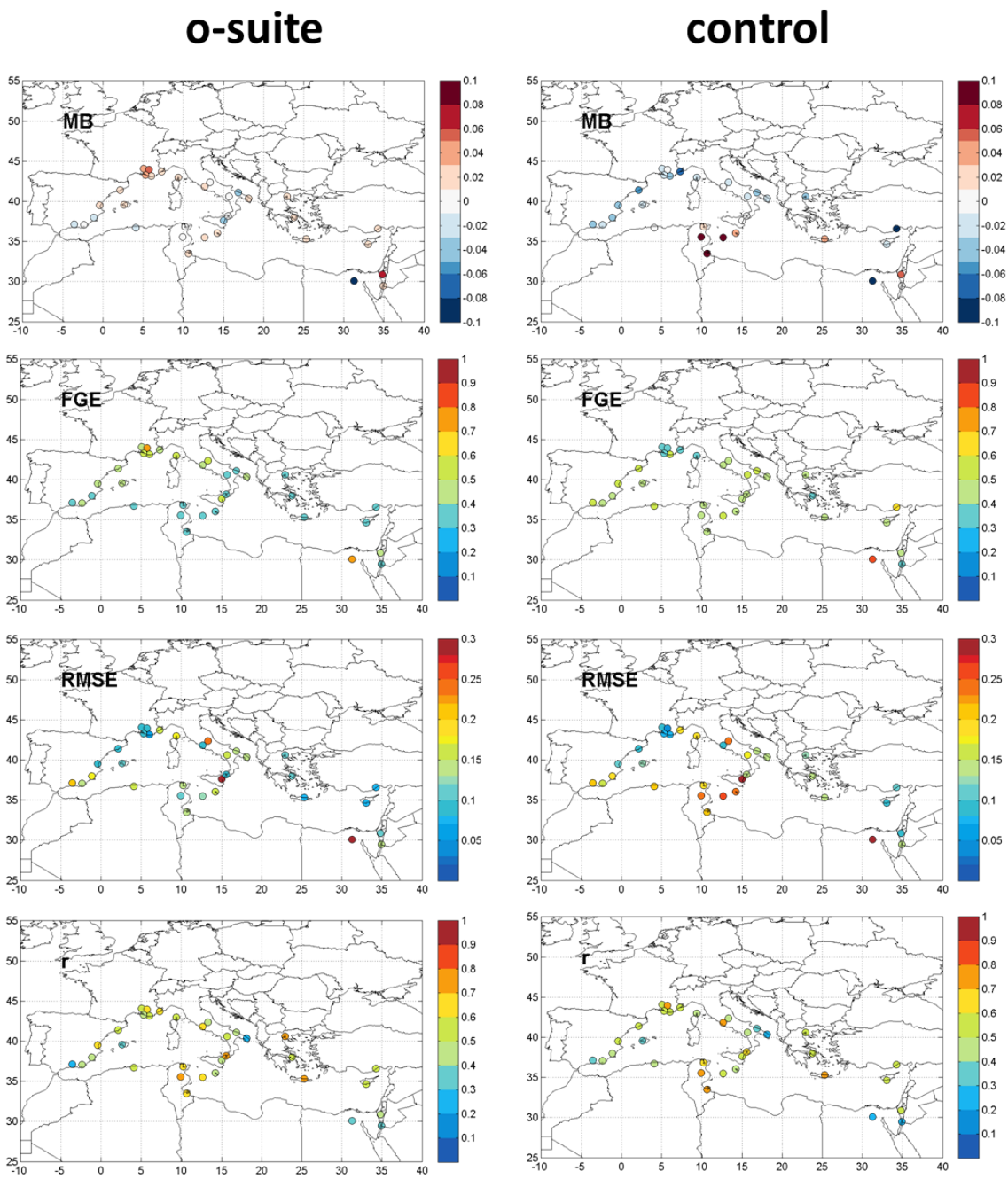

Figure 3.5.10: Skill scores (MB, FGE, RMSE and r) for 24-hour forecasts of CAMS o-suite and control for the study period. AOD from AERONET is the reference.

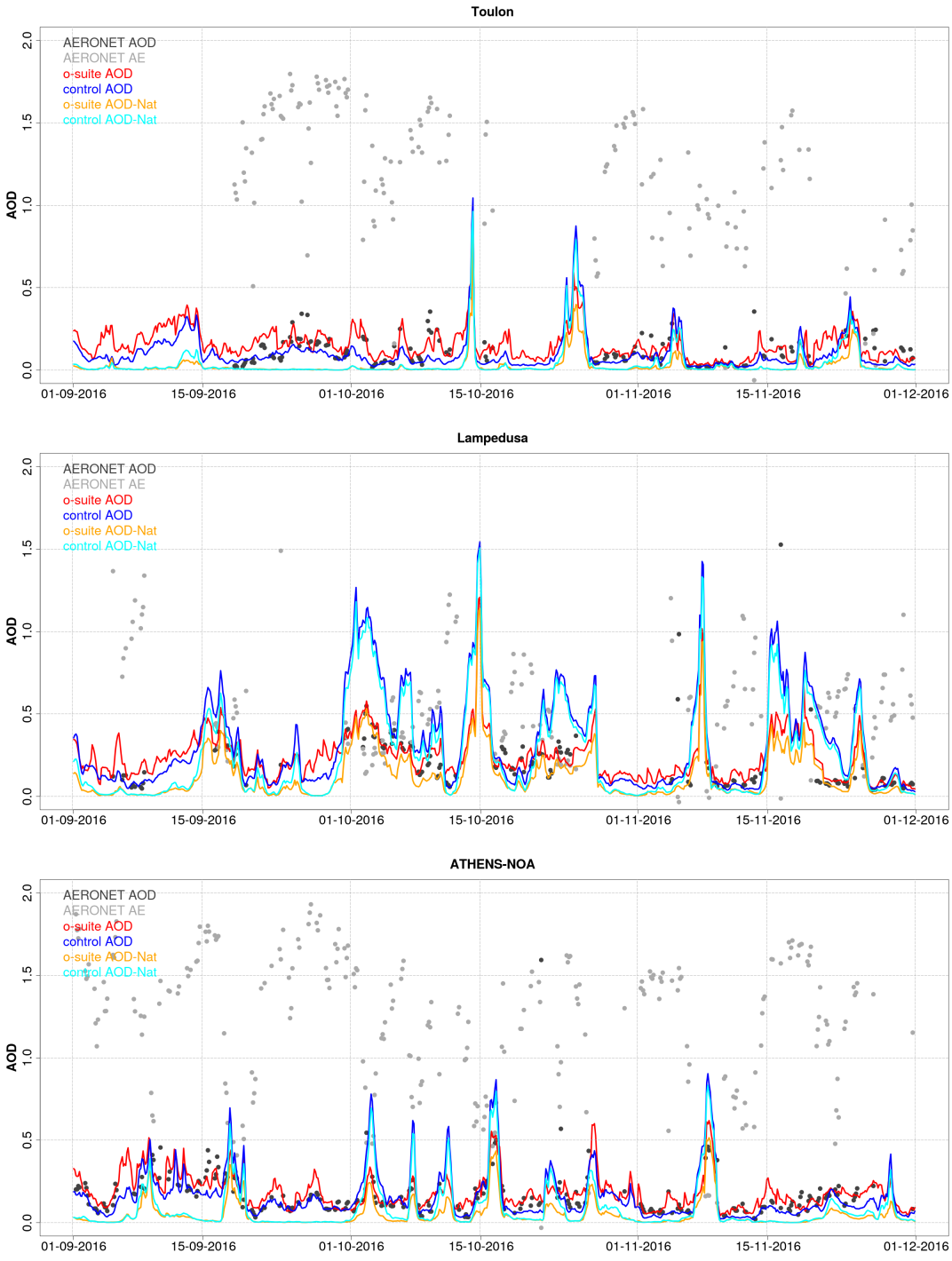

Figure 3.5.11: AOD from AERONET (black dot), AOD o-suite (red line), AOD control (blue line), AOD-Nat o-suite (orange line), AOD-Nat control (cyan line), for the study period over Barcelona (Spain), IMAA Potenza (Italy) and Athens (Greece). AOD-Nat corresponds to the natural aerosol optical depth that includes dust and sea-salt.

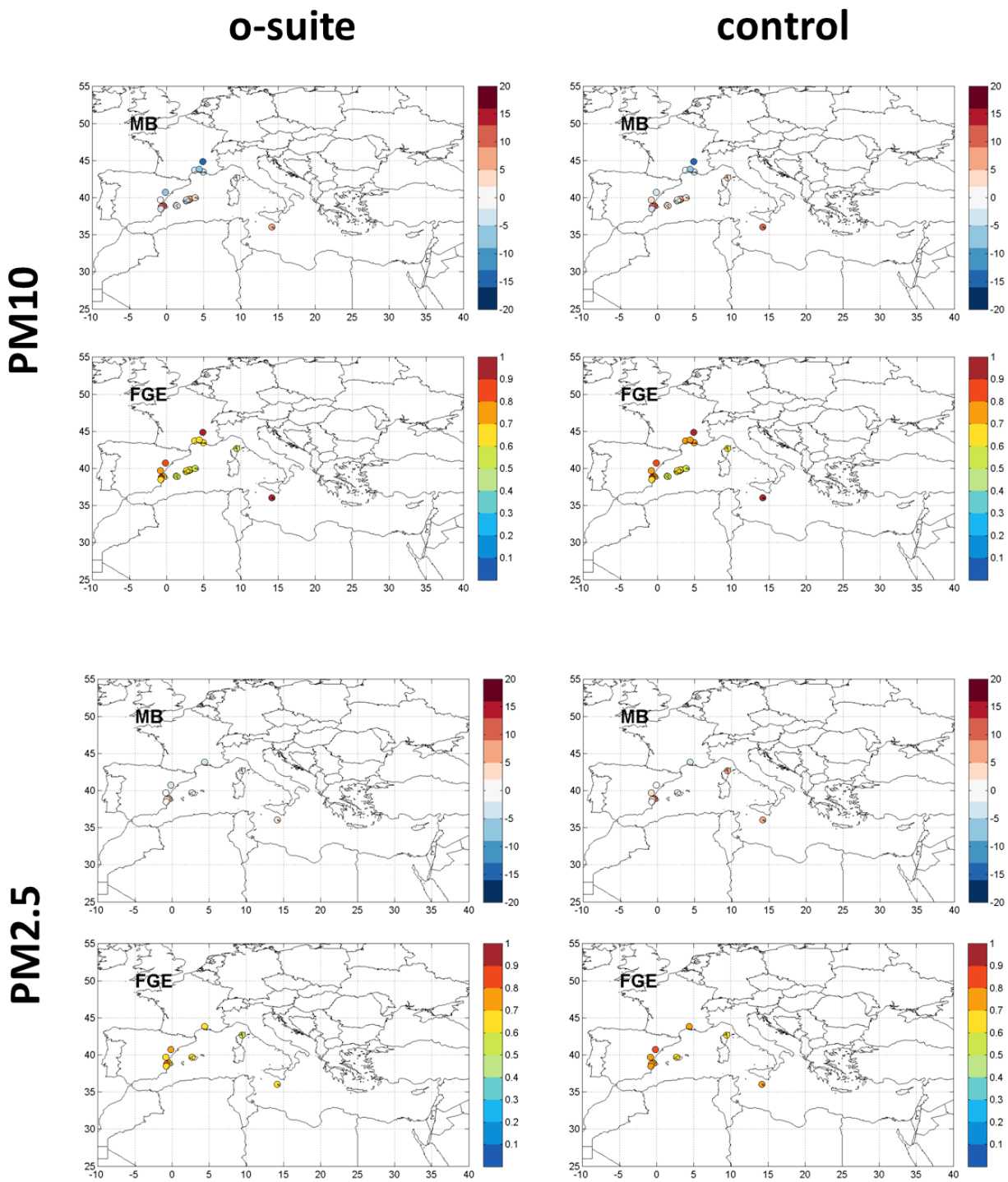

Figure 3.5.12: Skill scores (MB and FGE) for 24-hour forecasts of CAMS o-suite and control for the study period. PM10 and PM2.5 from Airbase are the reference. Only background suburban and rural available stations are displayed.

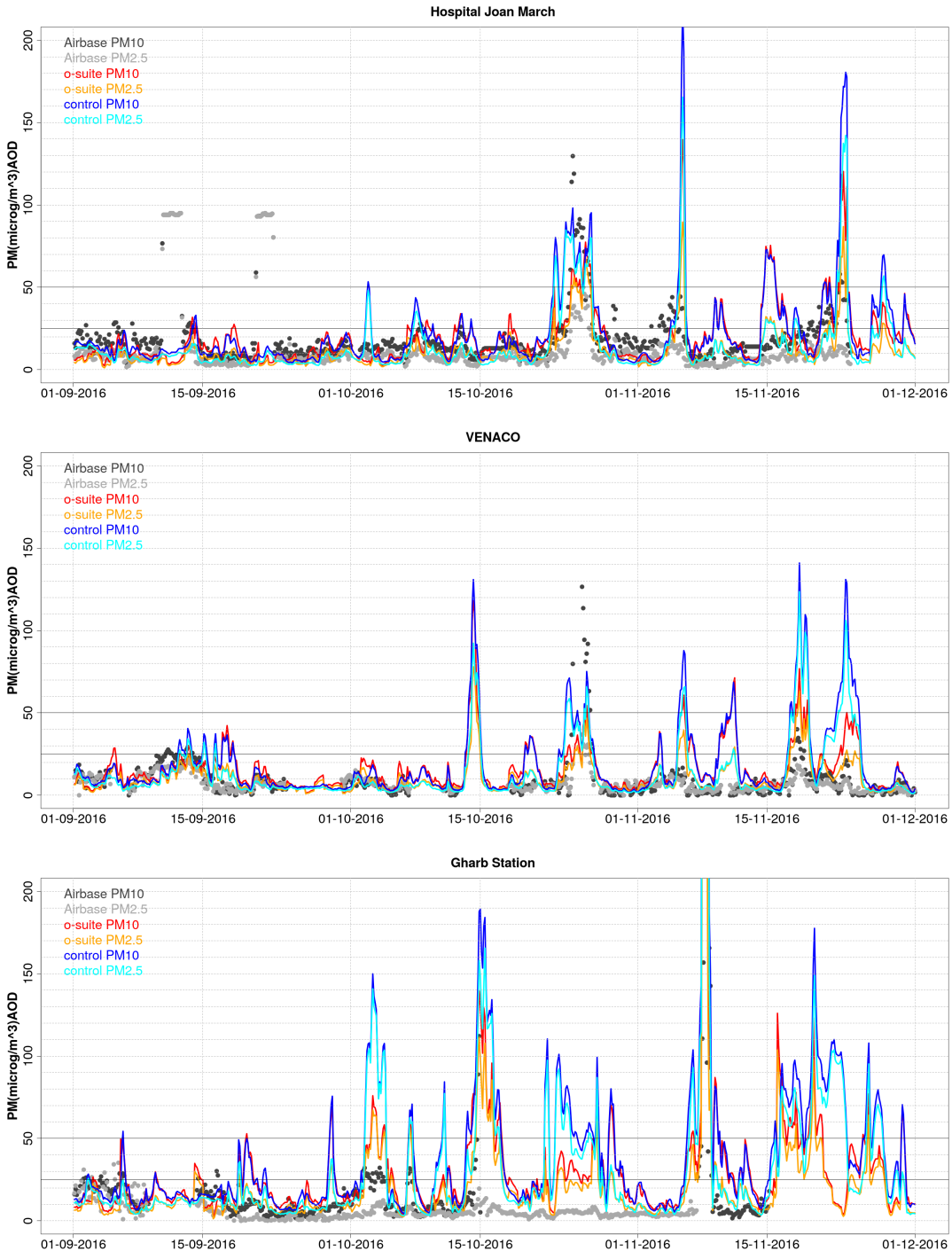

Figure 3.5.13: PM10 and PM2.5 Airbase observations (black and grey dots, respectively), PM10 and PM2.5 o-suite (red and orange lines, respectively) and PM10 and PM2.5 control (blue and cyan lines, respectively) for the study period over Hospital Joan March (Balearic Islands, Spain), Venaco (Corse, France) and Gharb Station (Malta).

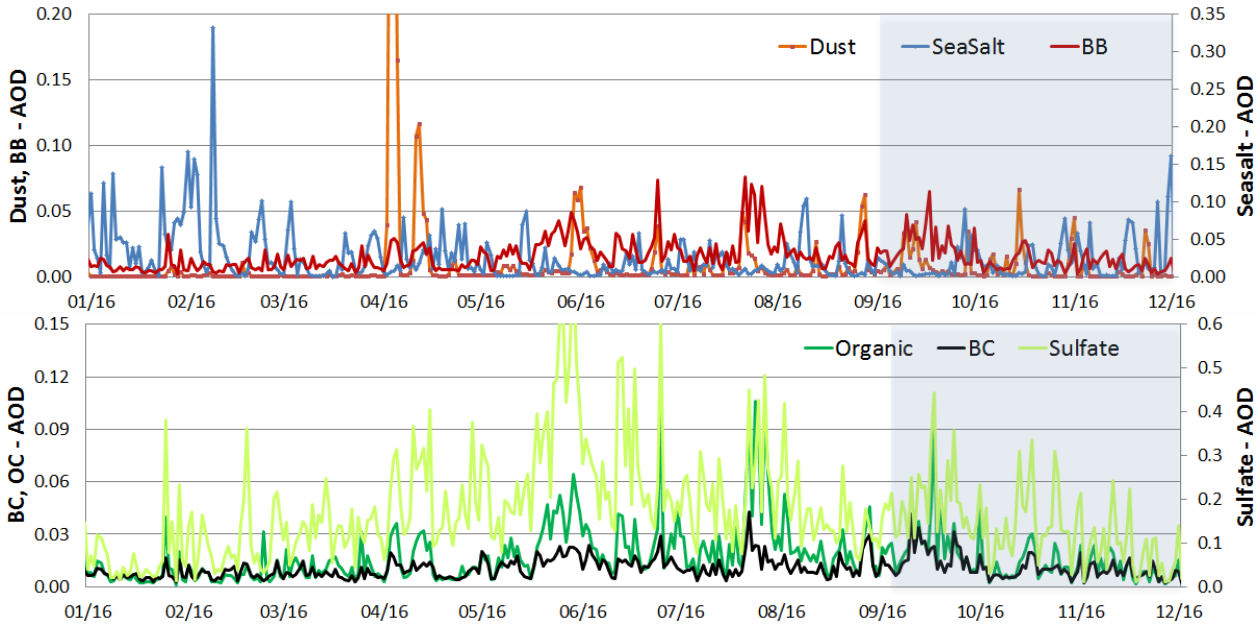

Figure 3.5.14: Maximum daily AOD around Soltau (53N/10E ±1° lat/lon) for aerosols included in the IFS model from 01-11/2016: sea salt (blue), dust (orange), biomass burning (=OC+BC - red), BC (black), organic (green), and sulfate (light green). Note the different y-axes for the aerosol species.

3.5.4 Backscatter profiles

The technical specifications of the data sources, evaluation parameters and methods are described in the report CAMS-84 D8.1. In this section, the vertical variation of the backscatter coefficient (bsc) profiles are evaluated, i.e. correlation and standard deviation of o-suite '0001' and control run 'gjjh' vs ceilometers, and summarized in Taylor plots. The vertically integrated bsc is not the focus, because it reveals similar but less accurate information like AOD. Likewise, a skill measure for the horizontal extension/positioning of plumes/layers is not a primary goal of this evaluation. We focus on cases with pronounced layers, because correct representation of thin or small-scale structures still is a large challenge for the model, indicated by low (or no) correlation. A statistical summary is given in Taylor plots. Issues discussed in former reports will be revised in depth only after significant model upgrades, which are announced for spring 2017.

Period Overview

The model aerosol optical depth (AOD) is used to select periods with significant aerosol plumes over Germany. Figure 3.5.14 shows this for Soltau (53N, 10E), central Germany, separately for contributions of mineral dust (SD), sea salt (SS), biomass burning (BB), black (BC) and organic carbon (OC), as well as sulfate (SU). A SD event on 14/15 Oct 2016 and advection of mixed SD/BB plumes via/from Spain and/or Greece around mid-Sept 2016 are confirmed by the ceilometers. As during early summer 2016 the BB plume is associated with enhanced sulfate. The background values of SO_4 and OC decrease slowly during the SON period.

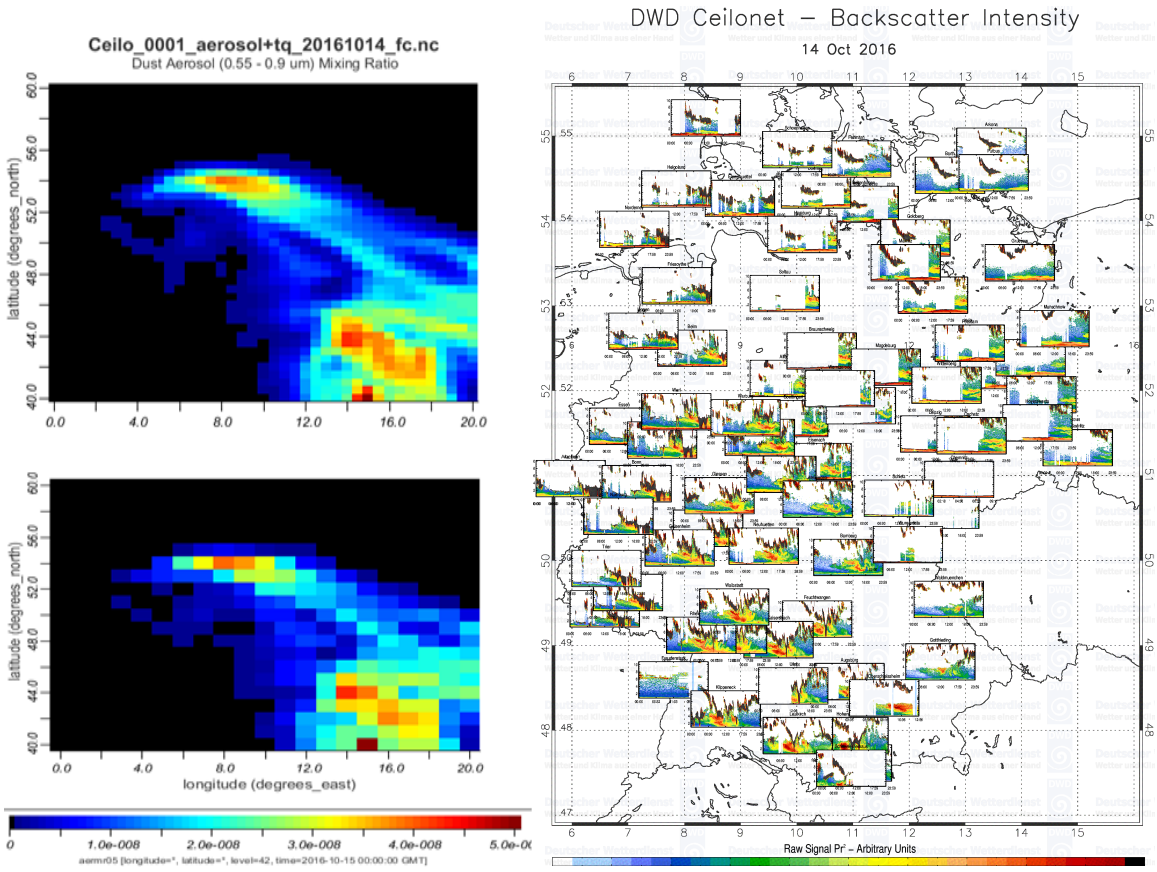

Figure 3.5.15: Left: Dust mass mixing ratio (d_p=0.55-0.9 µm) from o-suite on 15 Oct 2016 on a 0.5° (top) and 1° grid (each 0.5° resolution!). Right: Station-overview of ceilometer backscatter showing the passage of a SD plume on 14 Oct 2016, visible as orange-red layer in 2-5 km altitude.

Saharan Dust, 14/15 Oct 2016:

A compact SD plume crossed Germany from SW to NE from 141016, ~03 UT till 151016, ~12UT. It was centered at altitudes between 2 and 5 km a.s.l., and corresponding to the passage time of about 15 hours, extended over 300-500 km. It was terminated by an air-mass change associated with a warm-front on 15 Oct.

The modelled extension and movement of the SD plume as illustrated in Fig 3.5.15 by the dust AOD, is confirmed by the temporal evolution at the stations in the DWD ceilometer network. The arrival of the plume at the stations is given by its turning-up on the time-axis, proceeding from SW (~03 UT) to NE (~18-21 UT). Maybe owing to the increased model reolution from 1° to 0.5°, the plume appears roughly as bounded as in the ceilometer overview in Fig. 3.5.15. The fact that the plume is not really smoother at a 1° lat/lon grid instead of a 0.5° grid, suggests that the model fields may also be retrieved from the archive at a reduced resolution and resampled afterwards, which saves factor 4 of file size.

The shape of the profile and the BSC values are similarly well captured by both, o-suite and control run (Fig. 3.5.16). Only, gjjh has a bit high BSC and positions the profile peak by about 1 km too high.

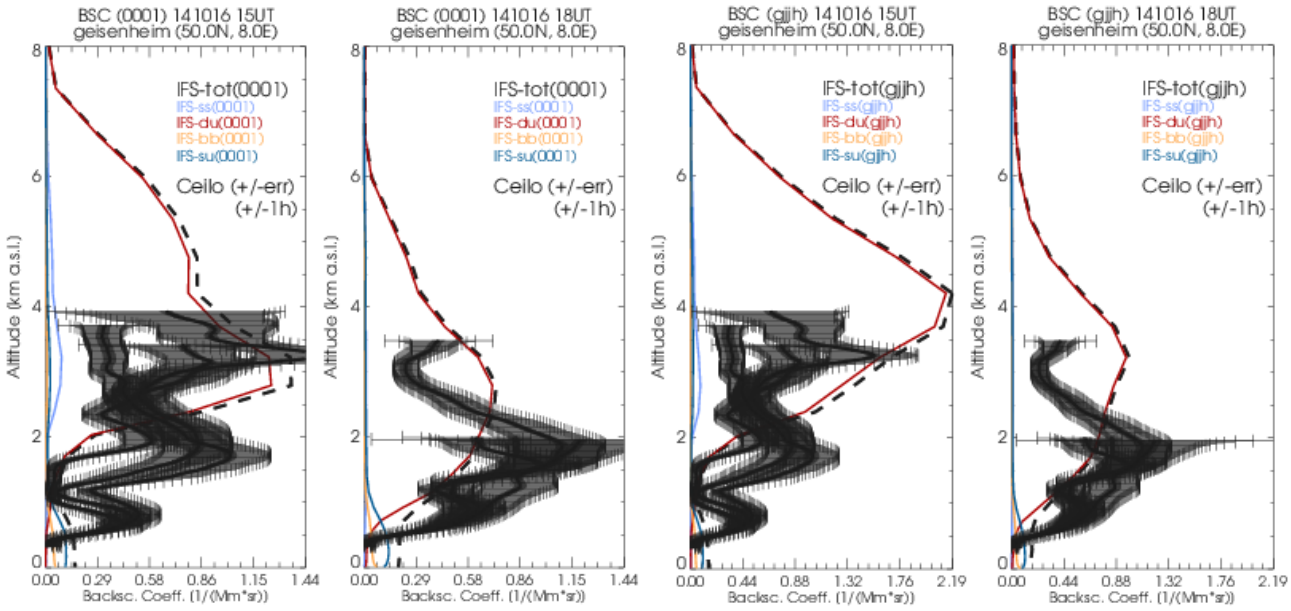

Figure 3.5.16: Bsc-profiles at Geisenheim on 14 Oct 2016 (left o-suite, right control), split up for contributions from sea-salt (light blue), dust (red), biomass burning (orange) and sulfate (dark blue), as well as the total aerosol (dashed black). Solid black lines: Ceilometer total bsc with estimated error bars, plotted for -1h, +/-0h, +1h around the time of the 3-hly model profile.

Mixed Saharan dust and biomass burning plume, 08-20 Sept 2016:

According to the fire radiative power map, available e.g. under http://macc.copernicus-atmosphere.eu/d/services/gac/nrt/fire_radiative_power!Europe!Fire%20Radiative%20Power!macc!od!enfo!fire_radiative_power!2016090600!/, and to HYSPLIT trajectories (Fig. 3.5.17) smoke from either (or both) fires in northern Spain or Greece were transported to Germany around the period 8-20 Sept 2016. Partly, also SD was contained in this air-mass. During the whole period, the ceilometers show dense aerosol layers over Germany, initially at altitudes up to 6 km, but repeatedly the smoke fraction settled to the boundary layer, in agreement with enhanced soot and O_3 concentrations measured at the GAW station Hohenpeißenberg. Though ceilometers cannot characterize the particle type, these layers can most likely be attributed to both fire and dust emissions.

On 17 Sep 2016, when the largest BB fraction during the SON period is predicted by the model, the o-suite has a sulfate layer in 3-4 km which is much weaker in the control run, and in this respect agrees better to the observations (Fig. 3.5.18 – selected station: Soltau). Both runs produce a similarly enhanced sea salt fraction in the boundary layer but still underestimate the observed bsc by roughly a factor of 2. Both runs capture the top height of the aerosol layers in the free troposphere as well as the broad double peak in the profile, but as before, the shallow layering structure is missed.

On 10 Sep 2016, 00UT-09UT, many stations exhibit high bsc in the PBL and pronounced aerosol layers up to 4 km height in the free troposphere. The FT layer is better reproduced by gjjh than by the o-suite at most stations and often has bsc of correct magnitude. The o-suite seems to redistribute the assimilated AOD to lower altitudes. As stated earlier, the assimilation repeatedly

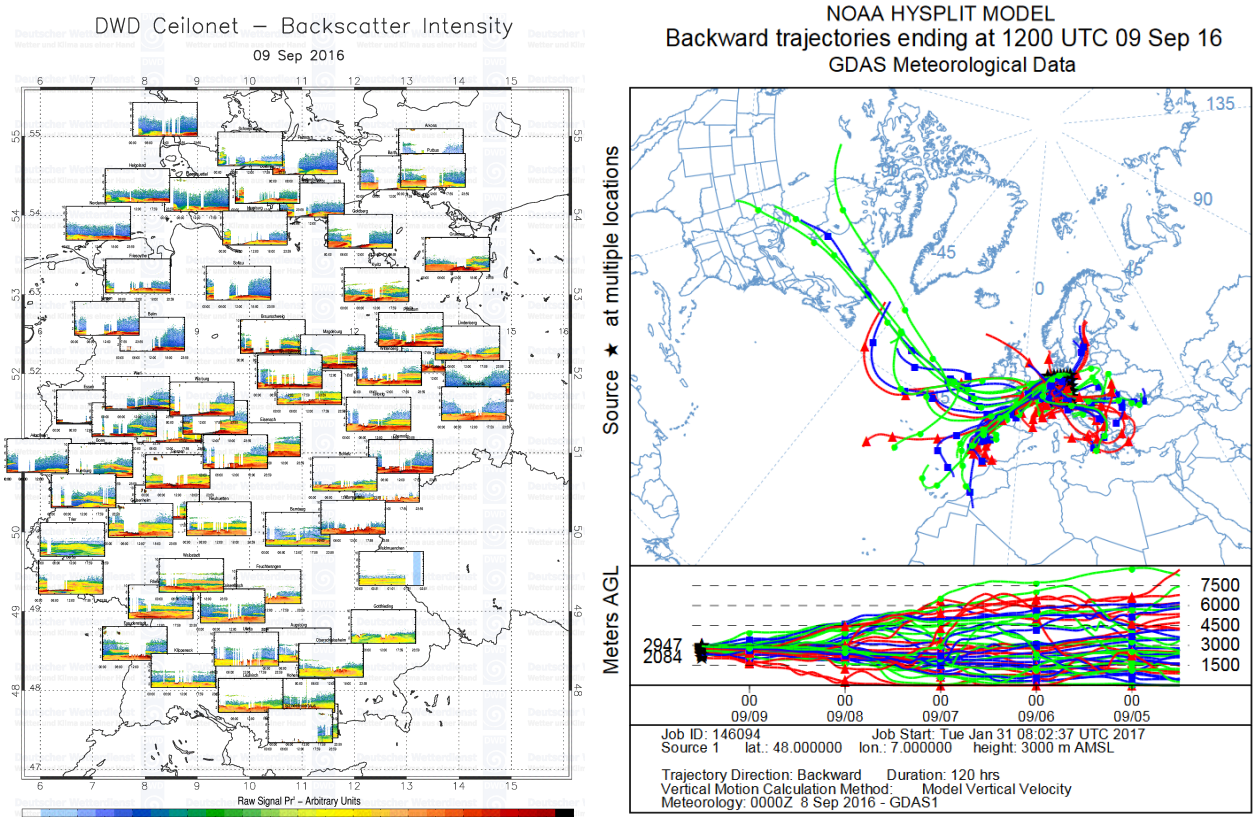

Fig. 3.5.17: German ceilometer network (time-height sections Pr²) and HYSPLIT back-trajectory matrix (48N/7E to 53N/14E by 1°) for 9 September 2016, indicating air-asses arriving in Germany from forest fire regions in NE Spain and Greece.

seems to have an adverse effect on the shape of the vertical profile. Fig. 3.5.18 (top panel) shows this for station Soltau. The o-suite reproduces the large PBL bsc (SU, SS, BB and DU) better than the control run, but nearly fails to produce the layer above, which is attributed to DU by the control run. However, the bsc of both, PBL and the above layer, are only about half as large as observed. The same behavior is found at the southern German stations, but there gjjh roughly captures the observed bsc.

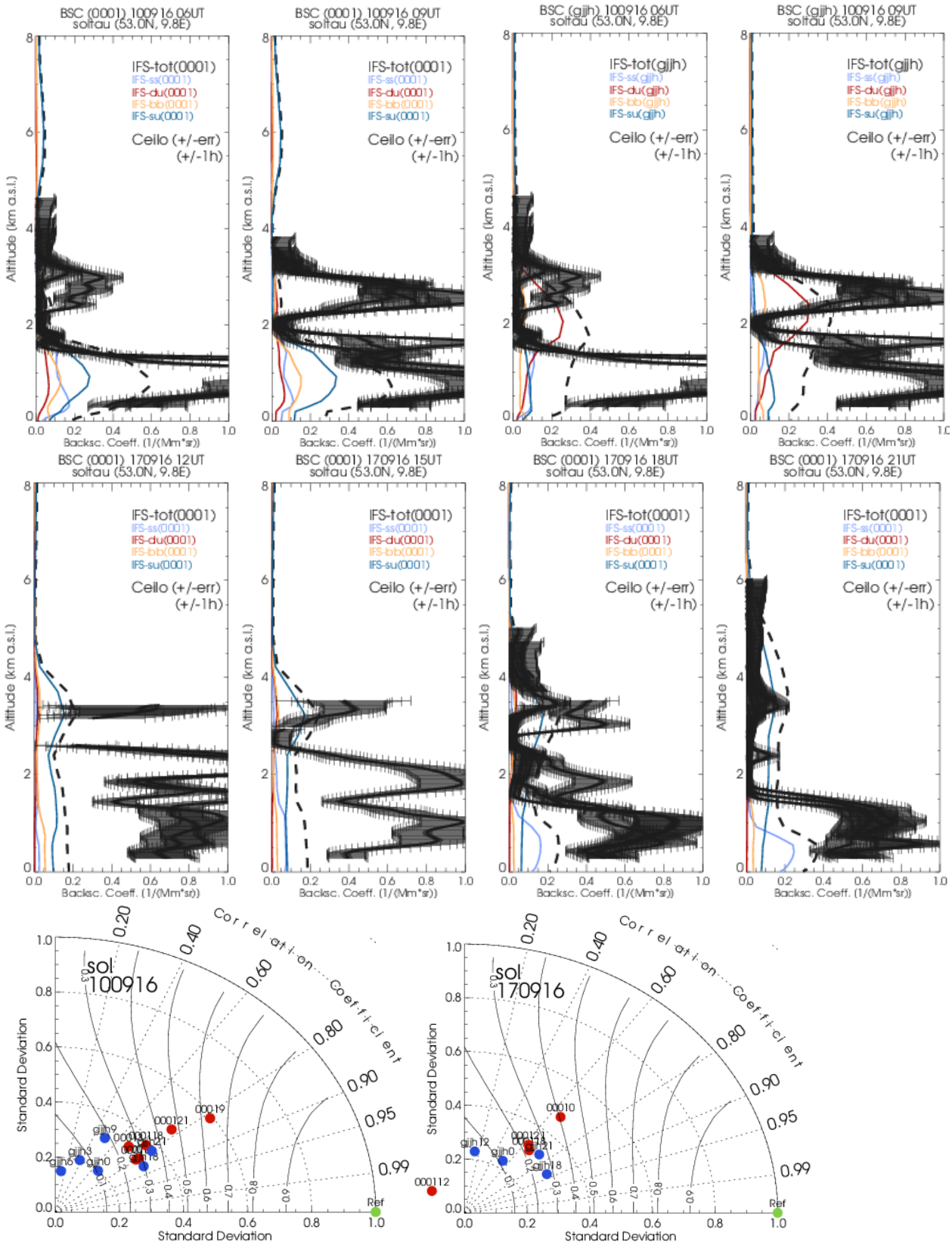

Figure 3.5.18: Upper panels: Bsc-profiles at Soltau (53°N) on 10 (o-suite + gjjh) and 17 Sep 2016 (o-suite), as in Fig 3.5.15. Lower panel: Taylor polar plots with standard deviation vs correlation coefficient of the 3-hourly profiles for Soltau on 10 and 17 Sep 2016. O-suite red, control blue.

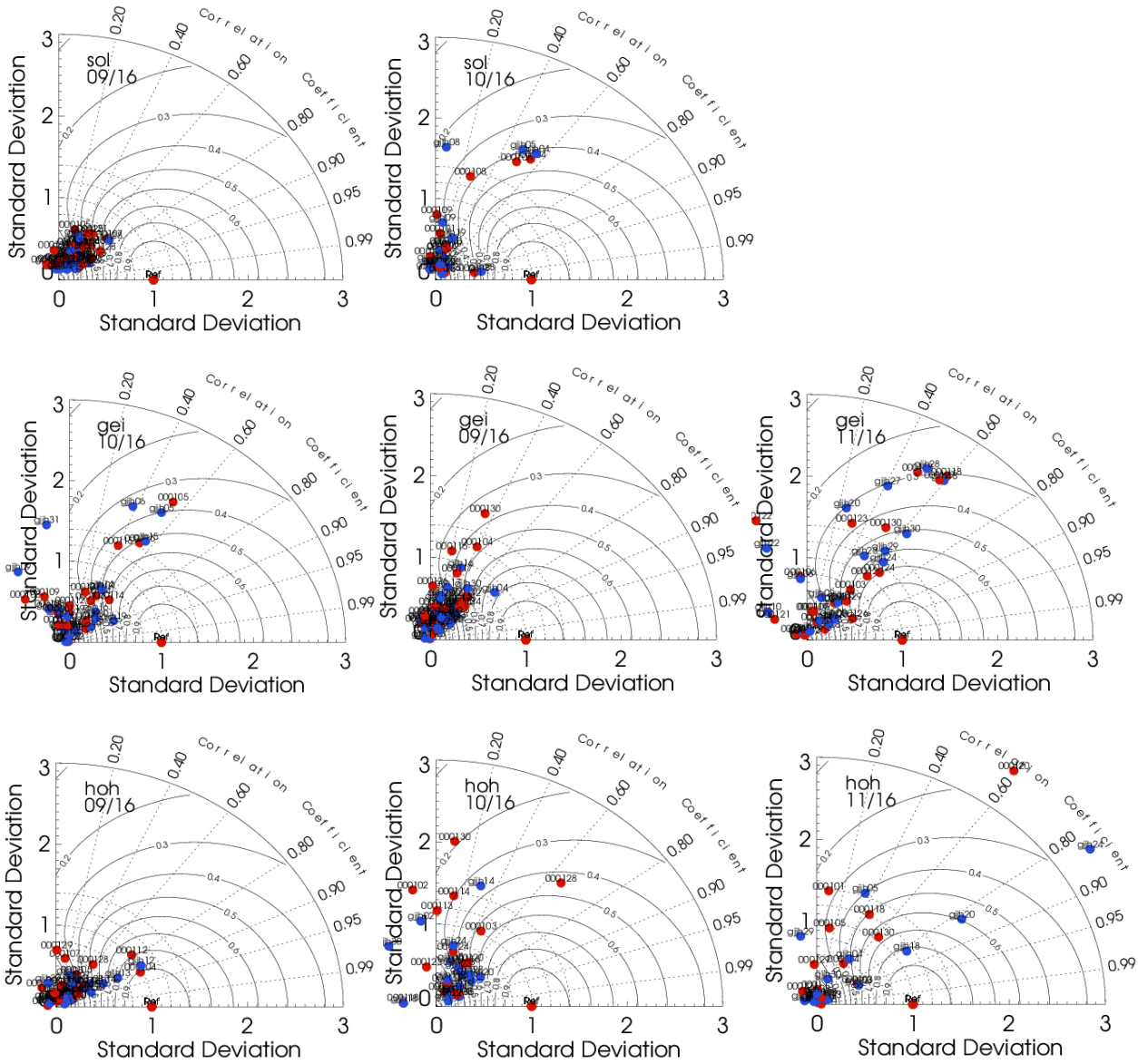

Fig. 3.5.19: Taylor polar plots with daily average standard deviation vs correlation coefficient for the three German sites Soltau (53°N), Geisenheim (50°N) and Hohenpeißenberg (48°N) for Sep, Oct and Nov 2016. O-suite red, control blue.

Summary:

The reproduction of detailed aerosol profiles is a serious challenge, as for all global models. Dense particle layers are generally better reproduced than thin ones, large gradients and fast changes are smoothed, structures often spatially and temporally shifted. The vertical variability (standard deviation) in the model is mostly smaller than observed and not following shallow layers, reflecting in the bullet clouds near the axis origin in the Taylor plots (Fig. 3.5.19). The fractions skill score concept is currently explored for assessments of displacement errors in future reports.

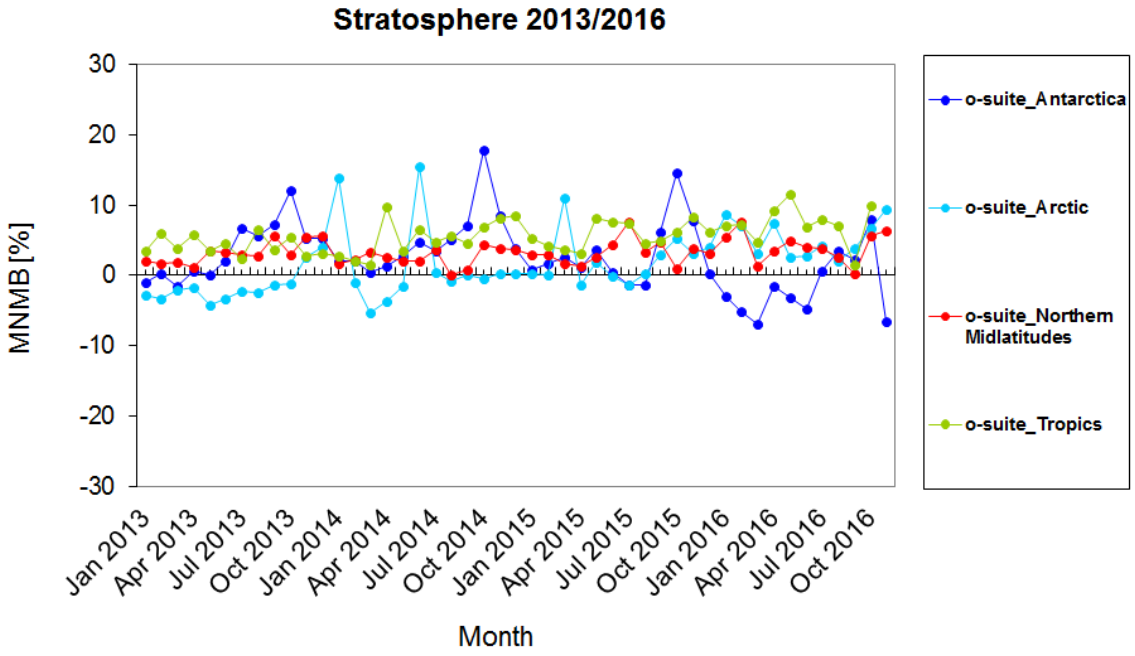

Figure 3.6.1: MNMBs (%) of ozone in the stratosphere from the o-suite against aggregated sonde data in the Arctic (light blue), Antarctic (dark blue) northern midlatitudes (red) and tropics (green).

3.6 Stratospheric ozone

3.6.1 Validation against ozone sondes

In what follows, we present the results of the stratospheric ozone evaluation against ozone soundings from the NDACC, WOUDC, NILU and SHADOZ databases. The sondes have a precision of 3-5% (~10% in the troposphere for Brewer Mast) and an uncertainty of 5-10%. For further details see Cammas et al. (2009), Deshler et al. (2008) and Smit et al (2007). Model profiles of the o-suite are compared to balloon sondes measurement data of 44 stations for the period January 2013 to November 2016 (please note that towards the end of the validation period fewer soundings are available). As C-IFS-CB05 stratospheric composition products beyond O_3 in the o-suite is not useful we provide only a very limited evaluation of the control experiment. A description of the applied methodologies and a map with the sounding stations can be found in Eskes et al. (2016). Both runs, the o-suite and the control run, show MNMBs mostly within the range -7 to +10%, for all regions and months (some exceptions with MNMBs of up to 18% for single months in the high latitude regions), see Fig. 3.6.1 and 3.6.2.

Ozone partial pressures in the stratosphere are mostly slightly overestimated (MNMBs between 2-8%) in all latitude bands, except for the Arctic (before 2015) and Antarctic summer season. MNMBs in Antarctica during the ozone hole season, from August to November, remain below ±15% for the o-suite.

For the latest quarter (SON), except for the Northern midlatitudes, the control run performs slightly better than the o-suite.

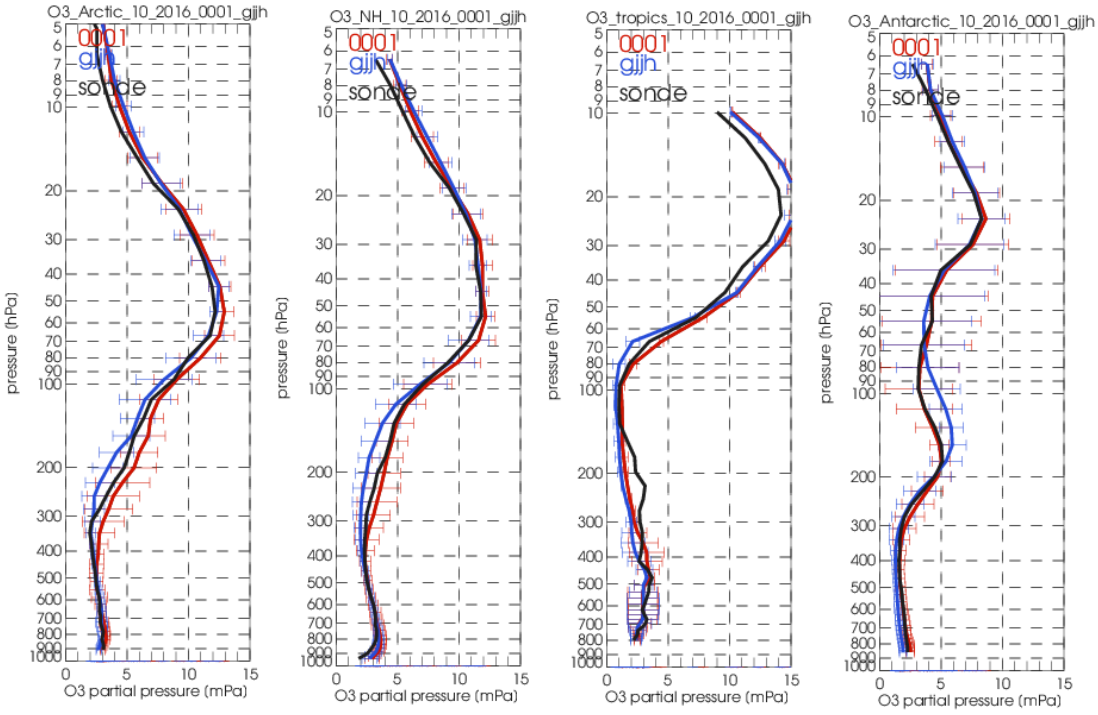

Figure 3.6.2: Comparison between mean O_3 profiles (units: mPa) of o-suite (red), and control (blue) in comparison with observed O_3 sonde profiles (black) for October 2016 for the various latitude bands: Arctic, NH-mid latitudes, Tropics and Antarctic.

Fig. 3.6.2 compares the averaged profiles in each region during October 2016. The vertical distribution of stratospheric ozone is quite well represented for all regions by the o-suite, with little overestimation above 20hPa.

3.6.2 Validation against observations from the NDACC network (MWR, LIDAR)

In this section we present a comparison between the CAMS o-suite and control run models against MWR and LIDAR observations from the NDACC network. A detailed description of the instruments and applied methodologies for all NDACC instruments can be found at http://nors.aeronomie.be. MWR (microwave) at Ny Alesund (79°N, 12°E, Arctic station) and Bern (47°N, 7°E, northern midlatitude station). LIDAR at Lauder, New Zeeland (46°S, 169.7°E, altitude 370m) and Hohenpeissenberg, Germany (47°N, 11°E, altitude 1km)

Table 3.6.1: Seasonal relative mean bias (MB, %), standard deviation (STD, %) of the partial (upper stratospheric 25km – 65km) ozone column for the considered period and number of observations used (NOBS), compared to NDACC microwave observations at Ny Alesund and Bern (mean bias and stddev in %).

		DJF			MAM			JJA			SON		
		MB	stddev	nobs	MB	stddev	nobs	MB	stddev	nobs	MB	stddev	nobs
o-suite	Ny.Ale	14.50	6.51	213	6.35	5.42	229	-0.43	5.56	267	10.23	8.65	257
	Bern	0.74	3.43	527	0.97	2.82	609	0.09	2.78	571	0.05	2.50	557

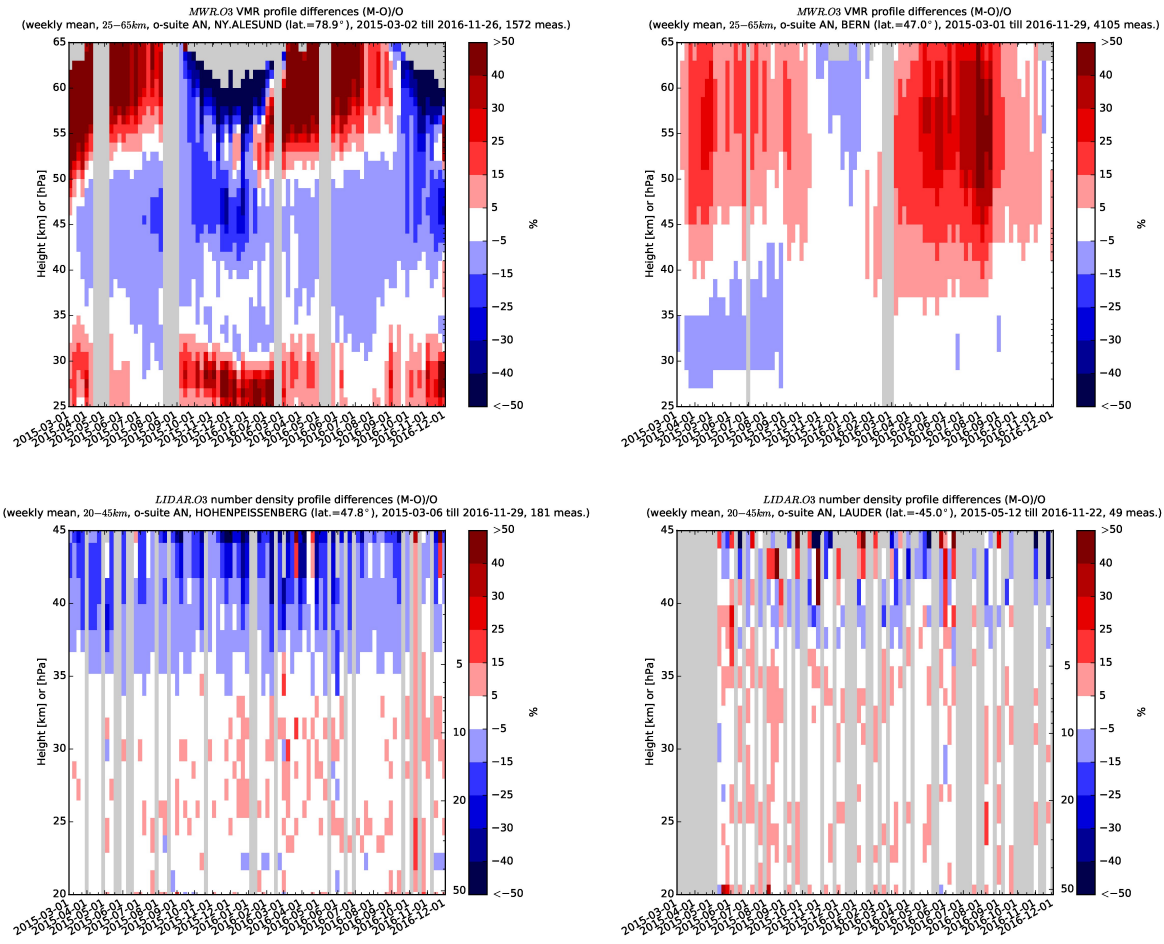

Figure 3.6.3: Comparison of the weekly mean profile bias between the O3 mixing ratios of o-suite and the NDACC station at Ny Alesund, Bern, Hohenpeissenberg and Lauder. For the LIDAR stations (bottom row), the measurement uncertainty above 35km is comparable to the observed profile bias.

From Table 3.6.1, the upper stratospheric partial column bias at Bern during Sept. 2015 –November 2016 is nearly vanishing (uncertainty on the partial column is 6%). At Ny Alesund, the o-suite overestimated the stratospheric ozone concentration with more than 10% during SON/DJF and this vanishes during summer JJA.

In MAM-JJA 2015 and 2016, both MWR stations observe a significant (i.e. comparable to the measurement uncertainty) overestimation of the upper stratospheric/mesospheric ozone content, and the converse is seen during autumn and winter SON-DJF, underestimating up to -30% (Ny Alesund), see Fig. 3.6.3. At BERN the difference between o-suite and MWR at 25-35km is negligible since Sept 2015 (compared to the MWR profile uncertainty).

At Lauder and Hohenpeissenberg (LIDAR), the o-suite slightly overestimates the observed ozone (<10%) between 25km and 35km. The uncertainty on the LIDAR concentration increases with altitude and above 35km the observed differences are comparable to the measurement uncertainty (>10%, see http://nors.aeronomie.be/projectdir/PDF/NORS_D4.2_DUG.pdf)

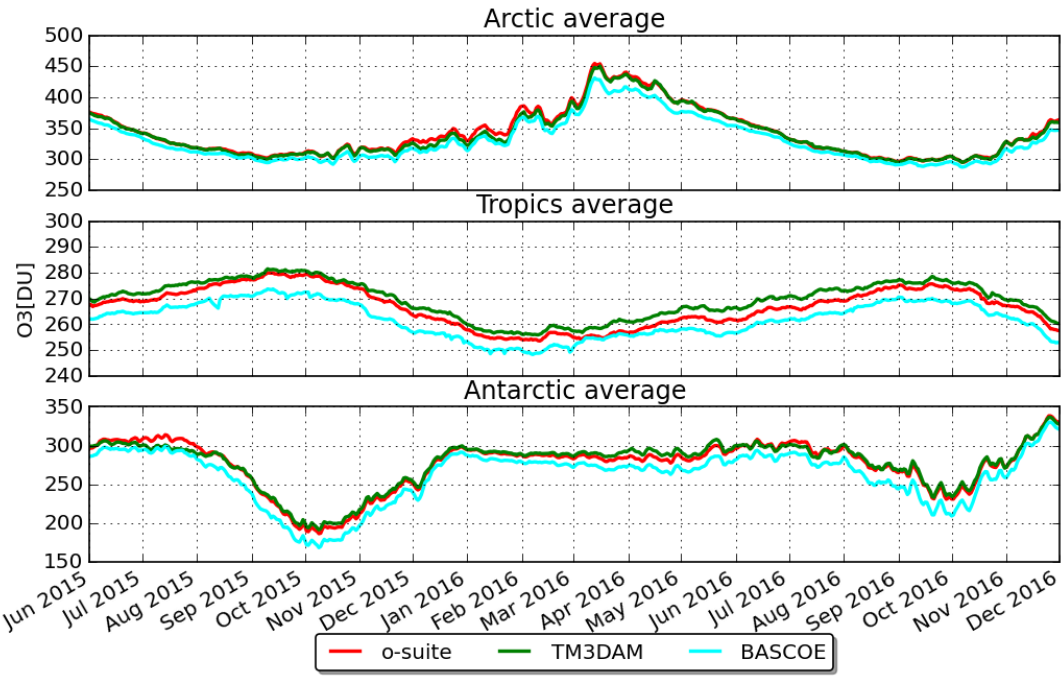

Figure 3.6.4: Zonally averaged ozone total column (Dobson Units) in the Arctic (60°N-90°N), Tropics (30°S-30°N) and Antarctic (90°S-60°S) during the period 2015/06/01-2016/12/01.

3.6.3 Comparison with dedicated systems and with observations by limb-scanning satellites

This section compares the output of the o-suite for the last period, based on the methodology described by Lefever et al. (2015). It also compares the model output with observations by limb-scanning satellite instruments. The combination of these comparisons delivers a good picture of the performance of the CAMS o-suite analyses w.r.t. stratospheric ozone. We also include the comparisons for the o-suite forecasts of stratospheric ozone. These forecasts have a lead time of 4 to 5 days and are represented by dotted lines in the figures.

All datasets are averaged over all longitudes and over the three most interesting latitude bands for stratospheric ozone: Antarctic (90°S-60°S), Tropics (30°S-30°N) and Arctic (60°N-90°N). In order to provide global coverage, the two mid-latitude bands (60°S-90°S and 60°N-90°N) are also included in some comparisons with satellite observations.

System intercomparison for total columns

Fig. 3.6.4 shows the ozone total column over the polar and tropical latitude bands, including results from TM3DAM (green lines) and BASCOE (cyan lines). Since TM3DAM applies bias corrections to the GOME-2 data based on the surface Brewer-Dobson measurements, we use the results from TM3DAM as a “reference” for the ground-truth.

Everywhere there is an underestimation for BASCOE of about 10-20 DU. This is due to the fact that BASCOE does not assimilate any observations of the total ozone column, but only Aura-MLS profiles and does not account for tropospheric sources of ozone. The o-suite results are much closer to those by TM3DAM:

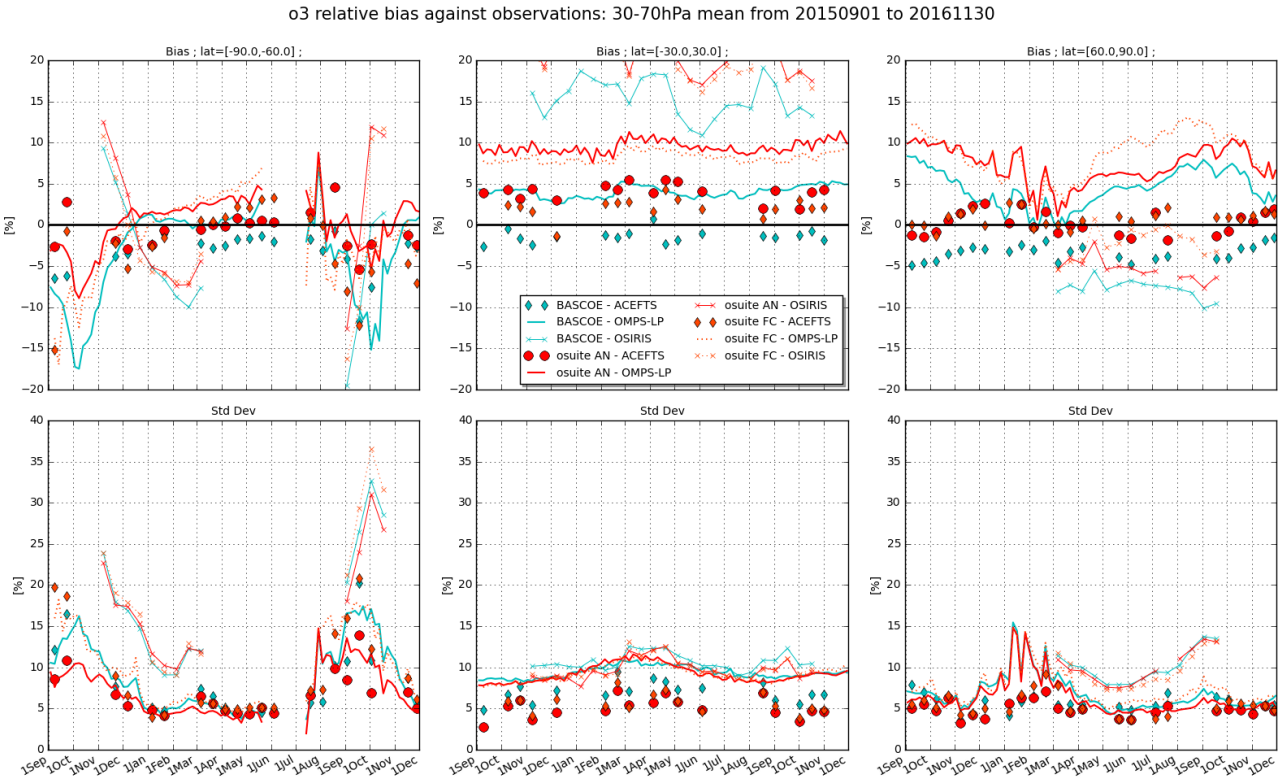

Figure 3.6.5: Time series comparing ozone from o-suite analyses (red, solid), o-suite forecasts 4th day (red, dotted), and BASCOE (cyan) with observations by OMPS-LP, OSIRIS and ACE-FTS for the period 2015-09-01 to 2016-12-01 in the middle stratosphere (30-70hPa averages): top row, normalized mean bias (model-obs)/obs (%); bottom row, standard deviation of relative differences (%).

- In the Arctic, the o-suite gives similar results to TM3DAM, except for the period of mid November 2015 to mid-February 2016, where it presents a slight overestimation of about 10 DU, i.e. ~3%.
- In the Tropics, the seasonal maximum of ozone, ranging from 270 to 290 DU, is reached in September. The o-suite presents slight underestimations w.r.t. TM3DAM of about 2-6 DU, i.e. ~2%.
- In the Antarctic, the o-suite matches TM3DAM during the whole period except for the month of July 2015 (overestimation reaching 15DU in mid-July).

Comparison with independent limb satellite datasets

In this section, we use observations from three satellite limb sounding instruments for comparison with the o-suite analyses and 4th day forecasts. For reference, we include also the BASCOE analyses which are very constrained by the AURA MLS offline profiles.

Fig. 3.6.5 and Fig. 3.6.6 present, in the upper row, the timeseries over the last 15 months of the bias of the o-suite against the three instruments for respectively two regions of the lower stratosphere and UTLS (30-70hPa and 70-100hPa). The bottom row of Fig. 3.6.5 and 3.6.6 shows the standard deviation of the differences and can be used to evaluate the random error in the analyses.

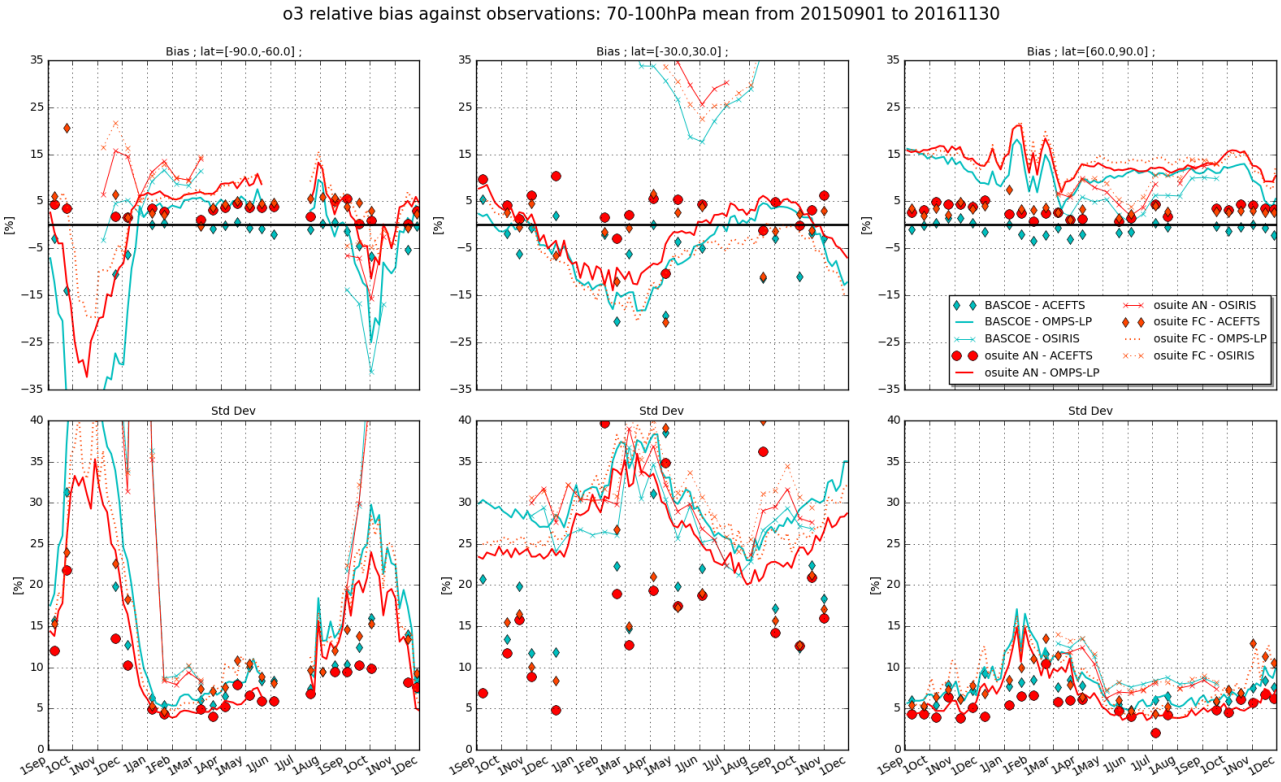

Figure 3.6.6: Time series comparing ozone from o-suite analyses (red, solid), o-suite forecasts 4th day (red, dotted), and BASCOE (cyan) with observations by OMPS-LP, OSIRIS and ACE-FTS for the period 2015-09-01 to 2016-12-01 in the middle stratosphere (70-100hPa averages): top row, normalized mean bias (model-obs)/obs (%); bottom row, standard deviation of relative differences (%).

It must be noted that the different instruments have a variety of spatial and temporal coverage: OSIRIS does not cover the North hemisphere from November to February and the South hemisphere from March to August; for a 3 month period and over the latitude bands considered, OMPS and Aura MLS (not shown) provide daily data with about 10^5 valid profiles, while OSIRIS provide about 2500 valid profiles and ACE-FTS around 700 profiles in the polar region and 200 profiles in the tropics. The bias with OSIRIS observations (against the o-suite but also BASCOE) are very irregular and in contradiction with the other instruments, and seem not appropriate for a validation purpose.

Compared to OMPS-LP in the 30hPa to 70hPa region, there is a systematic overestimation by the o-suite in the tropics and the North polar region (up to 10%), and a variable bias (up to ±10%) in the South polar region with a maximum ; in the 70hPa to 100hPa region, the north polar bias increases up to 20% in February 2016, while the variability of the bias is much stronger in the south polar region.

Compared to ACE-FTS, the bias is limited to ±6%, with a seasonal variation for the polar regions and a systematic positive sign in the tropics for the 30hPa to 70hPa region.

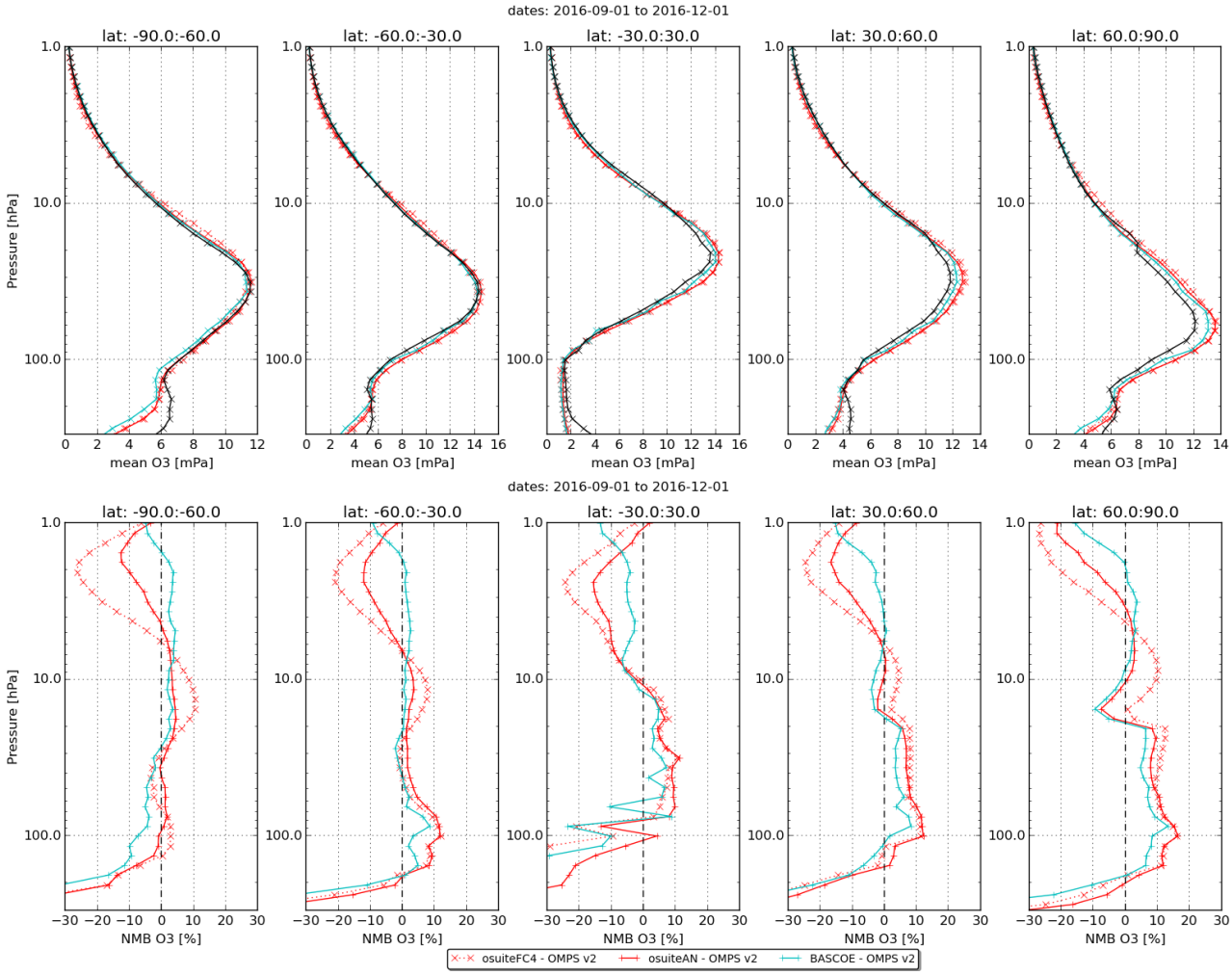

Figure 3.6.7: Mean value expressed in partial pressure (top) and normalized mean bias (bottom) of the ozone profile between o-suite analyses (red, solid), o-suite forecasts 4th day (red, dotted) and BASCOE (cyan line) with OMPS-LP v2 observations for the period September-October-November 2016.

Fig. 3.6.7 displays vertical profiles of the relative biases between the o-suite or BASCOE and OMPS-LP. The difference is averaged over the most recent 3-month period considered in this validation report, i.e. September-November 2016. In the northern hemisphere, a vertical discontinuity of the relative differences is noted at 20 hPa, but this is a spurious feature due to a vertical discontinuity in the OMPS retrievals used here (transition from UV to visible detector).

This quantitative comparison with OMPS-LP confirms the good agreement in the middle stratosphere while the lower stratosphere (< 70hPa) reveals stronger discrepancies. The comparison with BASCOE (which assimilates the offline Aura-MLS dataset) confirms that the lower stratospheric vertical oscillations seen against Aura-MLS in the Tropical band (not shown) are an artifact.

Fig. 3.6.8 displays vertical profiles of the relative biases between the o-suite or BASCOE and ACE-FTS. The difference is averaged over the most recent 3-month period considered in this validation report, i.e. September-November 2016. The bias is mainly within 10% between the tropopause and 40km, and mostly within 5% between 15km and 35km except in the tropics.

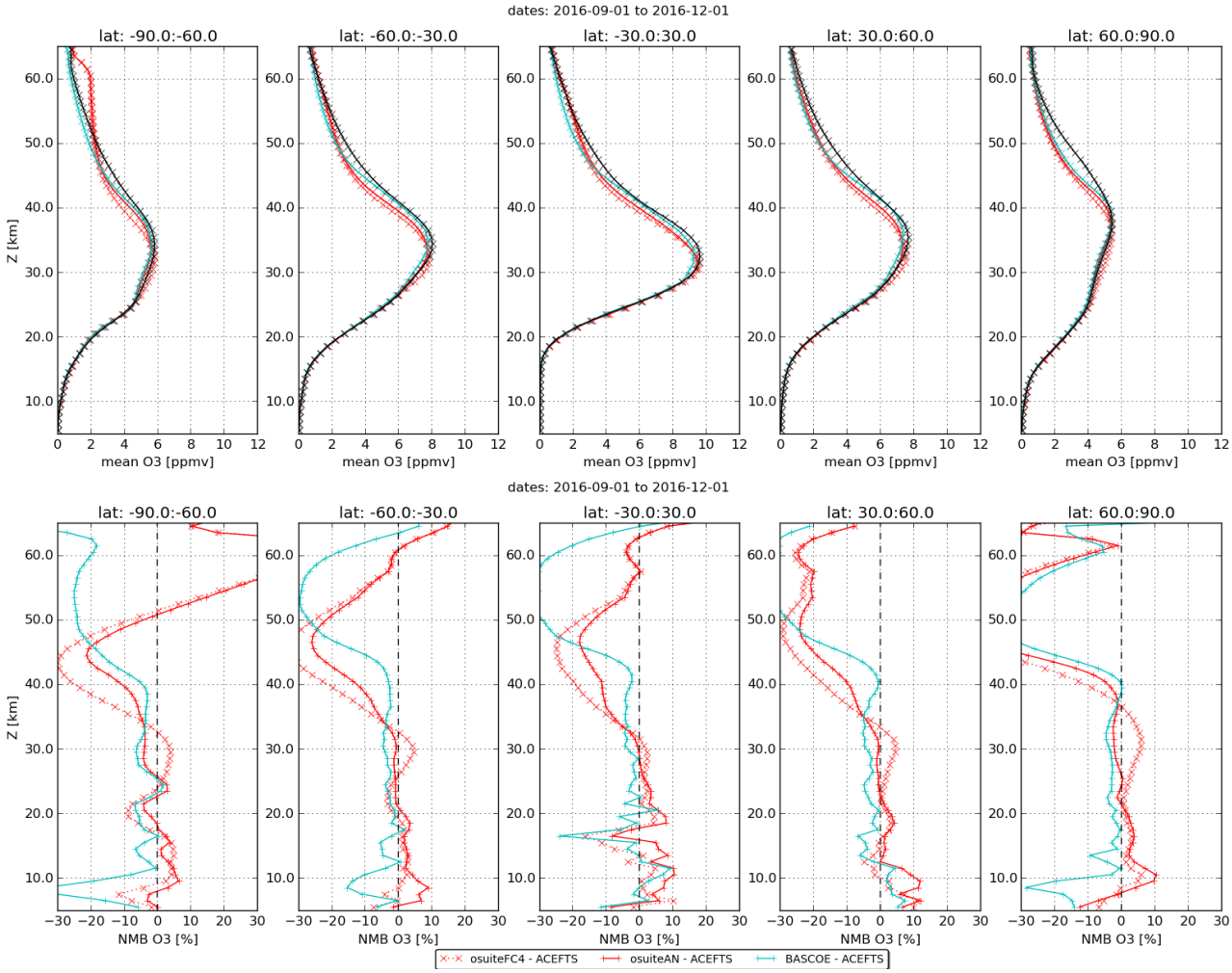

Figure 3.6.8: Mean value expressed in partial pressure (top) and normalized mean bias (bottom) of the ozone profile between o-suite analyses (red, solid), o-suite forecasts 4th day (red, dotted) and BASCOE (cyan line) with ACE-FTS observations for the period September-October-December 2016.

This quantitative comparison with ACE-FTS confirms the good agreement in the middle and lower stratosphere.

3.7 Stratospheric NO_2

In this section, nitrogen dioxide from SCIAMACHY/Envisat satellite retrievals (IUP-UB v0.7) and GOME-2/MetOp-A satellite retrievals (IUP-UB v1.0) are used to validate modelled stratospheric NO_2 columns. Monthly mean stratospheric NO_2 columns from SCIAMACHY and GOME-2 have relatively small errors of the order of 20% in the tropics and in mid-latitudes in summer and even lower errors at mid-latitudes in winter. As the time resolution of the saved model files is rather coarse and NO_x photochemistry in the stratosphere has a large impact on the NO_2 columns at low sun, some uncertainty is introduced by the time interpolation at high latitudes in winter.

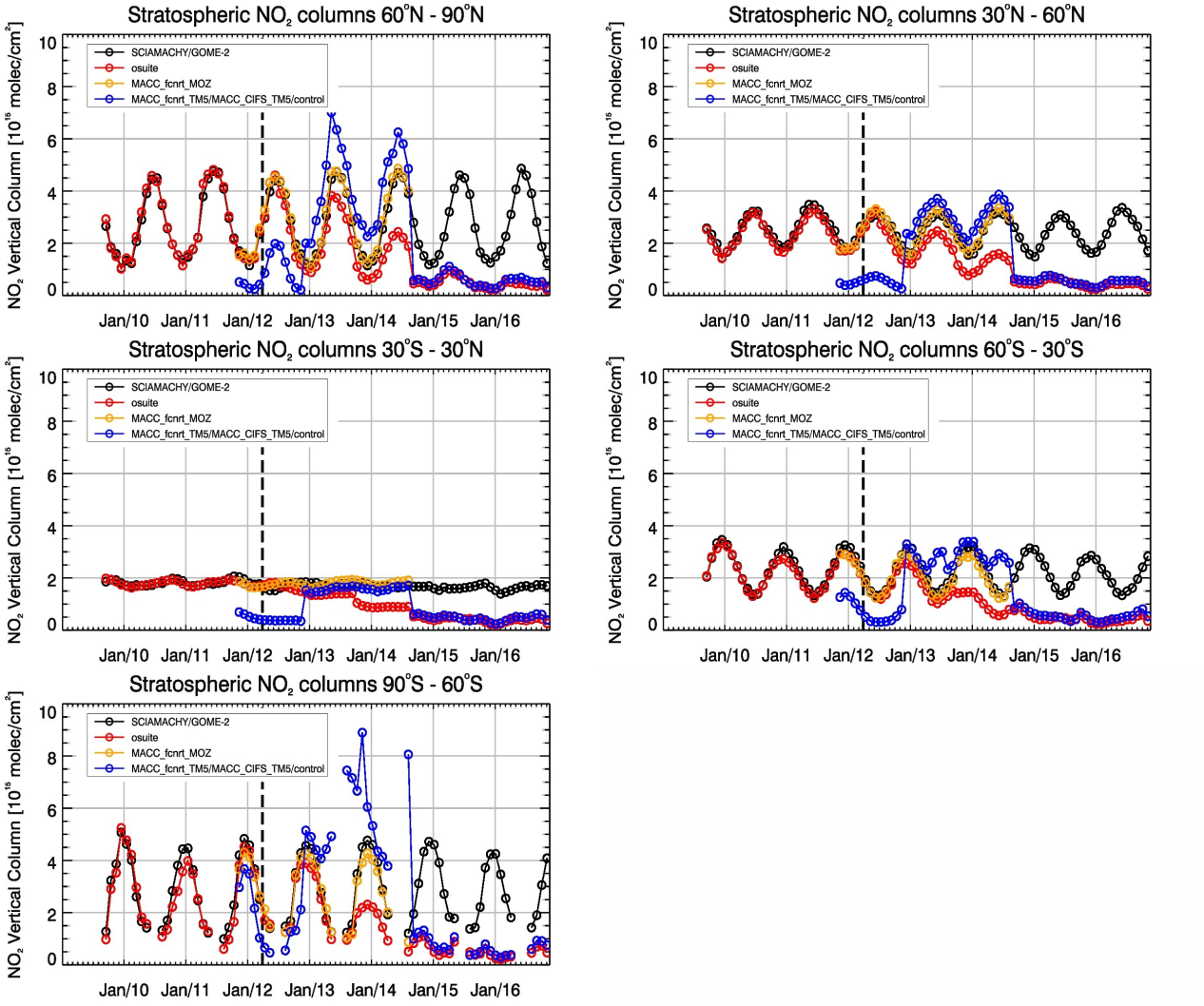

Figure 3.7.1: Time series of average stratospheric NO_2 columns [10^{15} molec cm^{-2}] from SCIAMACHY (up to March 2012) and GOME-2 (from April 2012) compared to model results for different latitude bands. See text for details. The blue line shows MACC_fcnrt_TM5 from November 2011 to November 2012, MACC_CIFS_TM5 results from December 2012 until August 2014 and control results from September 2014 onwards. The vertical dashed black lines mark the change from SCIAMACHY to GOME-2 based comparisons in April 2012.

As shown in Fig. 3.7.1, amplitude and seasonality of satellite stratospheric NO_2 columns are poorly modelled with CB05-based chemistry runs including the most recent version of the o-suite. There are no significant differences between o-suite and its control experiment. The significant differences between observations and CB05 chemistry runs, i.e. a strong underestimation of satellite retrievals by models, can be explained by the missing stratospheric chemistry for these model versions. The only constraint on stratospheric NO_x is implicitly made by fixing the HNO_3/O_3 ratio at the 10 hPa level. This assumption, in combination with the changing model settings for stratospheric O_3 for control compared to MACC_CIFS_TM5, may explain some of the jumps we see in stratospheric NO_2. In any of these runs the stratospheric NO_2 is poorly constrained. It clearly indicates that stratospheric NO_2 in the latest version of the o-suite is not a useful product and should be disregarded.

Comparison of the o-suite from July 2012 until August 2014 with the other model runs and satellite observations shows that the previous version of the o-suite stratospheric NO_2 columns have a systematic low bias relative to those from MACC_fcnrt_MOZ and satellite observations for all latitude bands. For example, o-suite values are a factor of 2 smaller than satellite values between 60°S to 90°S for October 2013. Best performance was achieved with the MOZART chemistry experiments without data assimilation (MACC_fcnrt_MOZ, running until September 2014), especially northwards of 30°S. Details on the NO_2 evaluation can be found at: http://www.doas-bremen.de/macc/macc_veri_iup_home.html.

4. Validation results for greenhouse gases

This section describes the NRT validation of the pre-operational, high resolution forecast of CO_2 and CH_4 from 1st December 2015 to 30 November 2016 based on observations from 15 surface stations. Over this period the high resolution forecast corresponds to two experiments: gf39 and ghqy, see also Sec. 2.1.3. The same experiments are used for the validation of CO_2 and CH_4 simulations using ICOS surface data and TCCON total column data.

4.1 CH_4 and CO_2 validation against ICOS observations

In the present comparison we consider 24 hours daily means of observed and simulated time series, without distinction of nighttime and daytime data although they often have different footprints which could justify a separate analysis. It is important to note the change of experiment on March 1st 2016, leading to an abrupt change of CO_2/CH_4 mole fractions at some sites like Amsterdam Island (Figures 4.1.1 and 4.1.2). We should also note that compared to the first reports we have changed the model grid boxes used to compare with observations at three coastal stations: Finokalia (FKL), Biscarrosse (BIS) and St Denis in Reunion Island (STD). Initially we were extracting the closest continental grid box for each site, but due to the influence of local emissions (anthropogenic and/or biospheric) this was resulting in an overestimated variability at diurnal and synoptic scales. For those three stations we are now using the closest marine grid box. This change has greatly improved the comparison with observations at FKL, and has little impact for BIS. For STD the situation is more complicated since we have to choice between two coastal grid boxes (Figure 4.1.3). The eastern and closest box (#1) improved the CH4 comparison; whereas the western coastal box (#2) improved the CO2 comparison. By default the gridbox #1 is used for the model evaluation.

Figure 4.1.1 and 4.1.2 show the CO_2 and CH_4 comparisons at four selected stations in South hemisphere (Amsterdam I.), North hemisphere (Mace Head, Trainou tall tower) and in the tropics (Lamto). The remote station of Amsterdam Island is the site where we have the best correlation coefficients for CO_2 (0.90) and CH_4 (0.89). It should be noted that the change of experiment (gf39 to ghqy) induces a discontinuity in the simulations, and so may bias the metrics in a few cases. For example the correlation coefficient for CH_4 at Amsterdam I. is significantly higher (0.98) when looking only at the last experiment (ghqy) compared to the combination of the two experiments (0.89).

The figure 4.1.4 presents the annual metrics for all surface stations based on comparisons of the daily means mole fractions. Regarding the CO_2 metrics, it appears that stations in South Hemisphere and tropics (RUN, STD, GUY, LTO, CHC) have significantly lower correlation coefficients compared to the European stations. However, as explained before, the best is obtained at the remote station of Amsterdam I., located in the Southern Indian Ocean. So the poorer performance of the model is not an intrinsic feature in South hemisphere but can be explained by the more difficult environment surroundings the monitoring sites. Tropical stations like LTO and GUY are located in places characterized by very strong biospheric sources. In addition the infrastructures of the sites are not as developed as in Europe where tall towers have been erected as part of ICOS in order to minimize the influence of local emissions. For the three tall towers (OHP, OPE, TRN) we see an improvement of the CO_2 correlation coefficient going form the lowest to the highest sampling lines. The two

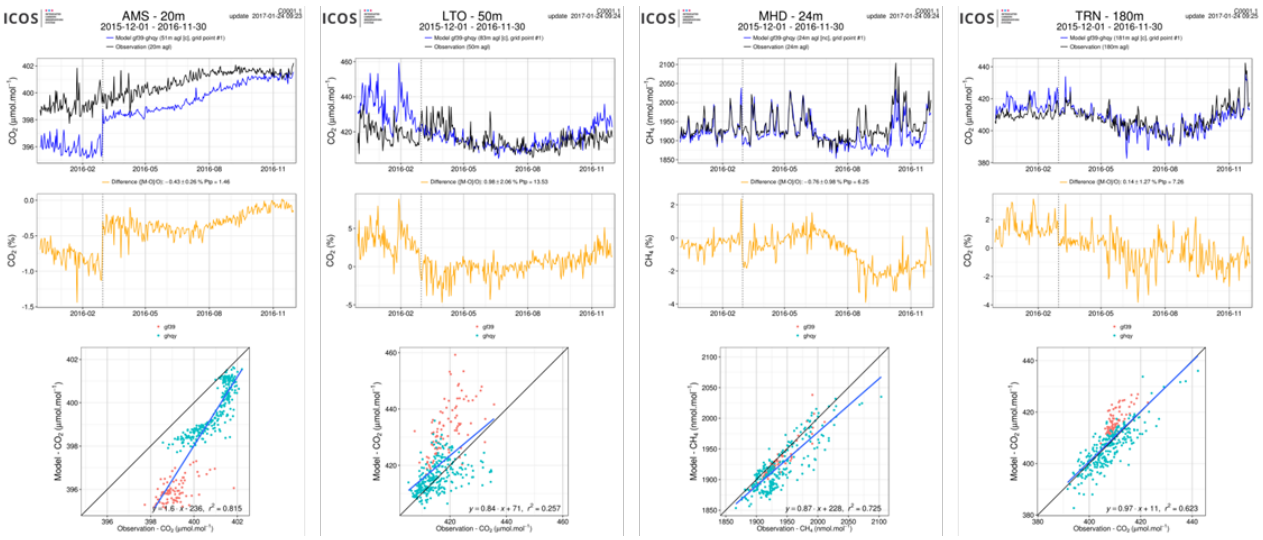

Figure 4.1.1: Above: Comparison of CO_2 daily means observed (red) and simulated (blue) at four stations (Amsterdam I., Mace Head, Lamto and Trainou tall tower). Middle: differences of the observations minus the simulations. Below: Linear fit between observations and simulations. The blue points correspond to the ghqy experiment, initialized on March 1st, 2016.

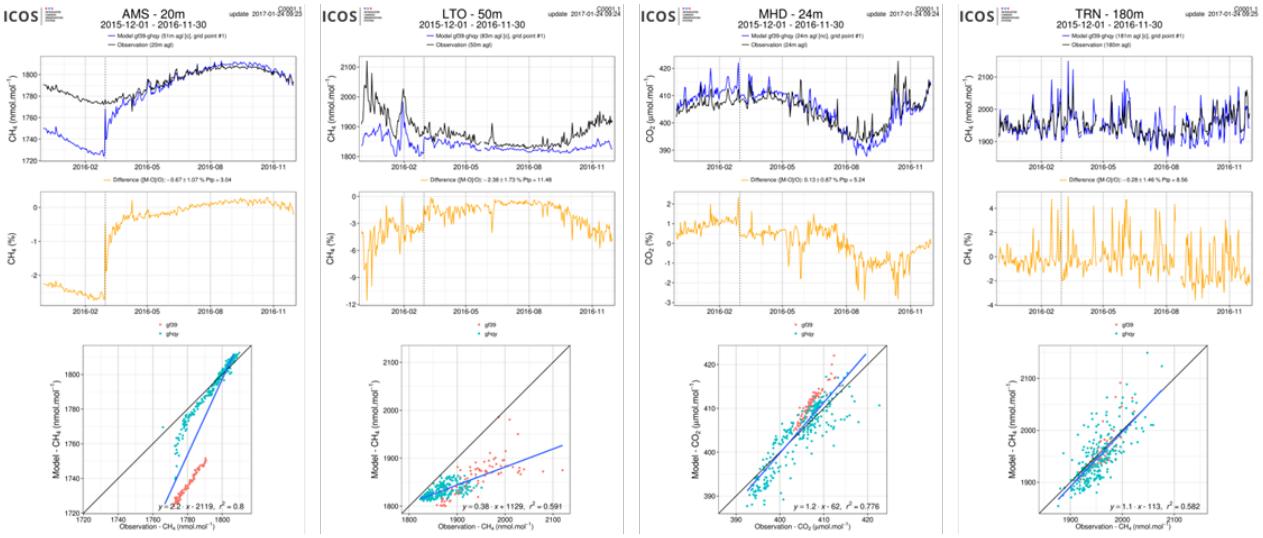

Figure 4.1.2: Same as figure 4.1.1 for CH_4

mountain station located in France (PDM, PUY) display even higher correlation coefficients. Overall the mean correlation coefficient is equal to 0.75 for European stations. It is very similar for CH_4 (0.73) and there is not so much systematic difference for stations located in tropics and south hemisphere.

In the last figure we have merged all European stations in on category, and all tropical/south hemisphere sites in another one, in order to evaluate the seasonal patterns of the metrics. It appears that the seasonal cycle of the CO_2 is significantly overestimated by the model in North hemisphere. Positive biases up to 8 ppm in winter are followed by negative biases up to -5 ppm in late summer. In the tropics/SH sites we find a more systematic negative CO_2 bias of -1.5 ppm. For CH_4 the biases are generally close to zero, except for few months which display negative ones. In

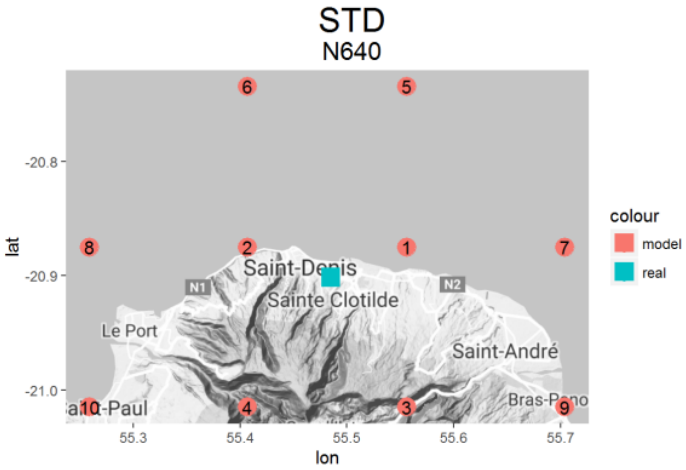

Figure 4.1.3: Location of the coastal station STD, La Réunion Island, and of the model grid boxes. By default the grid 1 is used to compare with observations.

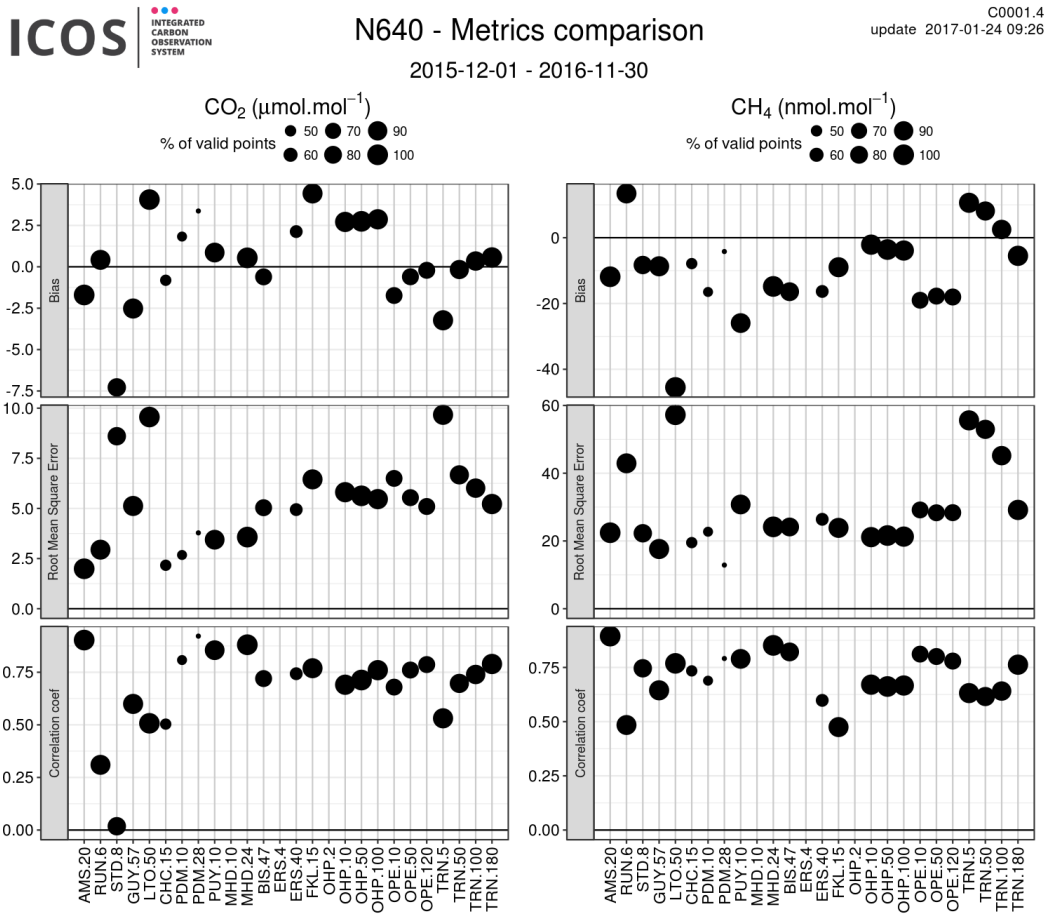

Figure 4.1.4: Annual metrics (bias, RMSE and coefficient correlation) calculated from the model-data comparison for daily means of CO_2 (left) and CH_4 (right) at the 15 sites (with multiple sampling heights at the last three sites). The size of each point relates to the percentage of available data. This figure uses both GF39 and GHQY experiments from 1st December 2015 to 30 November 2016.

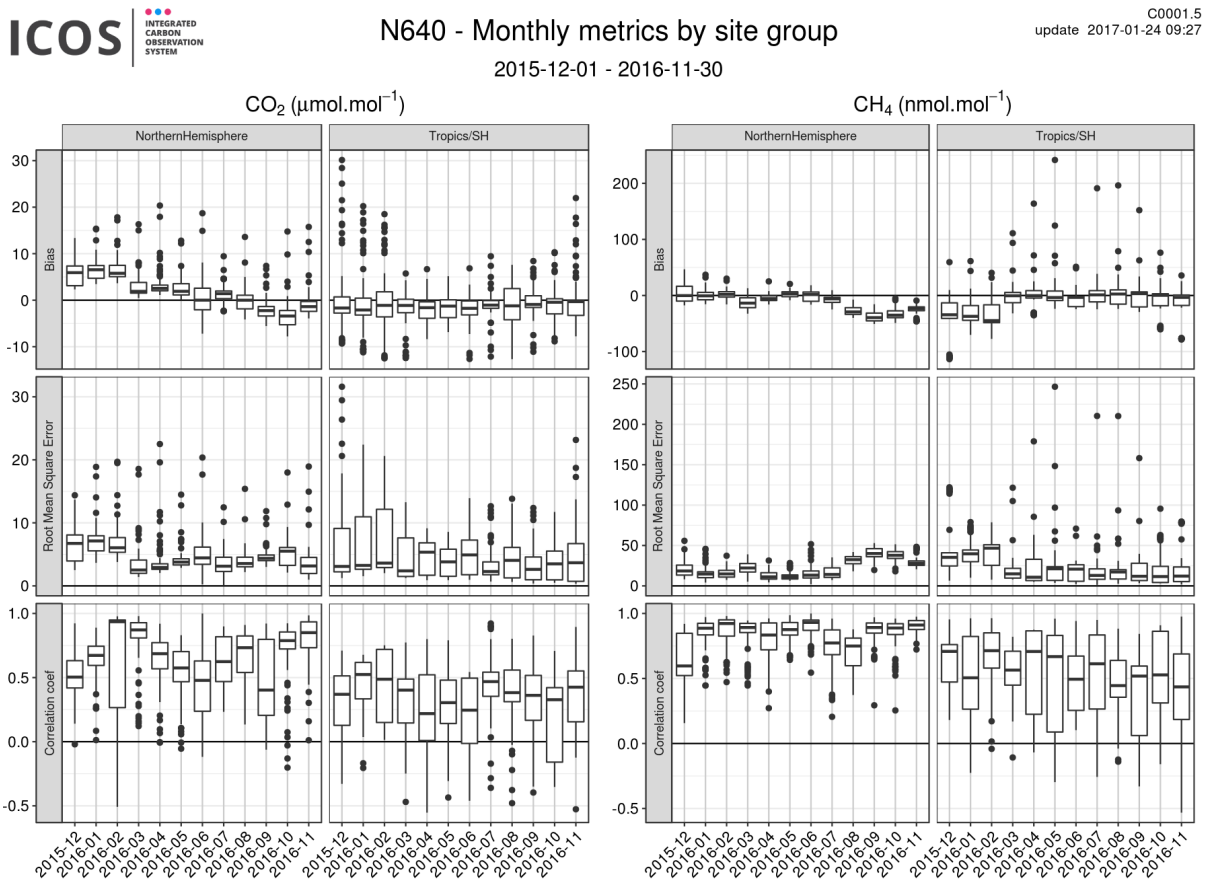

Figure 4.1.5: Annual metrics (bias, RMSE and coefficient correlation) calculated from the model-data comparison for daily means of CO_2 (left) and CH_4 (right) for two groups of stations: North hemisphere (Western Europe) and Tropics/South hemisphere. This figure uses both GF39 and GHQY experiments from 1st December 2015 to 30 November 2016.

North Europe negative biases of more than -20 ppb are observed from August to November 2016. Similar features are observed in tropics/SH for the gf39 model experiment from December to February 2016.

4.2 CH_4 and CO_2 validation against TTCON observations

For the validation column averaged mole fractions of CO_2 and CH_4 (denoted as XCO2 and XCH4) from the Total Carbon Column Observing Network (TCCON) are used. Column averaged mole fractions provide different information than the in situ measurements and are therefore complementary to the in situ data. For example if models suffer from problems in vertical transport, the combination of TCCON and surface in situ measurements will provide a means to detect this.

For the model validation the official TCCON data cannot be used due to its availability of typically one year after the measurement. Some TCCON sites are providing rapid delivery data (RD-TCCON data), which is available at least one month after the measurement. TCCON sites that deliver RD-TCCON data currently include Trainou (France), Bialystok (Poland) and Reunion (France). Over the course of the project more TCCON sites might contribute. This largely depends on funding for the fast data product.

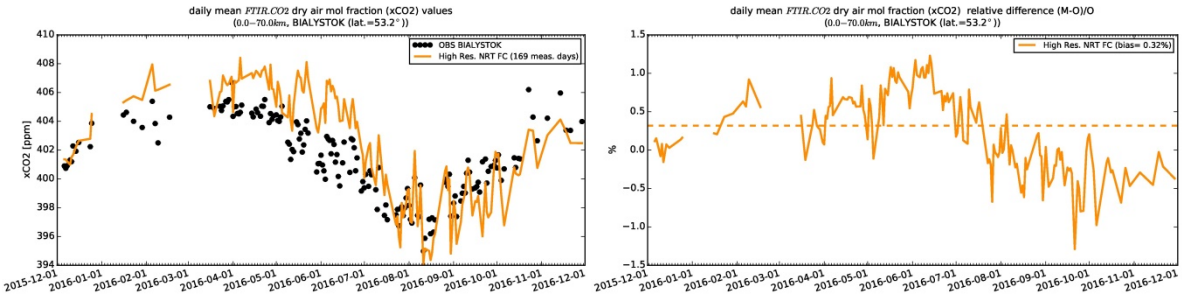

Figure 4.2.1: Time series of column averaged mole fractions (left) and relative difference (right) of carbon dioxide (CO_2) at the TCCON site Bialystok compared to high resolution NRT FC data (yellow)

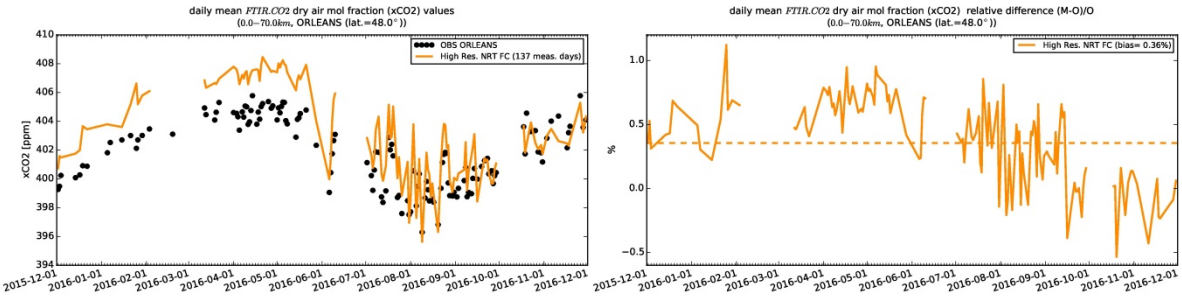

Figure 4.2.2: Time series of column averaged mole fractions (left) and relative difference (right) of carbon dioxide (CO_2) at the TCCON site Orleans compared to high resolution NRT FC data (yellow)

The validation routines used for TCCON data are the same as used for the NDACC network and are documented in Langerock et al. (2015). The routines have been adapted to use the TCCON data format.

4.2.1 Evaluation against TCCON CO_2

The data presented in the Figures 4.2.1-4.2.3 show a comparison for a full seasonal cycle from December 2015 – November 2016. At Bialystok (Fig. 4.2.1) and Orleans (Fig. 4.2.2) the difference between the model and the measurement shows a very similar seasonal pattern. The model overestimates the XCO_2 at both sites for the period January to July, when the CO_2 is declining. From August to November the model underestimates the CO_2 at Bialystok. For Orleans there is a good agreement between model and measurement for the period August to November. Only the short term variations during the minimum are stronger in the model. Variations in the XCO_2 are dependent on large-scale flux pattern. These variations are largest when the north-south gradient is large, which is especially the case during June-August due to the strong boreal uptake during this time of the year. Therefore the largest short-term variations in XCO_2 are expected during these months. A reason for the larger variations in the model could be a too strong CO_2 north-south gradient in the model. A TCCON site at higher latitudes would help to determine the reason.

At Reunion (Fig. 4.2.3) the overall agreement of the annual means is good but the model shows short-term fluctuations of ± 1%, which are not seen in the measurements. These short-term variations of several ppm are not reasonable and mostly occur between October 2015 and January 2016.

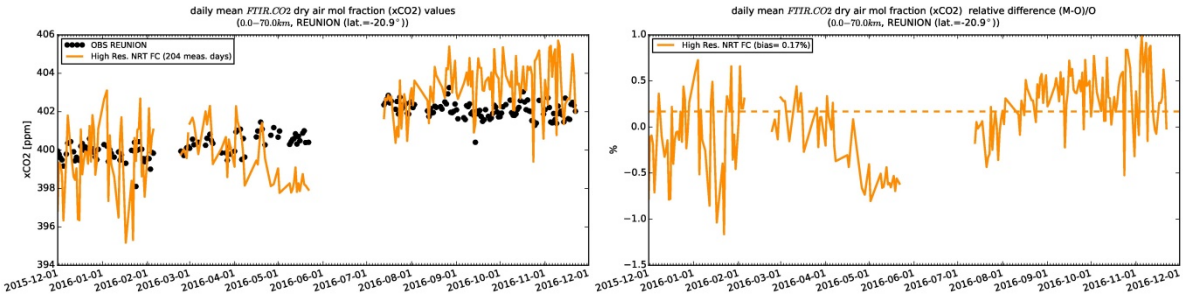

Figure 4.2.3 Time series of column averaged mole fractions (left) and relative difference (right) of carbon dioxide (CO_2) at the TCCON site Reunion compared to high resolution NRT FC data (yellow).

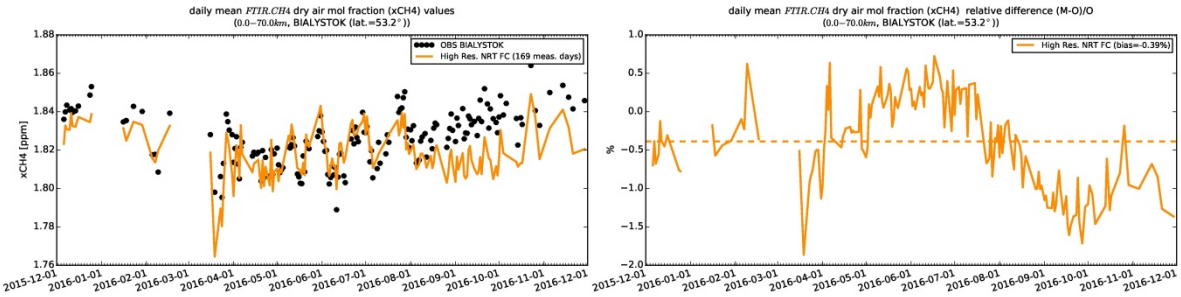

Figure 4.2.4: Time series of column averaged mole fractions (left) and relative difference (right) of methane (CH_4) at the TCCON site Bialystok compared to high resolution NRT FC data (yellow)

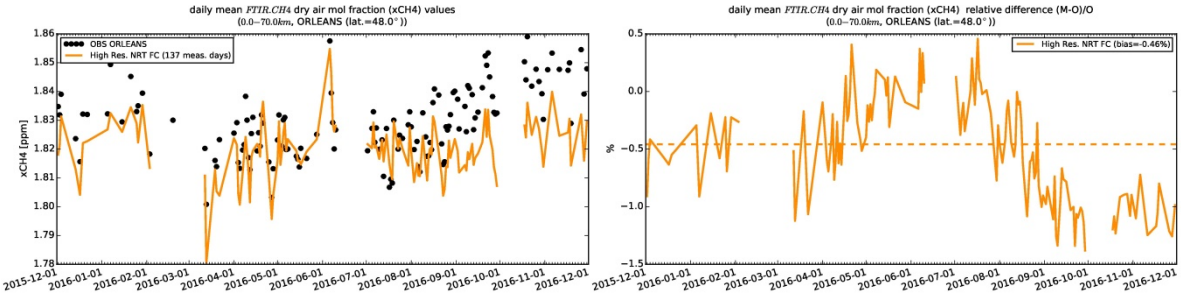

Figure 4.2.5: Time series of column averaged mole fractions (left) and relative difference (right) of methane (CH_4) at the TCCON site Orleans compared to high resolution NRT FC data (yellow)

4.2.2 Evaluation against TCCON CH_4

At Bialystok and Orleans (Figs. 4.2.4 and 4.2.5) the agreement between model and measurements worsens significantly from September 2016 onwards. Between September-November 2016 the model underestimates the seasonal amplitude by about 1%. At Reunion (Fig. 4.2.6) the modelled values were systematically too low between December 2015 and February 2016. This problem in the model seems to be resolved and from April 2016 onwards a good agreement between the measurements and the model is observed.

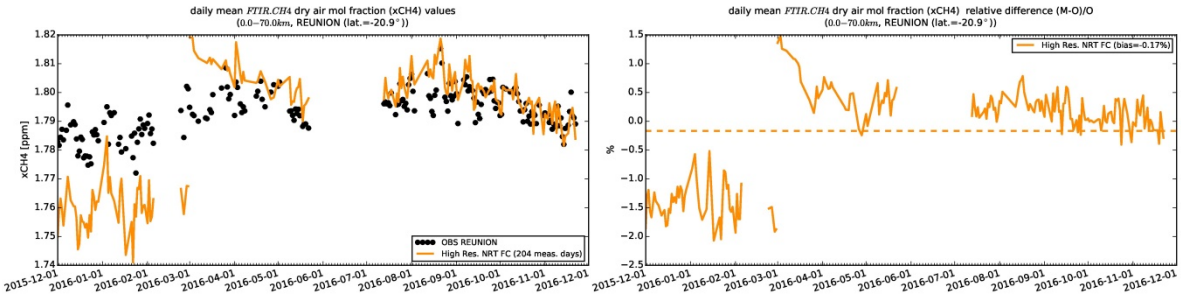

Figure 4.2.6: Time series of column averaged mole fractions (left) and relative difference (right) of methane (CH_4) at the TCCON site Reunion compared to high resolution NRT FC data (yellow).

5. Events

5.1 Dust event over Central-Eastern Mediterranean: 7-9 November 2016

The selected dust event corresponds to a dust plume that originated in Algeria, and move towards Central and Eastern Mediterranean in 7-9 November 2016 as it was detected ground visibility stations (see Fig. 5.1.1). The event was associated to the movement of a barometric trough that had associated the formation of clouds.

The full episode was well predicted by CAMS o-suite as it is showed the comparison of the dust aerosol optical depth (DOD) predicted by CAMS o-suite and observed AOD by MODIS from 6th to 9th November 2016 at 12UTC in Fig. 5.1.2. The model could predicted the arrival and the moment of the maximum peak of the dust plume over the affected AERONET sites in the Mediterranean although the maximum DOD concentration was underestimated (see Lampedusa and Athens-NOA in Figure 3.5.11).

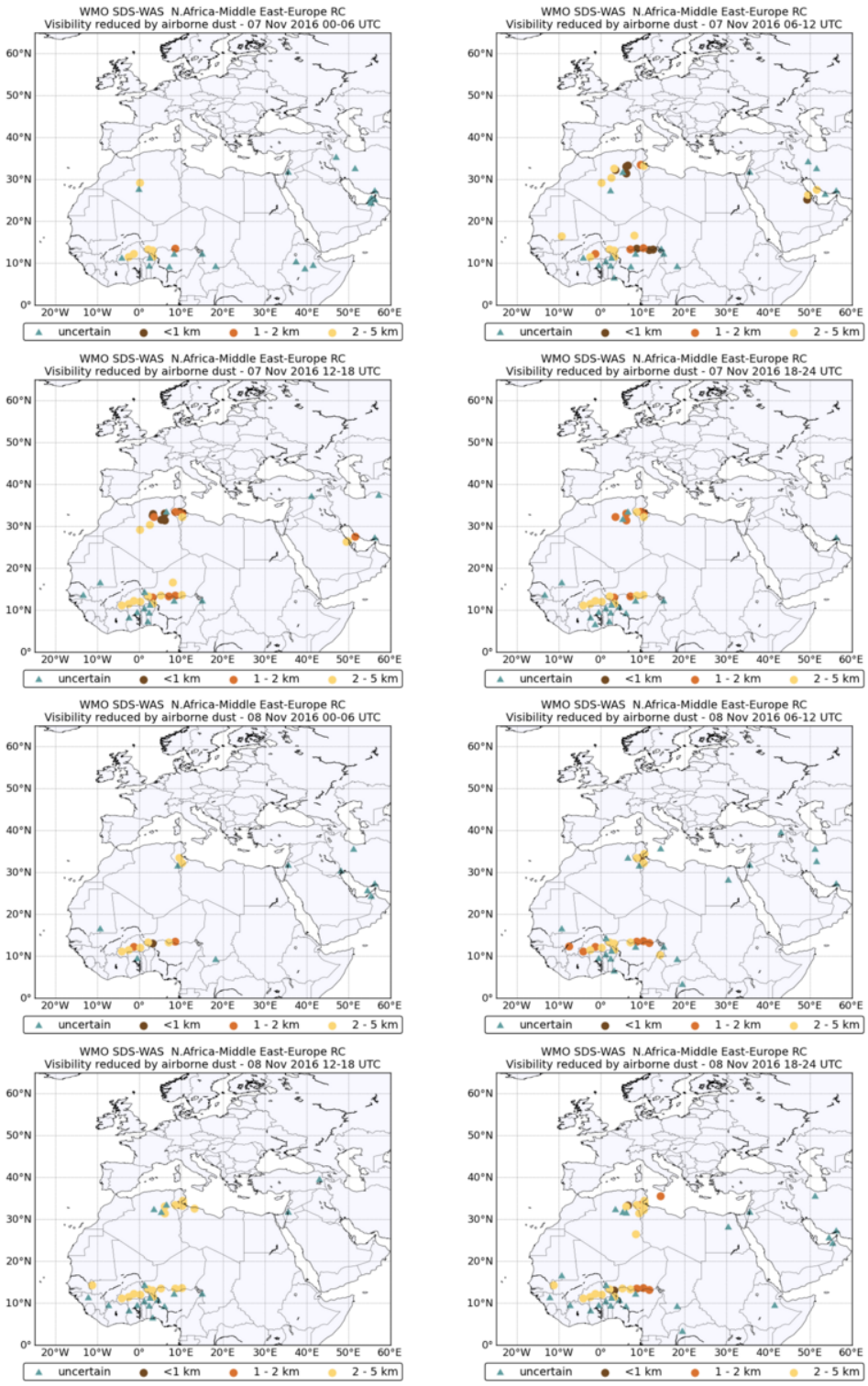

Figure 5.1.1. Visibility from METAR or SYNOP stations from SDS-WAS Regional Center during the case analysis from 7th to 8st November 2016. The maps show cases of visibility reduction by sand or dust to less than 5 km reported in METAR or SYNOP bulletins. More than 1,500 stations are checked every 6 hours. Brownish circles indicate stations where 'sand' or 'dust' has been explicitly reported. Triangles indicate stations where the present weather has been reported as 'haze', meaning that the visibility is reduced by particles of unspecified origin.

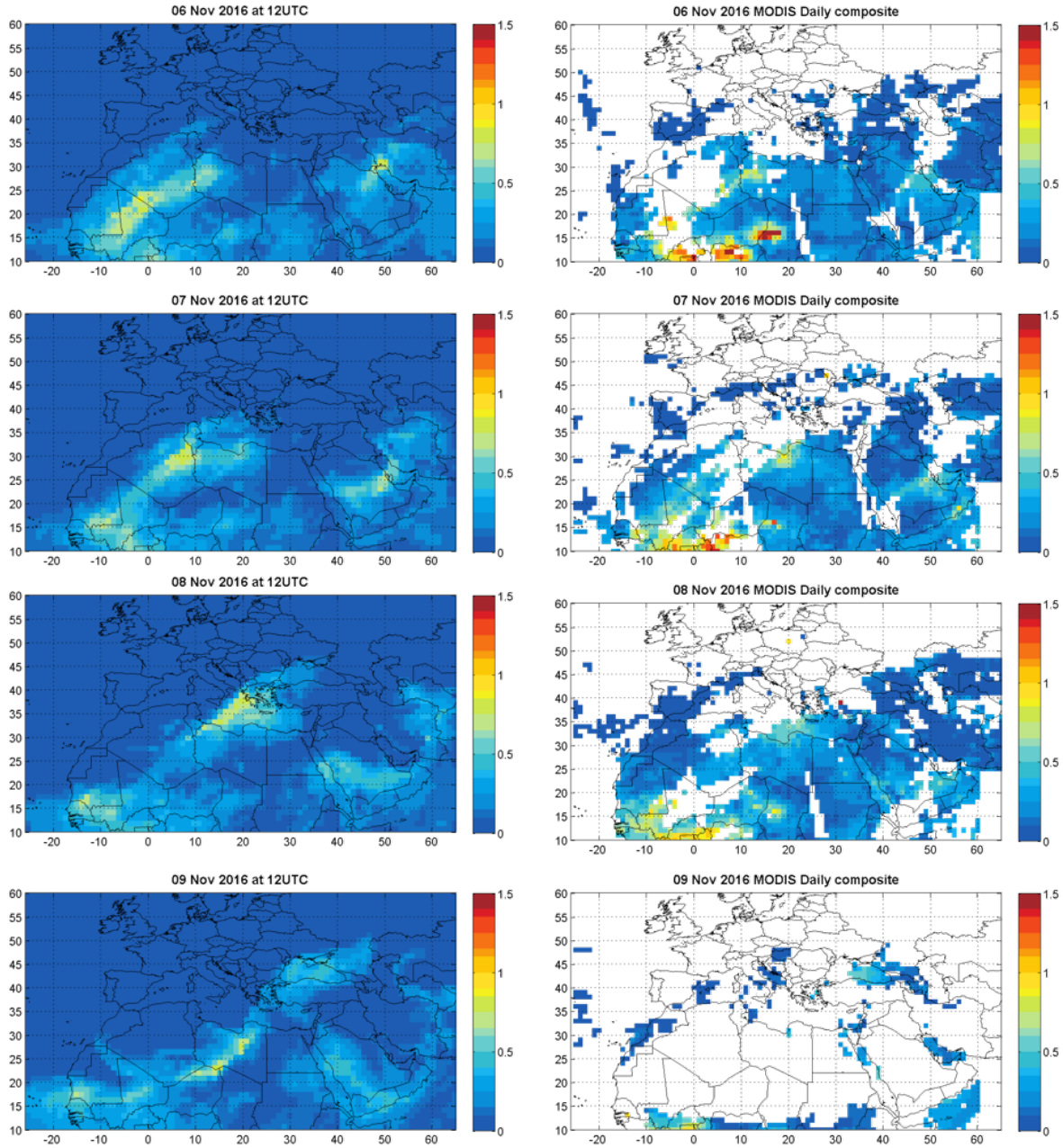

Figure 5.1.2. DOD from o-suite (right column) and AOD from MODIS combined Dark Target and Deep Blue near-real-time aerosol products (left column, MCDAODHD files), for November 6th- 9th, 2016 at 12UTC.

5.2 Fire case in Siberia, Russian Federation in September 2016

Several big fire events took place in Siberia, Russian Federation, in September 2016. IASI data show rapidly increasing CO over this region starting from September 18 and eastward transport across the continent later on (Fig. 5.2.1). Both model runs captured the location of the plume and the eastward transport of CO. Pictures from both model runs are very similar with slightly lower values in the control run. In the beginning of the fire event, on September 18, both runs overestimated CO values in the plume, but show an underestimation in the transportation pathway on September 23 and 25.

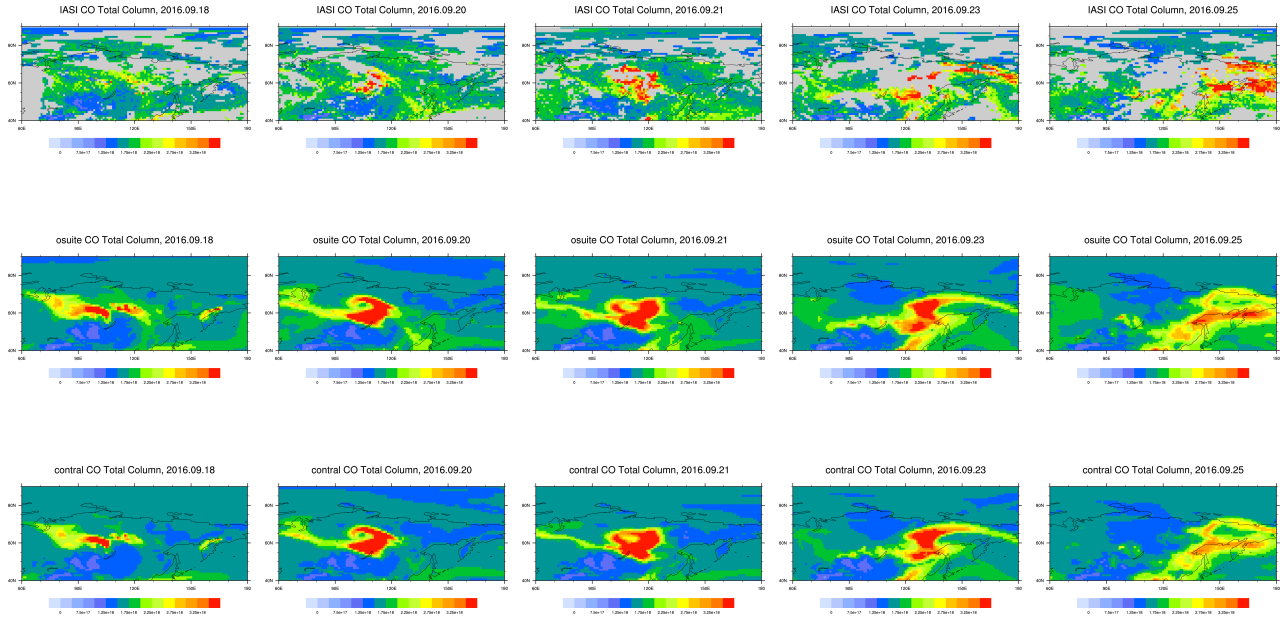

Fig. 5.2.1: CO total column from IASI (top), o-suite (middle) and control runs (bottom) for 18, 20, 21, 23 and 25 of September 2016 over the selected region.

5.3 Fire case in Siberia, Russian Federation in September 2016

Figure 5.3.1 shows an example of a synoptic event at Amsterdam Island which occurred in June 2016. During this season we observed sometimes an increase of the observed trace gases, like Radon, CO_2, CH_4, CO, black carbon. Such events cannot be explained by local emissions and are due to rapid advections (2-3 days) of pollutants from the southern Africa (Figure 5.3.2). This example demonstrates the capacity of the model to simulate this transportation over Indian Ocean, since both the amplitude and timing of the CH_4 spike is perfectly reproduced. For CO_2, the model underestimates the increase of concentrations and fails to reproduce the daily variation, indicating that the biospheric surface flux should be improved.

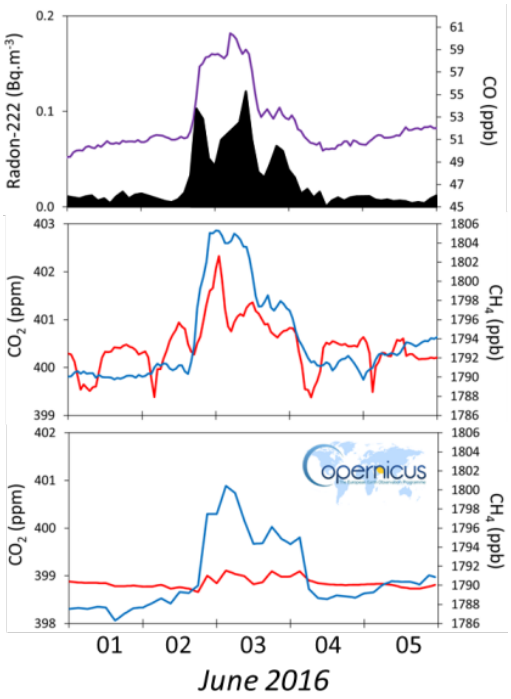

Figure 5.3.1: Short term variabilities of trace gases at Amsterdam Island during a radonic storm (01-05 June 2016) originating from Southern Africa. The above figure shows mole fractions of Radon-222 (black) and CO (purple. The middle figure shows mole fractions of CO_2 (red) and CH_4 (blue). The bootom figure shows simulations of CO_2 (red) and CH_4 (blue).

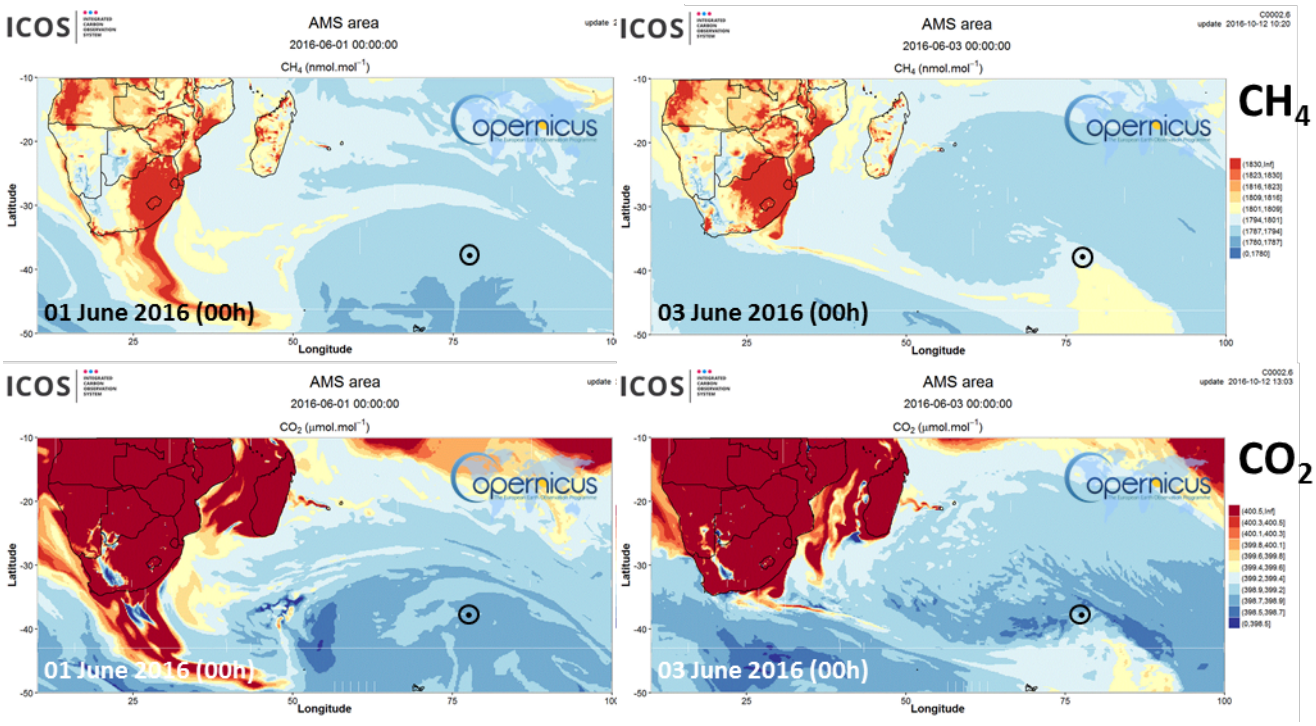

Figure 5.3.2: Simulated distribution of CH_4 (above) above and CO_2 (below) mole fractions at the surface level on 1st (left) and 3rd (right) June 2016. The black circle indicates the position of Amsterdam Island.

6. References

Agusti-Panareda, A., Monitoring upgrades of analysis/forecast system, MACC-III Deliverable D44.04, June 2015.

Bergamaschi, P., Frankenberg, C., Meirink, J. F., Krol, M., Villani, M. G., Houweling, S., Dentener, F., Dlugokencky, E. J., Miller, J. B., Gatti, L. V., Engel, A., and Levin, I.: Inverse modeling of global and regional CH4 emissions using SCIAMACHY satellite retrievals, J. Geophys. Res., 114, D22301, doi:10.1029/2009JD012287, 2009.

Benedetti, A., J.-J. Morcrette, O. Boucher, A. Dethof, R. J. Engelen, M. Fisher, H. Flentjes, N. Huneeus, L. Jones, J. W. Kaiser, S. Kinne, A. Mangold, M. Razinger, A. J. Simmons, M. Suttie, and the GEMS-AER team: Aerosol analysis and forecast in the ECMWF Integrated Forecast System. Part II : Data assimilation, J. Geophys. Res., 114, D13205, doi:10.1029/2008JD011115, 2009.

Boussetta, S., Balsamo, G., Beljaars, A., Agusti-Panareda, A., Calvet, J.-C., Jacobs, C., van den Hurk, B., Viterbo, P., Lafont, S., Dutra, E., Jarlan, L., Balzarolo, M., Papale, D., and van der Werf, G.: Natural carbon dioxide exchanges in the ECMWF Integrated Forecasting System: implementation and offline validation, J. Geophys. Res.-Atmos., 118, 1–24, doi: 10.1002/jgrd.50488, 2013.

Braathen, WMO Arctic Ozone Bulletin No 1/2016, DOI:10.13140/RG.2.1.4929.6403, 2016.

Cariolle, D. and Teyssèdre, H.: A revised linear ozone photochemistry parameterization for use in transport and general circulation models: multi-annual simulations, Atmos. Chem. Phys., 7, 2183-2196, doi:10.5194/acp-7-2183-2007, 2007.

Dee, D. P. and S. Uppala, Variational bias correction of satellite radiance data in the ERA-Interim reanalysis. Quart. J. Roy. Meteor. Soc.,135, 1830-1841, 2009.

Deeter, M. N., Emmons, L. K., Edwards, D. P., Gille, J. C., and Drummond, J. R.: Vertical resolution and information content of CO profiles retrieved by MOPITT, Geophys. Res. Lett., 31, L15112, doi:10.1029/2004GL020235, 2004.

Deeter, M. N., et al. (2010), The MOPITT version 4 CO product: Algorithm enhancements, validation, and long-term stability, J. Geophys. Res., 115, D07306, doi:10.1029/2009JD013005.

Deshler, T., J.L. Mercer, H.G.J. Smit, R. Stubi, G. Levrat, B.J. Johnson, S.J. Oltmans, R. Kivi, A.M. Thompson, J. Witte, J. Davies, F.J. Schmidlin, G. Brothers, T. Sasaki (2008) Atmospheric comparison of electrochemical cell ozonesondes from different maufacturers, and with different cathode solution strengths: The Balloon Experiment on Standards for Ozonsondes. J. Geophys. Res.113, D04307, doi:10.1029/2007JD008975

Dupuy, E., et al.: Validation of ozone measurements from the Atmospheric Chemistry Experiment (ACE), Atmos. Chem. Phys., 9, 287-343, doi:10.5194/acp-9-287-2009, 2009.

Elbern, H., Schwinger, J., Botchorishvili, R.: Chemical state estimation for the middle atmosphere by four-dimensional variational data assimilation: System configuration. Journal of Geophysical Research (Atmospheres) 115, 6302, 2010.

Emmons, L. K., D. P. Edwards, M. N. Deeter, J. C. Gille, T. Campos, P. Nédélec, P. Novelli, and G. Sachse, Measurements of Pollution In The Troposphere (MOPITT) validation through 2006 Atmos. Chem. Phys., 9, 1795-1803, 2009

Errera, Q., Daerden, F., Chabrillat, S., Lambert, J. C., Lahoz, W. A., Viscardy, S., Bonjean, S., and Fonteyn, D., 4D-Var Assimilation of MIPAS chemical observations: ozone and nitrogen dioxide analyses, Atmos. Chem. Phys., 8, 6169-6187, 2008.

Errera, Q. and Ménard, R.: Technical Note: Spectral representation of spatial correlations in variational assimilation with grid point models and application to the belgian assimilation system for chemical observations (BASCOE), Atmos. Chem. Phys. Discuss., 12, 16763-16809, doi:10.5194/acpd-12-16763-2012, 2012.

Eskes, H., Huijnen, V., Arola, A., Benedictow, A., Blechschmidt, A.-M., Botek, E., Boucher, O., Bouarar, I., Chabrillat, S., Cuevas, E., Engelen, R., Flentje, H., Gaudel, A., Griesfeller, J., Jones, L., Kapsomenakis, J., Katragkou, E., Kinne, S., Langerock, B., Razinger, M., Richter, A., Schultz, M., Schulz, M., Sudarchikova, N., Thouret, V., Vrekoussis, M., Wagner, A., and Zerefos, C.: Validation of reactive gases and aerosols in the MACC global analysis and forecast system, Geosci. Model Dev., 8, 3523-3543, doi:10.5194/gmd-8-3523-2015, 2015.

Eskes, H.J., V. Huijnen, S, Basart, A. Benedictow, A.-M. Blechschmidt, S. Chabrillat, H. Clark, Y. Christophe, E. Cuevas, H. Flentje, K. M. Hansen, J. Kapsomenakis, B. Langerock, M. Ramonet, A. Richter, M. Schulz, A. Wagner, T. Warneke, C. Zerefos: Observations characterisation and validation methods document. Copernicus Atmosphere Monitoring Service (CAMS) report, CAMS84_2015SC1_D84.8.1_2016Q2_201603, March 2016. Available from: http://atmosphere.copernicus.eu/user-support/validation/verification-global-services

Flemming, J., Huijnen, V., Arteta, J., Bechtold, P., Beljaars, A., Blechschmidt, A.-M., Diamantakis, M., Engelen, R. J., Gaudel, A., Inness, A., Jones, L., Josse, B., Katragkou, E., Marecal, V., Peuch, V.-H., Richter, A., Schultz, M. G., Stein, O., and Tsikerdekis, A.: Tropospheric chemistry in the Integrated Forecasting System of ECMWF, Geosci. Model Dev., 8, 975-1003, doi:10.5194/gmd-8-975-2015, 2015.

Franco, B., et al., Retrievals of formaldehyde from ground-based FTIR and MAX-DOAS observations at the Jungfraujoch station and comparisons with GEOS-Chem and IMAGES model simulations, Atmos. Meas. Tech., 8, 1733-1756, 2015

Gielen, C., Van Roozendael, M., Hendrick, F., Pinardi, G., Vlemmix, T., De Bock, V., De Backer, H., Fayt, C., Hermans, C., Gillotay, D., and Wang, P.: A simple and versatile cloud-screening method for MAX-DOAS retrievals, Atmos. Meas. Tech., 7, 3509-3527, doi:10.5194/amt-7-3509-2014, 2014.

Granier, C. et al.: Evolution of anthropogenic and biomass burning emissions of air pollutants at global and regional scales during the 1980–2010 period. Climatic Change (109), 2011

Holben, B. N., Eck, T. F., Slutsker, I., Tanré, D., Buis, J. P., Setzer, A., Vermote, E., Reagan, J. A., Kaufman, Y. J., Nakajima, T., Lavenu, F., Jankowiak, I., and Smirnov A.: AERONET – a federated instrument network and data archive for aerosol characterization, Remote Sens. Environ., 66, 1–16, 5529, 5533, 5537, 5544, 1998.

Hommel, R., Eichmann, K.-U., Aschmann, J., Bramstedt, K., Weber, M., von Savigny, C., Richter, A., Rozanov, A., Wittrock, F., Khosrawi, F., Bauer, R., and Burrows, J. P.: Chemical ozone loss and ozone mini-hole event

during the Arctic winter 2010/2011 as observed by SCIAMACHY and GOME-2, Atmos. Chem. Phys., 14, 3247-3276, doi:10.5194/acp-14-3247-2014, 2014.

Huijnen, V., et al.: The global chemistry transport model TM5: description and evaluation of the tropospheric chemistry version 3.0, Geosci. Model Dev., 3, 445-473, doi:10.5194/gmd-3-445-2010, 2010.

Inness, A., Blechschmidt, A.-M., Bouarar, I., Chabrillat, S., Crepulja, M., Engelen, R. J., Eskes, H., Flemming, J., Gaudel, A., Hendrick, F., Huijnen, V., Jones, L., Kapsomenakis, J., Katragkou, E., Keppens, A., Langerock, B., de Mazière, M., Melas, D., Parrington, M., Peuch, V. H., Razinger, M., Richter, A., Schultz, M. G., Suttie, M., Thouret, V., Vrekoussis, M., Wagner, A., and Zerefos, C.: Data assimilation of satellite-retrieved ozone, carbon monoxide and nitrogen dioxide with ECMWF's Composition-IFS, Atmos. Chem. Phys., 15, 5275-5303, doi:10.5194/acp-15-5275-2015, 2015.

Janssens-Maenhout, G., Dentener, F., Aardenne, J. V., Monni, S., Pagliari, V., Orlandini, L., Klimont, Z., Kurokawa, J., Akimoto, H., Ohara, T., Wankmueller, R., Battye, B., Grano, D., Zuber, A., and Keating, T.: EDGAR-HTAP: a Harmonized Gridded Air Pollution Emission Dataset Based on National Inventories, JRC68434, EUR report No EUR 25 299–2012, ISBN 978-92-79- 23122-0, ISSN 1831-9424, European Commission Publications Office, Ispra (Italy), 2012.

Jaross, G., Bhartia, P.K., Chen, G., Kowitt, M., Haken, M., Chen, Z., Xu, Ph., Warner, J., Kelly, T. : OMPS Limb Profiler instrument performance assessment, J. Geophys. Res. Atmos 119, 2169-8996, 2014.

Kaiser, J. W., Heil, A., Andreae, M. O., Benedetti, A., Chubarova, N., Jones, L., Morcrette, J.-J., Razinger, M., Schultz, M. G., Suttie, M., and van der Werf, G. R.: Biomass burning emissions estimated with a global fire assimilation system based on observed fire radiative power, Biogeosciences, 9, 527-554, doi:10.5194/bg-9-527-2012, 2012.

Kramarova, N. A., Nash, E. R., Newman, P. A., Bhartia, P. K., McPeters, R. D., Rault, D. F., Seftor, C. J., Xu, P. Q., and Labow, G. J.: Measuring the Antarctic ozone hole with the new Ozone Mapping and Profiler Suite (OMPS), Atmos. Chem. Phys., 14, 2353-2361, doi:10.5194/acp-14-2353-2014, 2014.

Lahoz, W. A., Errera, Q., Viscardy, S., and Manney G. L., The 2009 stratospheric major warming described from synergistic use of BASCOE water vapour analyses and MLS observations, Atmos. Chem. Phys. 11, 4689-4703, 2011

Lambert, A, et al., Aura Microwave Limb Sounder Version 3.4 Level-2 near real-time data user guide, http://disc.sci.gsfc.nasa.gov/Aura/data-holdings/MLS/documents/NRT-user-guide-v34.pdf

Langerock, B., De Mazière, M., Hendrick, F., Vigouroux, C., Desmet, F., Dils, B., and Niemeijer, S.: Description of algorithms for co-locating and comparing gridded model data with remote-sensing observations, Geosci. Model Dev., 8, 911-921, doi:10.5194/gmd-8-911-2015, 2015.

Lefever, K., van der A, R., Baier, F., Christophe, Y., Errera, Q., Eskes, H., Flemming, J., Inness, A., Jones, L., Lambert, J.-C., Langerock, B., Schultz, M. G., Stein, O., Wagner, A., and Chabrillat, S.: Copernicus stratospheric ozone service, 2009–2012: validation, system intercomparison and roles of input data sets, Atmos. Chem. Phys., 15, 2269-2293, doi:10.5194/acp-15-2269-2015, 2015.

Liu, Z., et al., Exploring the missing source of glyoxal (CHOCHO) over China, Geophys. Res. Lett., 39, L10812, doi: 10.1029/2012GL051645, 2012

Massart, S., Flemming, J., Cariolle, D., Jones, L., High resolution CO tracer forecasts, MACC-III Deliverable D22.04, May 2015, available from http://www.gmes-atmosphere.eu/documents/macciii/deliverables/grg

Morcrette, J.-J., O. Boucher, L. Jones, D. Salmond, P. Bechtold, A. Beljaars, A. Benedetti, A. Bonet, J. W. Kaiser, M. Razinger, M. Schulz, S. Serrar, A. J. Simmons, M. Sofiev, M. Suttie, A. M. Tompkins, and A. Untch: Aerosol analysis and forecast in the ECMWF Integrated Forecast System. Part I: Forward modelling, J. Geophys. Res., 114, D06206, doi:10.1029/2008JD011235, 2009.

Richter, A., Burrows, J. P., Nüß, H., Granier, C, Niemeier, U.: Increase in tropospheric nitrogen dioxide over China observed from space, Nature, 437, 129-132, doi: 10.1038/nature04092, 2005

*Richter, A., Begoin, M., Hilboll, A., and Burrows, J. P.: An improved NO2 retrieval for the GOME-2 satellite instrument, Atmos. Meas. Tech. , **4**, 1147-1159, doi:10.5194/amt-4-1147-2011, 2011*

Sindelarova, K., Granier, C., Bouarar, I., Guenther, A., Tilmes, S., Stavrakou, T., Müller, J.-F., Kuhn, U., Stefani, P., and Knorr, W.: Global data set of biogenic VOC emissions calculated by the MEGAN model over the last 30 years, Atmos. Chem. Phys., 14, 9317-9341, doi:10.5194/acp-14-9317-2014, 2014.

Smit, H.G.J., W. Straeter, B.J. Johnson, S.J. Oltmans, J. Davies, D.W. Tarasick, B. Hoegger, R. Stubi, F.J. Schmidlin, T. Northam, A.M. Thompson, J.C. Witte, I. Boyd: Assessment of the performance of ECC-ozonesondes under quasi-flight conditions in the environmental simulation chamber: Insights from the Juelich Ozone Sonde Intercomparison Experiment (JOSIE), J. Geophys. Res. 112, D19306, doi:10.1029/2006JD007308, 2007.

Solomon, S., Haskins, J., Ivy, D. J. and Min, F.: Fundamental differences between Arctic and Antarctic ozone depletion, PNAS 2014 111 (17) 6220-6225, doi:10.1073/pnas.1319307111, 2014.

Stavrakou,T., First space-based derivation of the global atmospheric methanol fluxes, Atm. Chem. Phys., 11, 4873-4898, 2013.

Strahan, S.E., A.R. Douglass, and P.A. Newman, The contributions of chemistry and transport to low arctic ozone in March 2011 derived from Aura MLS observations, J. Geophys. Res. Atmos., 118, 1563–1576, doi:10.1002/jgrd.50181, 2013.

Taha, G.; Jaross, G. R.; Bhartia, P. K.: Validation of OMPS LP Ozone Profiles Version 2.0 with MLS, Ozone Sondes and Lidar Measurements, American Geophysical Union, Fall Meeting 2014, abstract #A33J-3322, 2014.

Taylor, K.E.: Summarizing multiple aspects of model performance in a single diagram. J.Geophys. Res., 106, 7183-7192, 2001.

van der A, R. J. , M. A. F. Allaart, and H. J. Eskes, Multi sensor reanalysis of total ozone, Atmos. Chem. Phys., 10, 11277–11294, doi:10.5194/acp-10-11277-2010, www.atmos- chem-phys.net/10/11277/2010/, 2010

van der A, R., M. Allaart, H. Eskes, K. Lefever, Validation report of the MACC 30-year multi-sensor reanalysis of ozone columns Period 1979-2008, MACC-II report, Jan 2013, MACCII_VAL_DEL_D_83.3_OzoneMSRv1_20130130.docx/pdf.

van der A, R. J., Allaart, M. A. F., and Eskes, H. J.: Extended and refined multi sensor reanalysis of total ozone for the period 1970–2012, Atmos. Meas. Tech., 8, 3021-3035, doi:10.5194/amt-8-3021-2015, 2015.

*Vrekoussis, M., Wittrock, F., Richter, A., and Burrows, J. P.: GOME-2 observations of oxygenated VOCs: what can we learn from the ratio glyoxal to formaldehyde on a global scale?, Atmos. Chem. Phys., **10**, 10145-10160, doi:10.5194/acp-10-10145-2010, 2010*

Wittrock, F., A. Richter, H. Oetjen, J. P. Burrows, M. Kanakidou, S. Myriokefalitakis, R. Volkamer, S. Beirle, U. Platt, and T. Wagner, Simultaneous global observations of glyoxal and formaldehyde from space, Geophys. Res. Lett., 33, L16804, doi:10.1029/2006GL026310, 2006

WMO (2010), Guidelines for the Measurement of Atmospheric Carbon Monoxide, GAW Report No. 192, World Meteorological Organization, Geneva, Switzerland, 2010.

WMO (2013), Guidelines for the Continuous Measurements of Ozone in the Troposphere, GAW Report No. 209, World Meteorological Organization, Geneva, Switzerland, 2013.

Annex 1: Acknowledgements

Listed below are the authors contributing to the sections in this report. The authors contributing to the model description are also provided, as well as acknowledgements to the validation datasets.

Tropospheric reactive gases reactive gases

Annette Wagner, MPG (editor, O3 sondes, GAW data)
Hannah Clark, Valerie Thouret, CNRS-LA (IAGOS)
Harald Flentje, DWD (O3 sondes, GAW data)
Anne Blechschmidt and Andreas Richter, IUB Bremen (GOME-2 NO2, HCHO)
John Kapsomenakis, Christos Zerefos, AA (ESRL)
N. Sudarchikova, satellite IR observations (MPG)
Kaj Hansen, Ulas Im, AU (Arctic theme)
Bavo Langerock, BIRA (NDACC)

Tropospheric aerosol

Michael Schulz, MetNo (editor, Aerocom, Aeronet)
Anna Benedictow, Jan Griesfeller, MetNo (Aerocom, Aeronet)
Sara Basart, MTeresa Pay, Oriol Jorba, BSC-CNS (Aeronet, MODIS, AirBase, SDS-WAS NAMEE RC)
Emilio Cuevas, AEMET (Aeronet, MODIS, AirBase, SDS-WAS NAMEE RC)
Harald Flentje, DWD (Backscatter profiles)

Stratospheric reactive gases

Yves Christophe, BIRA (editor, model intercomparisons)
Simon Chabrillat, BIRA (model intercomparisons)
Annette Wagner, MPI-M (O3 sondes)
Bavo Langerock, BIRA (NDACC FTIR, MWR, UVVIS DOAS, LIDAR)
Anne Blechschmidt and Andreas Richter, IUB-UB Bremen (SCIAMACHY/GOME-2 NO2)

Greenhouse gases

Michel Ramonet, IPSL (ICOS)
Olivier Jossoud and Leonard Rivier, LSCE (ICOS)
Thorsten Warneke, UBC (TCCON)
Bavo Langerock, BIRA (TCCON)

Reactive gases and aerosol modeling

Johannes Flemming (ECMWF), Antje Inness (ECMWF), Angela Benedetti (ECMWF), Sebastien Massart (ECMWF), Anna Agusti-Panareda (ECMWF), Johannes Kaiser (KCL/MPIC/ECMWF), Samuel Remy (LMD), Olivier Boucher (LMD), Vincent Huijnen (KNMI), Richard Engelen (ECMWF)

Acknowledgements for the validation datasets used

We wish to acknowledge the provision of NRT GAW observational data by: Institute of Atmospheric Sciences and Climate (ISAC) of the Italian National Research Council (CNR), South African Weather Service, National Centre for Atmospheric Science (NCAS, Cape Verde), National Air Pollution Monitoring Network (NABEL) (Federal Office for the Environment FOEN and Swiss Federal Laboratories for Materials Testing and Research EMPA), Atmospheric Environment Division Global Environment and Marine Department Japan Meteorological Agency, Chinese Academy of Meteorological Sciences (CAMS), Alfred Wegener Institut, Umweltbundesamt (Austria), National Meteorological Service (Argentina), Umweltbundesamt (UBA, Germany)

We are grateful to the numerous operators of the Aeronet network and to the central data processing facility at NASA Goddard Space Flight Center for providing the NRT sun photometer data, especially Ilya Slutker and Brent Holben for sending the data.

We wish to acknowledge the provision of ozone sonde data by the World Ozone and Ultraviolet Radiation Data Centre established at EC in Toronto (http://woudc.org), by the Data Host Facility of the Network for the Detection of Atmospheric Composition Change established at NOAA (http://ndacc.org), by the Norwegian Institute for Air Research and by the National Aeronautics and Space Administration (NASA).

We wish to thank the NDACC investigators for the provision of observations at Ny Alesund, Bern, Jungfraujoch, Izaña, Xianghe, Harestua, Reunion Maido, Uccle, Hohenpeissen, Mauna Loa, Lauder and Haute Provence. Special thanks to the data providers at Ny-Alesund, Bern and Uccle for their support of the Arctic ozone depletion case study.

The authors acknowledge the help of Geir Braathen (WMO) for his support of the Arctic ozone depletion case study.

The authors acknowledge the NOAA Earth System Research Laboratory (ESRL) Global Monitoring Division (GMD) for the provision of ground based ozone concentrations.

The MOPITT CO data were obtained from the NASA Langley Research Center ASDC. We acknowledge the LATMOS IASI group for providing IASI CO data.

SCIAMACHY lv1 radiances were provided to IUP-UB by ESA through DLR/DFD.

GOME-2 lv1 radiances were provided to IUP-UB by EUMETSAT.

Index database and especially to the contributors to that database which provided the measurements for comparisons.

The authors acknowledge Environment and Climate Change Canada for the provision of Alert ozone data and Sara Crepinsek – NOAA for the provision of Tiksi ozone data. Surface ozone data from the Zeppelin Mountain, Svalbard are from www.luftkvalitet.info. Surface ozone data from the Villum Research Station, Station Nord (VRS) were financially supported by “The Danish Environmental Protection Agency” with means from the MIKA/DANCEA funds for Environmental Support to the Arctic Region. The Villum Foundation is acknowledged for the large grant making it possible to build VRS in North Greenland.

We acknowledge the National Aeronautics and Space Administration (NASA), USA for providing the http://osirus.usask.ca/OMPS limb sounder data (http://npp.gsfc.nasa.gov/omps.html) and the Aura-MLS offline data (http://mls.jpl.nasa.gov/index-eos-mls.php).

We acknowledge the University of Saskatchewan, Canada for providing the OSIRIS (http://osirus.usas.ca/) observations data and the Canadian Space Agency and science teams for providing validation observations by ACE-FTS on the Canadian satellite SCISAT-1.

The TCCON site at Orleans is operated by the University of Bremen and the RAMCES team at LSCE (Gif-sur-Yvette, France). The TCCON site at Bialystok is operated by the University of Bremen. Funding for the two sites was provided by the EU-project ICOS-INWIRE and the University of Bremen. The TCCON site at Réunion is operated by BIRA-IASB, in cooperation with UReunion and is funded by BELSPO in the framework of the Belgian ICOS program.

We acknowledge the provision of CO_2/CH_4 data from SNO-RAMCES/ICOS network coordinated by LSCE/OVSQ (CEA-CNRS-UVSQ, Université Paris-Saclay), as well as Laboratorio de Física de la Atmósfera (UMSA, Bolivia), Environmental Chemical Processes Laboratory (ECPL/UoC, Greece), Station Géophysique de LAMTO, Ivory Coast), C-CAPS/NUIG/EPA (Ireland), BIRA-IASB (Belgium) and the following research institutes in France: LaMP/OPGC, P2OA/LA/OMP, OPE/ANDRA, OHP/PYTHEAS, OPAR/LACY/OSUR, UMR EcoFoG, IPEV, IRD.

Some references will be added: to the SDS-WAS NAMEE Regional Center to provide the multimodel product, as well, AirBase for the air quality PM10/PM2.5 observations.

Copernicus Atmosphere Monitoring Service

ECMWF - Shinfield Park, Reading RG2 9AX, UK

Contact: info@copernicus-atmosphere.eu